Silicon Micromachined Devices for *In Vitro* and *In Vivo* Studies of Neural Networks

Thesis by
Svetlana Tatić-Lučić

In Partial Fulfillment of the Requirements
for the Degree of
Doctor of Philosophy

California Institute of Technology
Pasadena, California

1995

(Defended August 31, 1994)

Acknowledgments

I wish to thank my thesis advisor Dr.Yu–Chong Tai for all the encouragement, enthusiasm and knowledge that he has shared with me. I consider myself fortunate to be one of his students. I also wish to thank my co–advisor, Dr. Jerome Pine, for all the support that he offered me when I needed it most. His generosity will never be forgotten.

Many thanks to my fellow students John Wright, Chang Liu, Raanan Miller, Amish Desai, Thomas Tsao, Viki Temesvary, Shuyun Wu and all the others who have shared with me all the good and bad times (not to mention the laboratory). My friends have been as always, a big support and consolation to me during the past five years. Thanks to Zoya Popović, Nataša Kovačević, Branislav Kecman, Suzana Veličković–Brown, Milivoje Brković, Cynthia Stewart, Jadranka Mezić, Nancy Winfree and many others for their unconditional friendship.

Finally, and most importantly, I would like to thank my husband Dragan. He was the one that convinced me to come to the United States to continue my education and who believed in me when few persons did. These have not been easy years for either of us, and without his support and endurance it would have been much more difficult to complete this work. Thank you!

Silicon Micromachined Devices for *In Vitro* and *In Vivo* Studies of Neural Networks

by

Svetlana Tatić–Lučić

In Partial Fulfillment of the
Requirements for the Degree of
Doctor of Philosophy

Abstract

The design, fabrication and mechanical testing of two new kinds of silicon–micromachined devices for both *in vitro* and *in vivo* extracellular stimulation and recording are investigated. The novelty of these devices is a neuron well structure fabricated in a 16-20 μm-thick silicon membrane using a double-sided micromachining technique. The neuron well is a trapezoidal cavity with a gold electrode at the bottom and a mechanical grillwork on the top. Through the grillwork, live embryonic neurons can be implanted, cultured, and then electro-physiologically studied inside the wells. This approach can tremendously improve the reliability and signal-to-noise ratio of extracellular recording of the cultured neurons compared to previous approaches.

First, a silicon-micromachined microchip for *in vitro* studies of cultured neural networks has been developed. The bottom of the neurochip has two different designs. One has a circular silicon-dioxide rim (0.8 μm step height) at the bottom (called dimpled bottom), and the other has only a flat bottom. The dimpled bottom is expected to provide a better mechanical seal between the cultured cell and the gold electrode, which would result in a better signal-to-noise ratio. Physiologically, it has been confirmed that the neuron growth inside the well is independent of the kind of bottom. So far, the neurochips' biocompatibility for up to a week has been demonstrated using both rat hippocampal and superior cervical ganglion (SCG) neuron cells. Next, silicon neuroprobes for *in vivo* studies of central nervous systems have also been successfully developed. These probes are developed using a modified neurochip technology. The mechanical properties of the neuroprobes are satisfactory, proven in bending, buckling, and even *in vivo* animal tests. Recently, the neuroprobes have been physiologically tested in rat hippocampus. For the first time, outgrowth of neurites from the cultured neurons inside the wells into the host hippocampus has been observed, which represents the very important evidence for the success of using neuroprobes.

In the future, although beyond the scope of this work, a lot more exciting electro-physiological research using these devices should be done. This should lead to further improvement over the prototypes, and finally produce a new generation of working neural prosthetic devices.

Contents

List of Figures

List of Tables

Chapter 1

Introduction

One of the principal techniques for studying the central nervous system is the recording of the potentials generated by single neurons. However, although it can provide important insight into the neural architecture, it does not provide any information about how the groups of neurons do connect and interact. The information about how groups of neurons do work together is essential for understanding how the brain functions, that old and overwhelming problem that has attracted the attention of so many scientists and people in general.

A variety of different methods of neural network analysis have been developed to analyze this problem. The majority of these studies are performed *in vivo*, meaning on live and intact nervous systems. However, some of them are done *in vitro* on cultured neurons. Both approaches are going to be described in more detail in the following sections.

1.1 *In Vitro* Studies of Neural Networks

In vitro studies of a neural networks have to start with dissociated cell cultures, which can be obtained by disassembly of part of a nervous system into individual cell components by means of chemical and/or mechanical processes. The dissociated neuron cells are then kept alive and cultured in a liquid environment which is similar to their original habitat. This environment, called cell medium, usually contains proteins, sugars, vitamins and other ingredients that are essential for the cells.

The main advantage of using cultured neurons is their easy accessibility and manipulation. Detailed electrophysiological studies have been demonstrated and essentially all parts

of the nervous system can be cultures including cerebellum [25, 42, 50], hypothalamus [4] and hippocampus [27, 2].

There are two ways to record and/or stimulate the electrical activity of the cultured neuron cells: intracellular and extracellular. Each method has its advantages and disadvantages and they are described in the following.

1.1.1 Intracellular Electrophysiology of Cultured Neurons

For many years, one problem of neurobiology research was to measure the potential inside a cell. One solution was to use a capillary micropipette, which is usually a glass tube with a small tip opening. Once filled with a saline solution, it becomes an electrode that is glass-insulated except at the tip, where electrical connection with the cell can be obtained by penetrating it through the cell membrane.

The pioneering studies of intracellular recording were started as early as 1939 by Hodgkin and Huxley [11]. The capillary electrodes they used had a tip size of about 100 microns in diameter and were introduced vertically into the cut end of a giant squid axon. The data they acquired is first-rate in quality as shown in Fig. 1-1. The first micropipette with a submicron tip was made by Ling and Gerard in 1949. [19]. Because of its small size, their pipette can be used for much smaller neurons and neural processes.

The advantage of the intracellular glass-pipette recording is a good signal–to–noise ratio. However, it is ill-suited for long-term experiments, because neurons rarely survive the penetrations long enough. In addition, it is very difficult to do more than two neurons at the same time [6]. On the other hand, extracellular recording seems to be more suitable for long-term stimulation and recording. The cost is a compromise in signal–to–noise ratio. A big improvement was the invention of the so-called patch-clamp technique, which is described next.

The Patch-Clamp Technique

Instead of piercing the neuron, a thin glass pipette of the proper shape can be tightly pressed against a cell membrane, thereby isolating a small patch of the membrane and the ion channels it contains. When properly initiated, the annulus of the membrane forms a

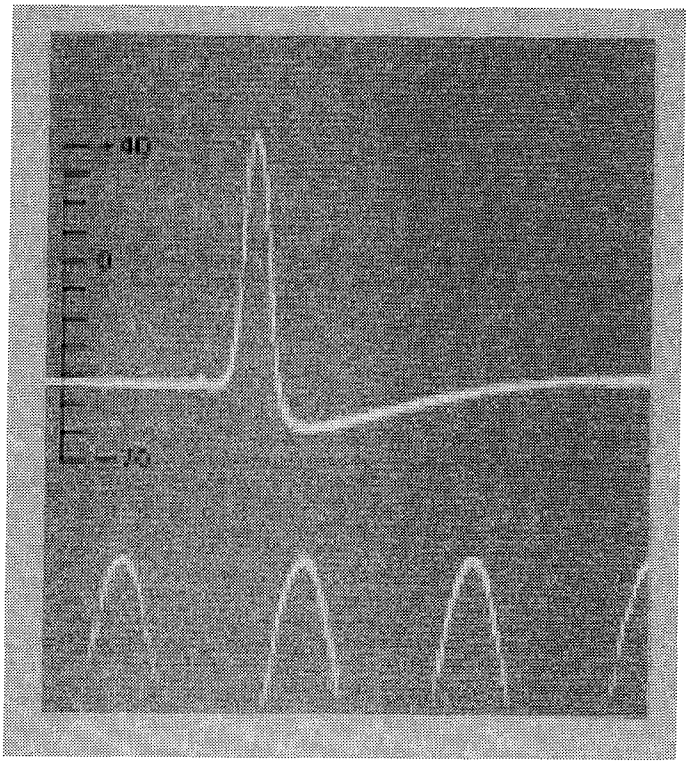

Figure 1-1: Intracellular recording of action potential from squid axon. Time base: 500Hz [11].

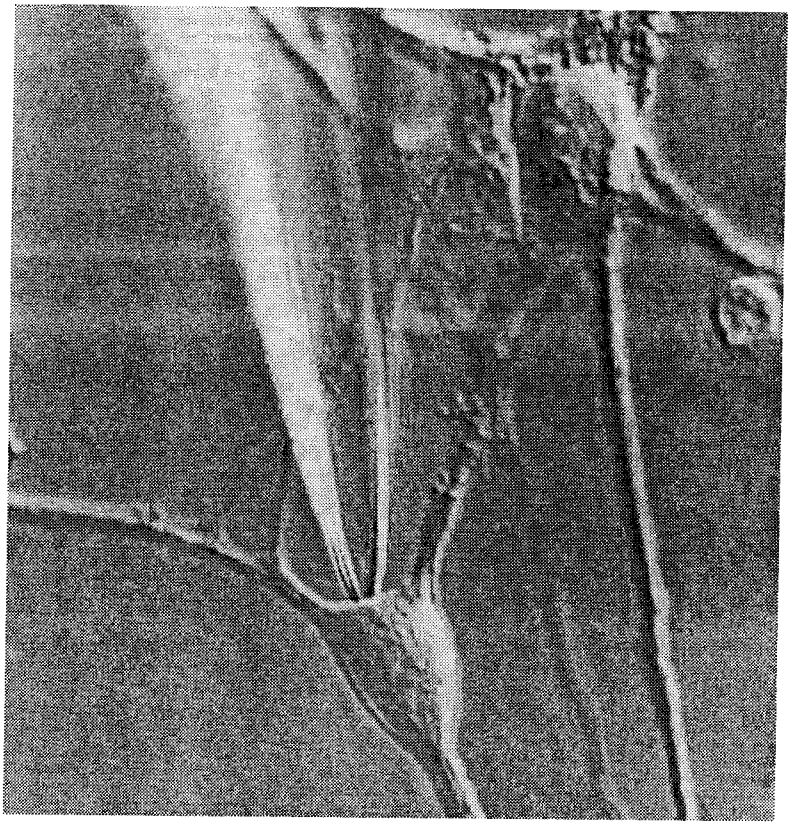

Figure 1-2: Tightly sealing a pipette against the surface of a neuron enables researchers to study the ion channels in the membrane. The pipette physically and electrically isolates the trapped channels [23].

tight seal with the interior of the pipette tip.(Figs.1-2. and 1-3.)

This seal has a resistance of gigaohms, and it is tight in electrical, chemical and mechanical senses [18]. The high resistance of a "giga-seal" reduces the background noise of the recording by an order of magnitude. Mechanically, other regions of the membrane will break before this seal. Consequently, the patch of membrane can be removed or a window opened to alter the cytoplasmic constituents of the cell [24] (Fig.1-3.c.).

It seems that this way of penetrating a cell inflicts much less damage than the standard microelectrode impalement, so it is widely used.

The patch-clamp technique differs from conventional micropipettes in some main points. First, cell penetration with a conventional micropipette usually results in cell injury if the cell is less than 20μm in diameter (which is usually the case for our more interesting, mammalian cells). Patch–clamping can be performed on cells less than 10μm in diameter

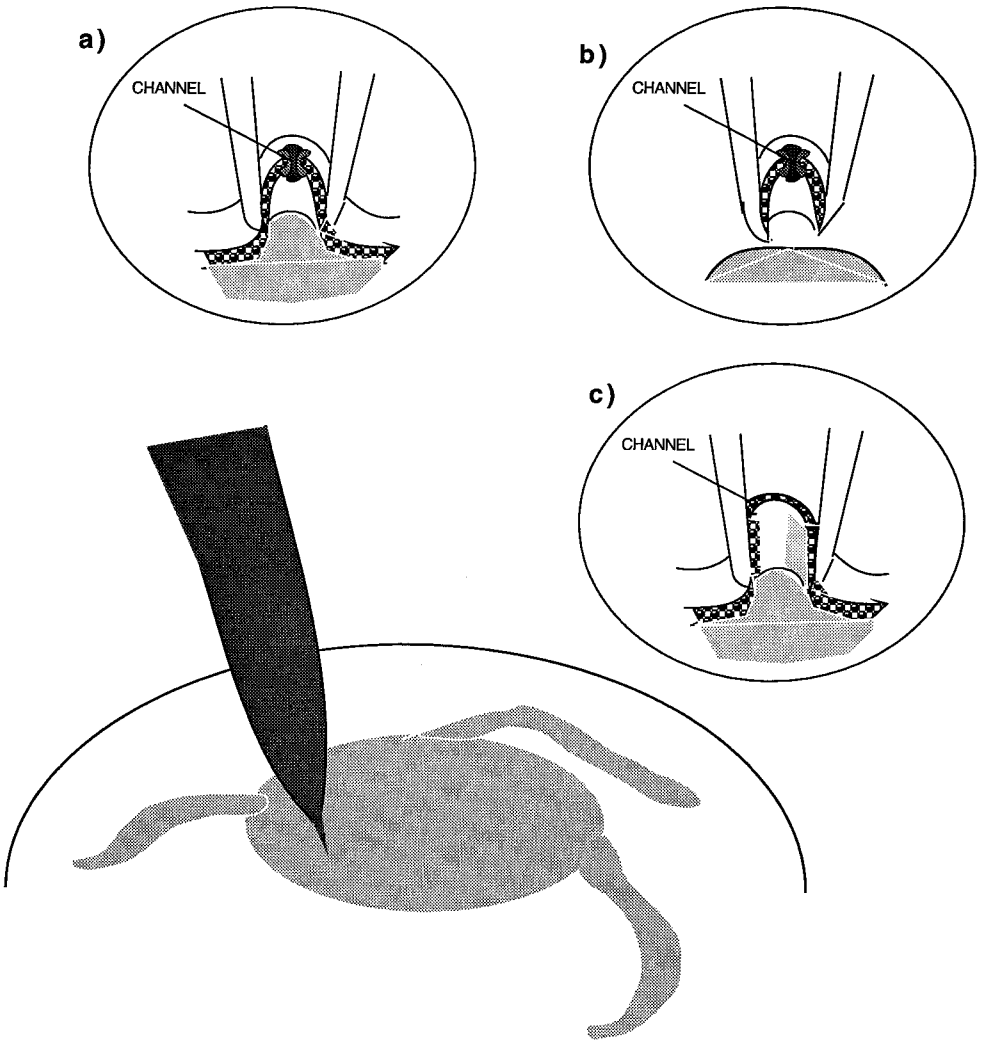

Figure 1-3: Three forms of patch clamping: a) By pressing a patch pipette against the enzymatically clean surface, researchers can place a gigaohm seal around a small patch of the cell membrane and the ion channels it contains, b) An experimenter may detach the membrane patch from the cell or c) If the membrane patch can be ruptured without breaking the giga–ohm seal, the experimenter can alter the constituents of the living cell's cytoplasm. (Adapted from [23].)

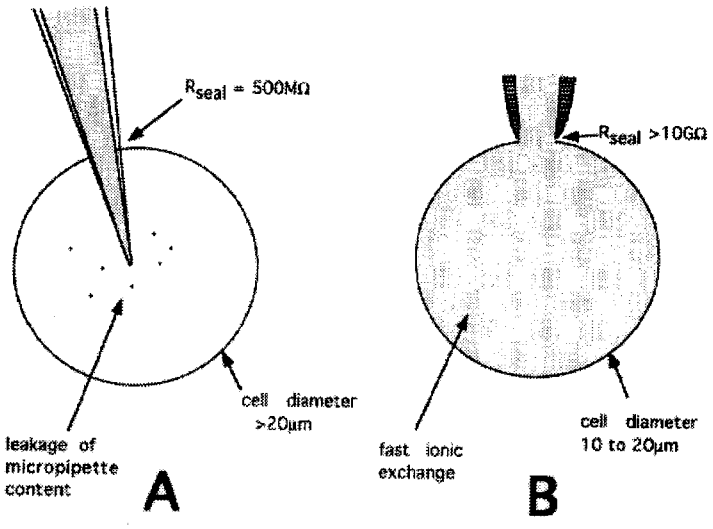

Figure 1-4: Comparison between conventional micropipette recording (A) and tight–seal whole–cell recording (B).

without signs of cell damage. Second, the obtained seal is much better than that formed by a micropipette (20GΩ when compared to 500 MΩ) (See Fig.1-4.).

Additionally, an alternative method of the patch–clamping was found where the cell is not penetrated, but the pipette is tightly pressed against the cell and stimulation and recording are performed. It is so–called loose–patch clamp technique.

The Loose Patch Clamp

Instead of isolating localized patches of membrane containing only one or at most a few channels, one can attempt to clamp a membrane area large enough to give a "macroscopic" current, such that it contains many channels distributed over an area of 5-50μm^2. The difference with respect to the ordinary patch-clamp technique is twofold. First, you clamp a larger area (pipette diameter is larger) and, second, no giga seals are required. This technique enables stable and localized electrophysiological data to be obtained [43].

1.1.2 Extracellular Recording of Cultured Neurons

Extracellular stimulation and recording techniques were among the first to be used in electrophysiology. The old-fashioned approach is to use a glass pipette, but instead of piercing

the cell, the pipette is put very close to the cell [14]. This method is, obviously, not harmful to the cell and is very repeatable. However, signal-to-noise ratio is bad, and it is difficult to perform experiments on more than 2-3 neurons at the time, because of the bulky micromanipulators.

The revival of extracellular recording happened after the realization that micromachining methods can be used for the fabrication of different extracellular and recording devices.

Multielectrode Dishes

It is possible to fabricate electrodes embedded in the culture-dish bottom and to perform extracellular recording and stimulation of neurons [49, 8, 33, 53]. Several hours after cell medium with dissociated neurons is poured into the culture dish, neurons tend to anchor to the floor of the culture dish and grow processes. (Fig.1-4.). Multielectrode dishes are noninvasive tools for studies of cultured neurons, providing the capability of long-term experiments of a multi-neuron network. They are very suitable for invertebrate neurons, because they tend to grow over electrodes and form a seal of several megaohms. These electrodes are embedded at the culture-dish bottom and act as loose–patch electrodes, stimulating and recording reliably [36].

However, in mammalian neuron cultures, which typically consist of much smaller neurons, the distance between electrodes and neurons is usually big. Signal-to-noise ratio is, consequently, small and postsynaptic potentials cannot be detected.

There is one more problem: a neuron being next to a electrode is a purely random process.

Also, it can happen that two or more neurons or neural processes are next to an electrode. This makes it very difficult to distinguish from where the signals originate.

Diving Board Electrodes

Trying to achieve one-to-one connections, Regehr built a silicon microdevice which can be used as a loose-patch electrode (Fig.1-6.) [38]. A cup-like electrode structure, positioned at the end of the long, slender beam can be maneuvered onto the neuron and then the other end glued to the bottom of the culture dish. Both stimulation and recording of neural signals can

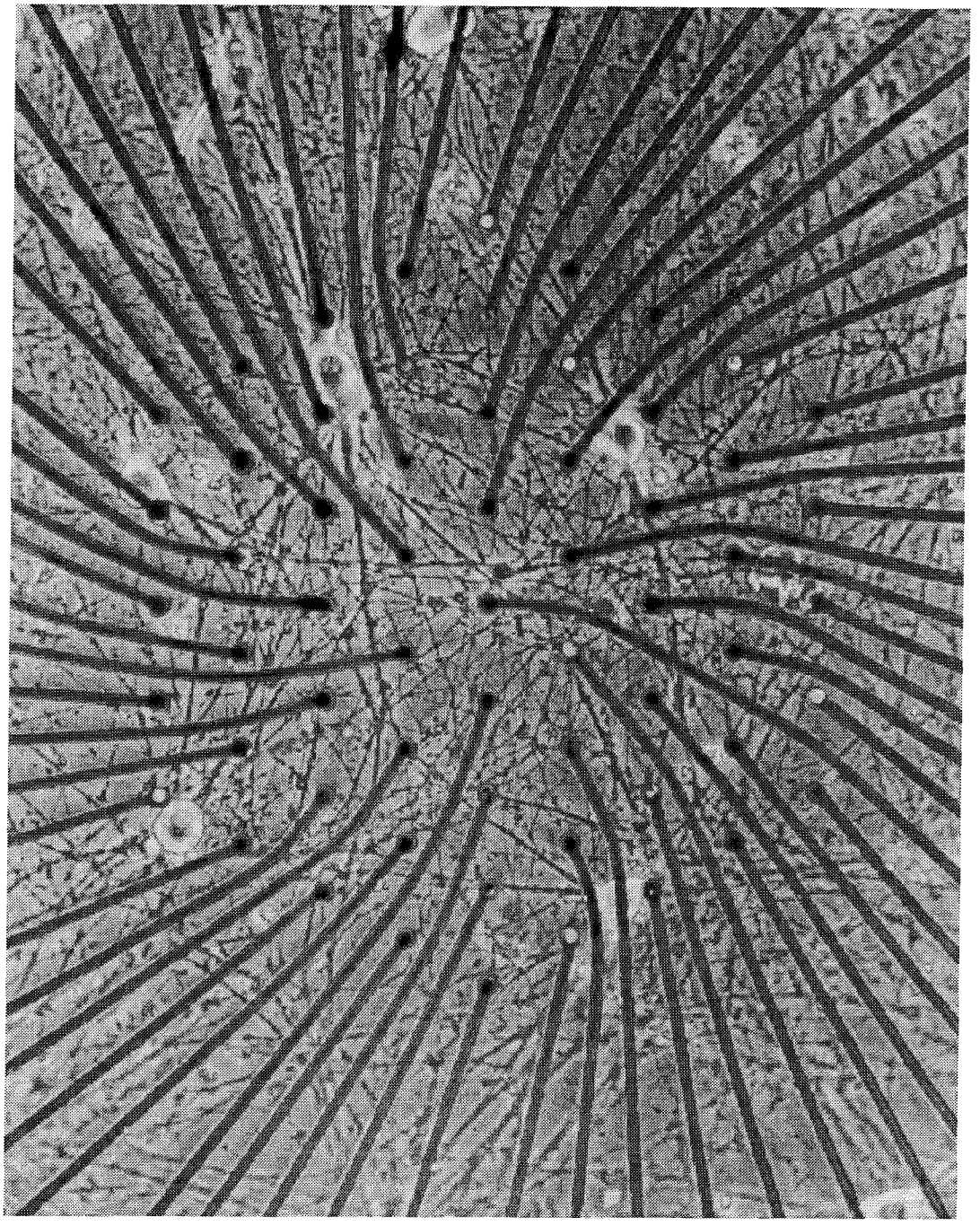

Figure 1-5: Neurons sealed at the bottom of the multielectrode dish.

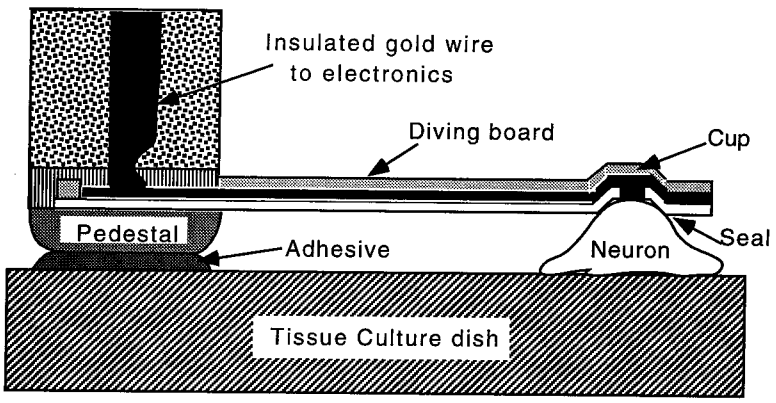

Figure 1-6: Schematic of a diving–board electrode in contact with a cell. (Adapted from [36]).

be performed. However, it is difficult to maneuver the electrode above the neuron and to use more than a few electrodes concurrently [14]. Also, their fabrication is not simple, especially when smaller, vertebrate neurons are used. These problems (especially the necessity of the maneuvering the electrode above the neuron) are overcome by the invention of the polyimide multiwell dishes.

Polyimide Multiwell Dishes

Polyimide multiwell dishes, developed a few years ago at Caltech, are similar to the multi–electrode arrays described earlier. The main difference is that the dish is not flat and the metal electrodes are embedded into the bottom of a neuron well. Neuron wells are fabricated using a photosensitive polyimide as a building material [14]. (See Fig.1-7). There are couple of advantages of well electrodes when compared to the other extracellular recording techniques. The most important ones are increased specificity and increased reproducibility. However, the long–term stability of the polyimide as the constitutive element of the neuron wells is questionable.

Neurochip: Motivation and the Basic Concept

Neither of the previously mentioned options is ideal. Multielectrode dishes (electrodes embedded at the bottom of the petri–dish) offer the possibility of recording and stimulating

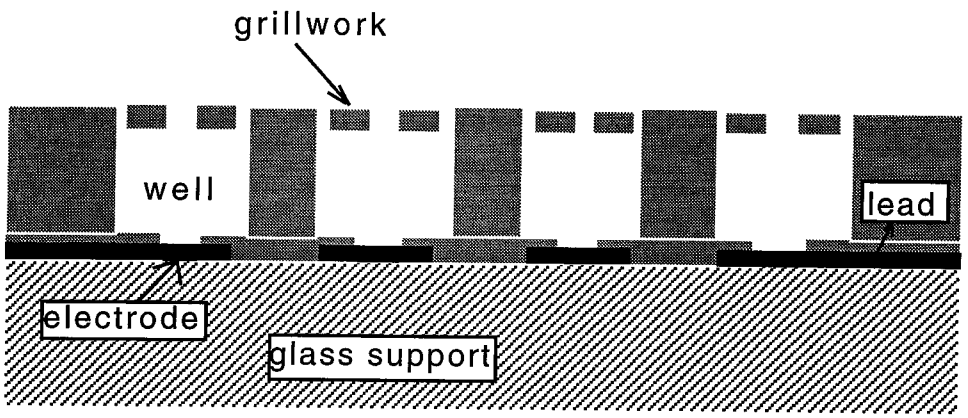

Figure 1-7: A typical cross-section through a line of four wells in a well electrode device. (Adapted from [7]).

from an abundance of neurons. The disadvantage is that the randomness of the neuron position vs. the electrode often causes troubles with the signals–they might be not present at all electrodes and they are difficult to be interpreted if they originate from more than one neuron at the same time.

Diving board electrodes are difficult to mount and inpractical for recording from more than a few neurons at the time, whereas the polyimide dishes suffer from long–term reliability problems. Obviously, a better tool is needed for the extracellular recording from the cultured neurons. The need exists to create a new device for *in vitro* studies of live neural networks which would enable one–to–one neuron–to–electrode correspondence and would be applicable to many neurons at the same time for long–term experiments, therefore avoiding the problems associated with the structures mentioned above.

The idea was born to fabricate structures based on silicon neuron wells similar to the polyimide wells that were previously described (See Fig.1-8) [17]. That structure would have one–to–one neuron–to–electrode correspondence, would not require the positioning of the electrode above the neuron and would have good long–term reliability because of the building material having better long–term properties than polyimide. One possible configuration of such a device is presented at Fig.1-9.

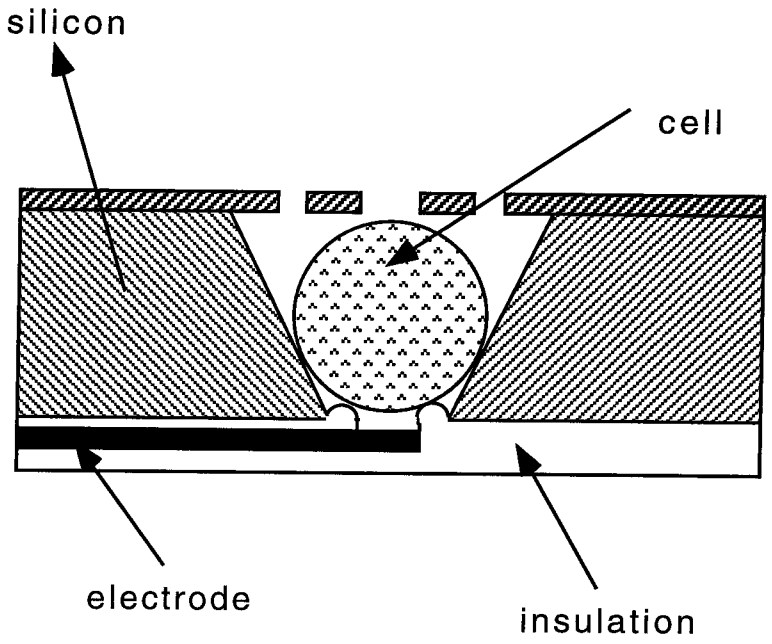

Figure 1-8: Schematic presentation of the silicon well.

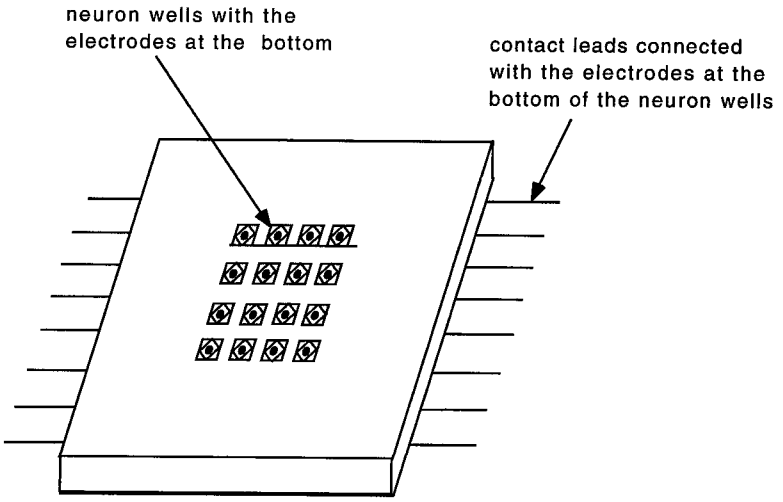

Figure 1-9: The idea of the neurochip

1.2 Devices for *In Vivo* Studies of Neural Networks

The great physiologist Sir Charles Sherrington compared the activity of brain cells to twinkling points of light [15]. Describing awakening from sleep, he wrote: "Swiftly the head-mass becomes an enchanted loom where millions of flashing shuttles weave a dissolving pattern, always a meaningful pattern, though never an abiding one; a shifting harmony of sub-patterns."

Obviously, he believed that investigation of spatiotemporal patterns of neuronal activity is crucial in understanding how the brain functions. However, the spatial aspect was usually neglected, due to the technological limitations that existed. The spatial pattern of neuronal activity was resolved by using arrays of metal multimicroelectrodes.

1.2.1 Multimicroelectrode Arrays

The first attempts to do multimicroelectrode recordings were done with single microelectrodes, which were rigidly coupled. [51]. Even now, one can frequently find bundled fine metal electrodes (insulated wires that are cut at the ends) applied as multimicroelectrodes. An interesting idea was implemented by O'Keefe and Bouma (1969.), who did temporary gluing of individual metal electrodes by polyethylene glycol, which melts and dissolves in the brain in a short time after the implantation [26].

Metal electrodes are still widely employed, but their serious drawbacks are undeniable: lack of control over electrode properties (the size of the exposed electrode sites and uniform spacing among the electrodes, for example), as well as prominent tissue damage caused by probe insertion being the most serious ones. It is exceedingly difficult, if not impossible, to produce fine wire bundle microelectrode arrays which are reproducible in their mechanical and electrical properties and which maintain their mechanical and electrical stability during insertion [21]. Also, it is not possible to separate electrical and mechanical properties of the array, because more electrodes (wires) means thicker bundles and stiffer arrays. These drawbacks were made possible to solve when the micromachining technology was developed.

1.2.2 Silicon Microprobes

Silicon micromachining permits the fabrication of micro-miniature devices for extracellular recording and stimulation which enable high-density recording with minimal brain intrusion. The basic structure of a neural probe consists of an insulated array of metal electrodes (usually gold, for biocompatibility reasons, insulated by silicon oxide, silicon nitride, oxynitride or polyimide) on a common substrate. The substrate is predominantly silicon, although metal foils have been used as well. The specific design depends on the specific application. The application can be chronic (long–term application) or acute (short–term experiments). Also, probes can be passive or active. Active probes have built–in circuitry which is necessary for signal processing.

From the seventies on, a lot of work has been done on micromachined probes [32, 16, 21, 29]. However, the first who explored this possibility, to the best of my knowledge, was Kensall Wise [57]. He used, for the first time, an integrated–circuit approach to the extracellular microelectrodes.

In Fig.1-10. one can see the design of his microelectrodes. They have been fabricated with gold deposited on a very thin silicon substrate and insulated by silicon oxide.

However, this structure was not practical until the early eighties, when anisotropic etch–stops were applied [55, 56]. Figure 1-11 shows a diagram of the probe structure being developed, while Fig.1-12 shows some SEM micrographs and photographs of the obtained structure. The key idea is the supporting substrate which is formed using a deep boron diffusion and a boron etch–stop in EDP. The probe is released by the dissolving of the undoped substrate wafer. This fabrication process is reliable and easy to control, so these probes are now extensively fabricated at the University of Michigan, in the variety of shapes for the different needs of the customers.

However, Michigan probes do have some drawbacks. They are stimulating all regions of the brain in exactly the same fashion, and there are some ideas that the stimulation should be performed in a more specific way. They are also very thin, because their thickness is determined by the maximum depth of the boron diffusion, which is not more than 15μm . Finally, they have rounded edges as a consequence of the boron diffusion (See Fig.1-12), and it is very difficult to stack them in three–dimensional arrays.

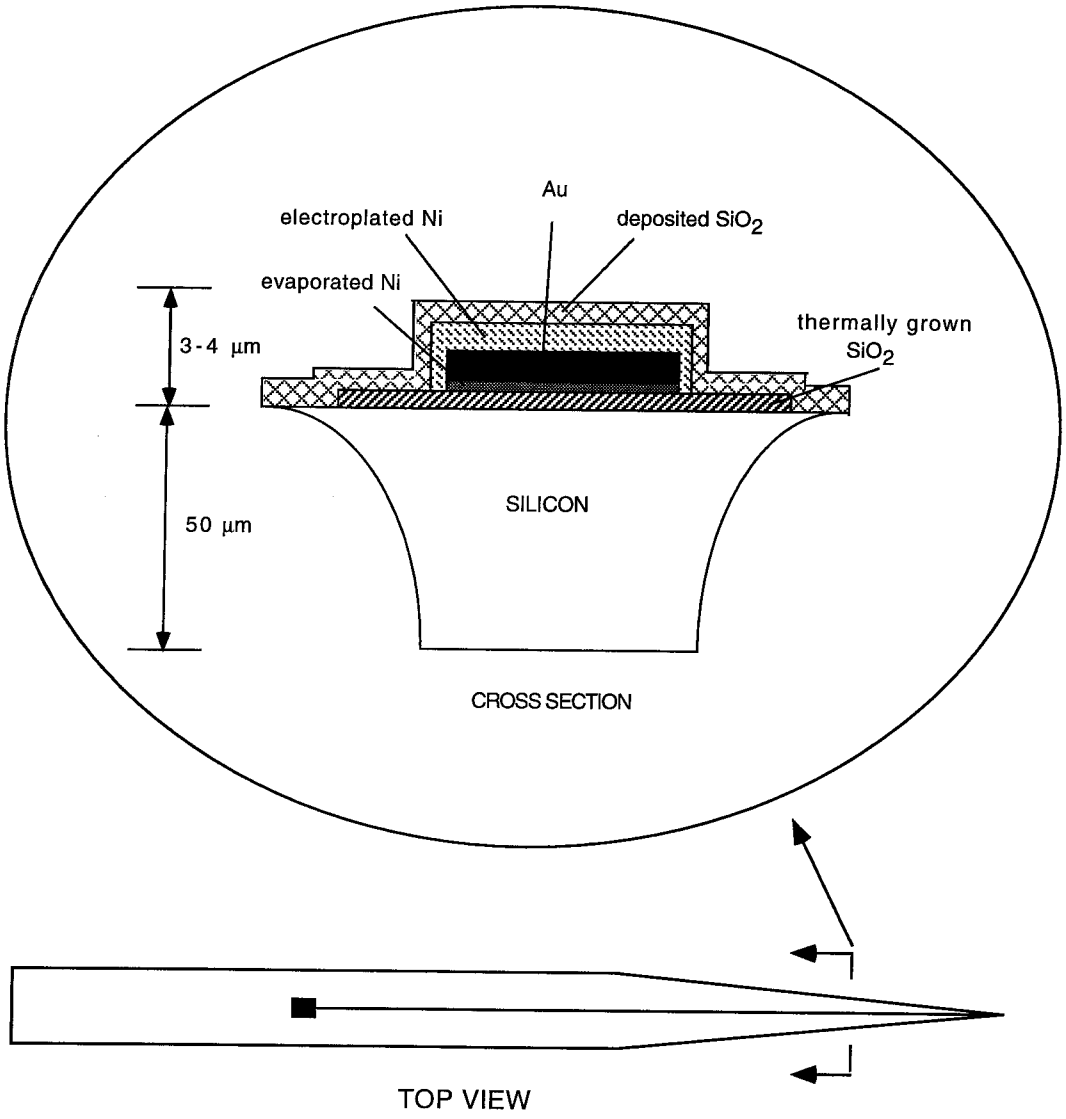

Figure 1-10: Cross section of a single–electrode microprobe. (Adapted from [55]).

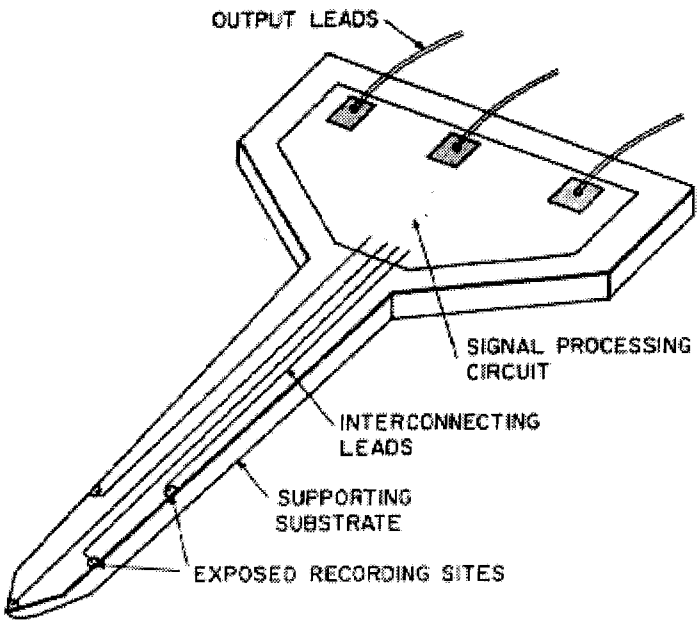

Figure 1-11: Schematic presentation of the silicon microprobe fabricated at the University of Michigan [54].

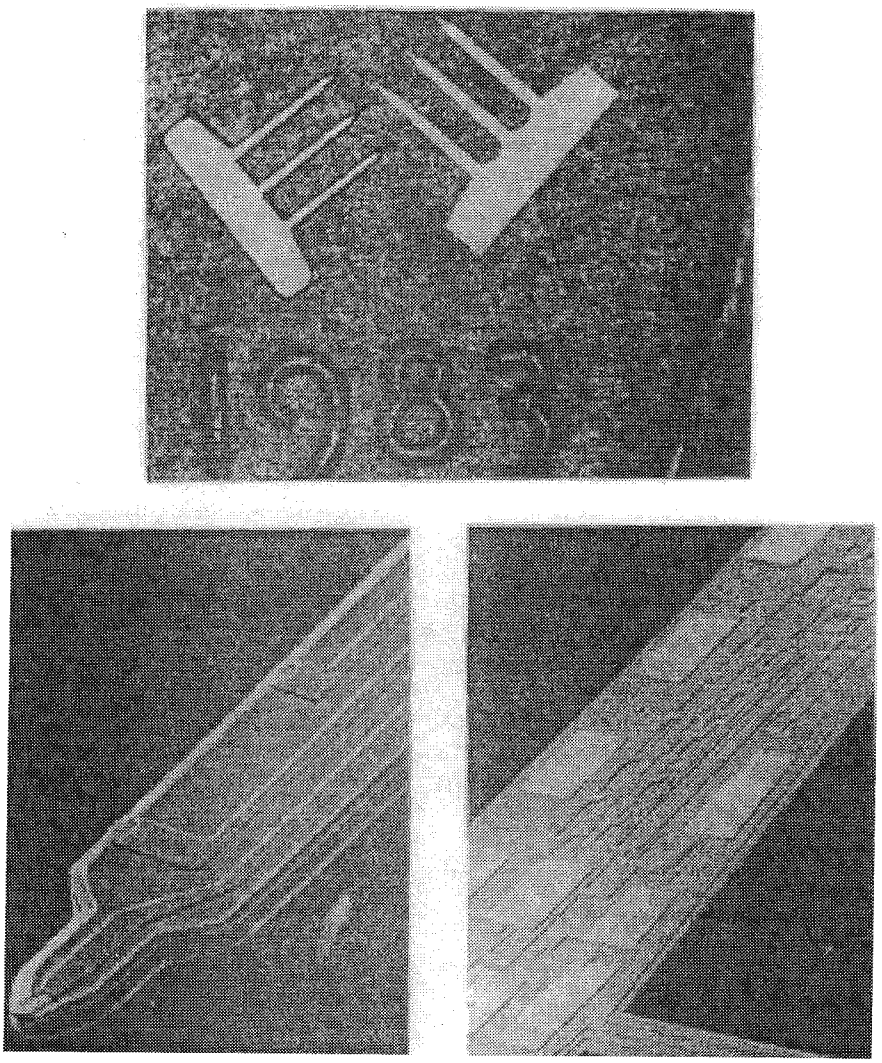

Figure 1-12: Several views of silicon microprobes fabricated at the University of Michigan. The probes are typically 15μm thick with a tapered shank width of 60-90μm. The photo in the lower right shows the rear portion of a probe containing NMOS test circuitry [54].

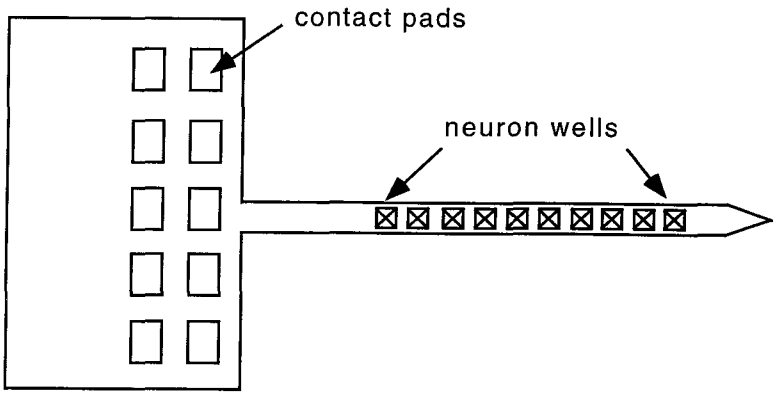

Figure 1-13: The basic structure of the neuron probe.

We have tried to solve the necessity for better devices for *in vivo* studies of neural networks with a novel approach: a cultured neuroprobe. It is described in the following section.

Cultured Neuroprobe: Motivation and the Basic Concept

We propose a new approach which uses "linking neurons" incorporated into neuron wells contained in the silicon micromachined neuroprobe. The probe is to be inserted into the animal's brain. Assuming that the cultured neurons do survive and make synapses there, highly specific connections can made with specific neurons. The name chosen for this structure is "cultured neuroprobe."

Cultured neuroprobes have several neuron wells at their tip, with leads running along the shank. The leads end up on the handle of the probes where contact holes are opened for the electrical communication with the electrode at the bottom of the neuron wells (Fig.1-13).

Note that the handle of the cultured neuroprobe would have, according to this configuration, the entire thickness of the silicon wafer to enable easy handling and, possibly, stacking of the probes when one wants to obtain a three–dimensional structure.

1.3 Overview

In the introduction of this thesis, various methods of *in vitro* and *in vivo* studies of neural networks are described and their advantages and disadvantages presented. The concept

of neuron wells and novel devices for extracellular stimulation and recording from neurons that are based on neuron wells (so–called neurochips and neuroprobes) is introduced.

Design considerations, the design itself and the fabrication process for the neurochips is presented in the following chapter. Fabrication requirements for the neurochip have led to the development of new micromachining methods: a novel technique for extra–accurate front–to–back alignment across a thin membrane and across a whole wafer, as well as the exposure in a 500μm–deep–cavity. Both neurochips containing neuron wells with dimpled and the flat bottoms are presented. Next, the experimental results with the neurochips are discussed.

The design and fabrication of the cultured neuroprobes are described in the next chapter. The mechanical testing that proves their mechanical strength is described, as well as preliminary results of the physiological experiments. Finally, we consider the potential of these devices and suggest the direction of the further research.

Chapter 2

Neurochip for *In Vitro* Studies of Neural Networks

The battle for the understanding of how the nervous system functions is very difficult, but the inventions of neuron culturing and silicon micromachining offer an elegant, promising solution to the problem. However, with the existing devices it was difficult to find an answer to even very basic questions, like how small neural networks interconnect or how electrical activity affects synaptic strength. In the following chapter we are going to describe the device which overcomes the difficulties associated with the use of the existing structures.

2.1 The Basic Concept of Neurochip

A structure was envisioned with an array of neuron wells containing electrodes at their bottom and grillwork on top (See Figs.2-1. and 1-9). We planned to have a neuron implanted in the well when it is very young. It is confined to the well by means of grillwork. Inside it grows, fills the well and forms a seal by pressing against the oxide ring at the bottom of the well. In principle this can be thought of as a loose–patch electrode. The exposed gold electrode and opening in oxide layer that is defining it are chosen to have the typical size of a loose–patch electrode. The schematic presentation of a neuron implanted in a neuron well is given in Fig.2-2, and Fig.2-3 shows the appropriate equivalent circuit. In this figure, Z_e is the equivalent impedance of the electrode. Since we are using a gold (metal) electrode, its impedance is predominantly capacitive. R_{seal} is the resistance of a layer of the cell medium squeezed between the cell and the rim of the electrode. C_m is the membrane capacitance (typically 1 μ F/cm^2).

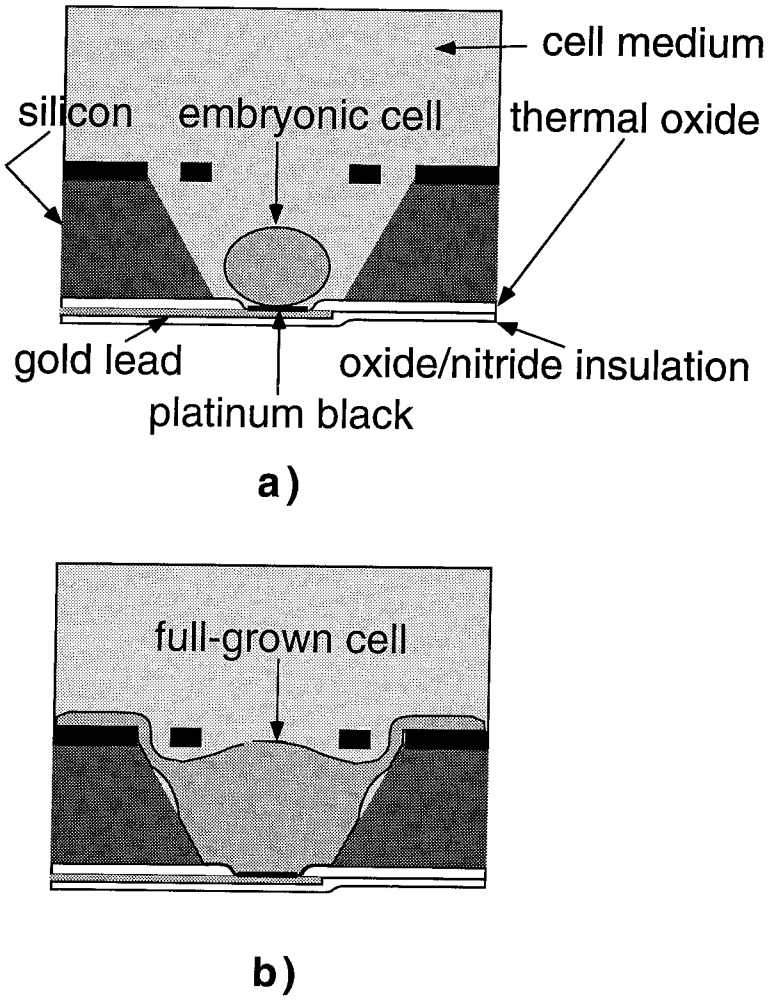

Figure 2-1: a) Neuron just implanted in well, b) Neuron increases in size and grows processes out of the well.

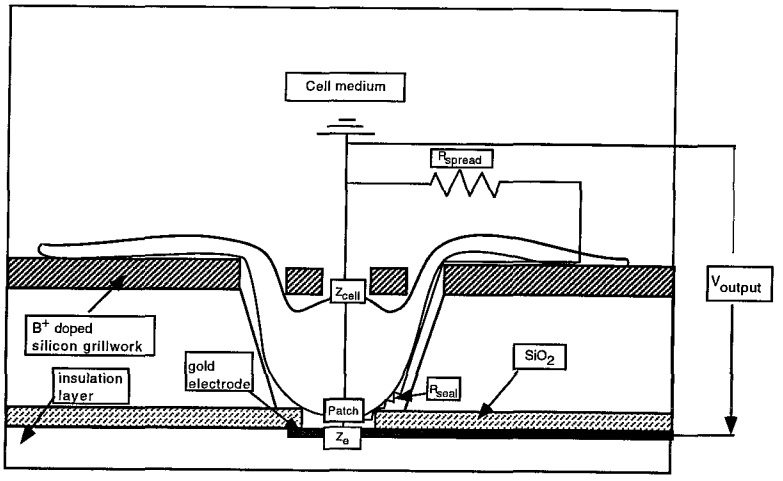

Figure 2-2: Schematic presentation of a neuron implanted in the neuron well.

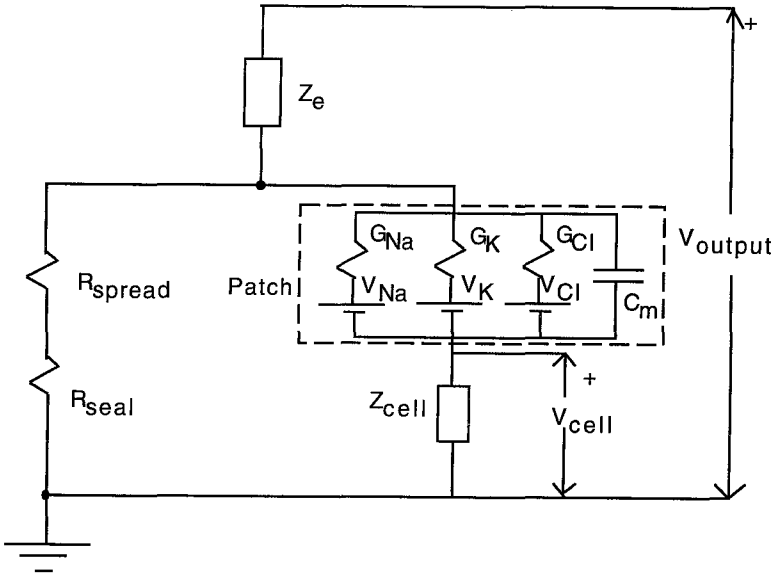

Figure 2-3: The equivalent circuit of a neuron implanted in the neuron well.

Ion*	Concentration (mM/l)		Reversal potential
	Inside	Outside	(mV)
K^+	400	10	-92
Na^+	50	460	55
Cl^-	40	540	-65

Table 2.1: The concentrations of the most important ions inside and outside the cell.

V_{Na}, V_K and V_{Cl} are so–called reversal potentials for Na^+, K^+ and Cl^- ions, respectively. Since Na, K and Cl channels are the dominant channels in the cell patch, channels of the other types will be neglected in this study. Due to the metabolically driven pumps, the concentration of different kind of ions (K^+, Na^+ and Cl^-) are different inside and outside the cell. The diffusion of ions outward will be exactly counterbalanced by the drift inward when the voltage across the membrane reaches the value V_r such that

$$V_r = -\frac{kT}{q} \ln \frac{N_{in}}{N_{ex}}, \tag{2.1}$$

where N_{ex} is ion density in the extracellular fluid and N_{in} is the density in the cytoplasm. These concentrations for the most important ions are given in Table 2.1. As for the other parameters shown in the equivalent circuit in Fig. 2-2.b, R_{spread} is the resistance of the extracellular solution linearly proportional to the resistivity of the medium ρ and Z_{cell} is the impedance of the cell, which can be approximated at the resting potential as a parallel connection of a resistor and a capacitor [38]. Finally, G_{Na}, G_K and G_{Cl} are total conductances of the Na, K and Cl channels of the cell.

In order to stimulate the cell, the membrane should be depolarized approximately 15mV in order to initiate the action potential of the neuron [37]. The stimulation is usually performed by passing a current pulse of intensity I_0 and duration Δt , with the current flowing from the ground into the electrode. In order to estimate the intensity of the pulse that would enable the firing of the neuron, one should make certain assumptions to simplify the circuit. R_{spread} should be much smaller than R_{seal} and Z_e should be negligible when compared with the other impedances in the equivalent circuit. This assumes the electrode

is designed and fabricated in a right way.

By the definition of capacitance, the voltage and current flowing through the cell capacitance satisfy the relation:

$$I_{C_{cell}} = C_{cell}\frac{dV_{cell}}{dt}. \tag{2.2}$$

If $\frac{dV_{cell}}{dt}$ is approximated by the ratio $\frac{\Delta V_{cell}}{\Delta t}$, equation (2.2) can be transformed into

$$\Delta V_{cell} = \frac{I_{C_{cell}}\Delta t}{C_i cell}. \tag{2.3}$$

The duration of the current pulse Δt is chosen to be much smaller than the time constant of the cell, which is usually a couple of miliseconds [38]. Knowing that, we can approximate the current flowing through the cell capacitance as the current that flows at the moment the current pulse is initiated. At that particular moment, the entire current that is entering the cell patch will flow through the cell capacitance C_{cell}, and not through the cell resistance R_{cell}, so we can obtain the relation

$$\Delta V_{cell} \approx \frac{\Delta t}{C_{cell}}(i_{C_m} + i_{Na} + i_K + i_{Cl}) \tag{2.4}$$

However, the total currents through the specific channel types (i_{Cl}, i_{Na} and i_K) are dependent on the channel density, which is a random (unknown) variable. So, the stimulus current has to be experimentally determined rather than precalculated.

As for the recording, it can be written that the measured voltage between the electrode and ground is:

$$V_{meas} = R_{seal}(i_c + i_{Cl} + i_K + i_{Na}), \tag{2.5}$$

$$V_{meas} = R_{seal}(C_{cell}\frac{dV_{cell}}{dt} + \frac{V_{cell} - V_{Na}}{R_{Na}} + \frac{V_{cell} - V_K}{R_K} + \frac{V_{cell} - V_{Cl}}{R_{Cl}}). \tag{2.6}$$

One component of the output voltage depends on the derivative of the V_{cell}, whereas the other component is linearly dependent on V_{cell}. For some related experiments [38] performed on *Helisoma* B19 neurons, the capacitive component of the current was dominant and that is expected in the case of the neuroprobe's neurons as well.

2.2 Neurochip Design

The design of the neurochip is shown in Fig.2-4. The neurochip has a 4x4 array of neuron wells situated at the center of a 9mm long, 3mm wide and 20μm thick silicon membrane [46]. The minimum size of the membrane is determined by a GCA4800 stepper's ability to do autofocusing at the bottom of a 500μm deep cavity. One side of the membrane has a 4x4 array of metal electrodes (Fig.2-4.a) and the other side has a corresponding grillwork array (Fig.2-4.b) which defines the neuron wells. Fig. 4-3.c. shows a schematic cross section of a neuron well. The depth of the neuron well, or the thickness of the membrane (20μm), is chosen to accomodate the size of the target rat superior cervical ganglion (SCG) neurons, which are about 15μm in diameter when fully grown.

We designed two different kinds of neurochips. One design has an oxide step on the bottom of the neuron well surrounding the electrode, and they are named "dimpled neurochips." The other design, which attempts to optimize the shape of the neuron well, has flat, purely golden bottom. These were baptized "flat neurochips."

2.3 Neurochip Fabrication

About thirty years ago [23] the astounding realization was made that the same methods applied for the fabrication of integrated circuits could be used for the manufacturing of tiny three-dimensional structures.

In the beginning, it looked like just another laboratory curiosity, suitable for paper publishing and attracting a lot of public attention, but little more. Fortunately, it survived the test of the time. It ends up that silicon is a mechanical material with many desirable properties, including high strength (See Table 2.2.).

Single crystal silicon shows a yield strength two times higher than steel and a Young's modulus very close to that of the steel. At the same time, it has a density very close to aluminum. It is important to mention that single crystal silicon does not deform plastically; it is entirely elastic. The hardness of it is comparable to the hardness of quartz and its thermal conductivity is about 50% higher than the thermal conductivity of steel. All of these characteristics make silicon a mechanical material with very desirable qualities. Add

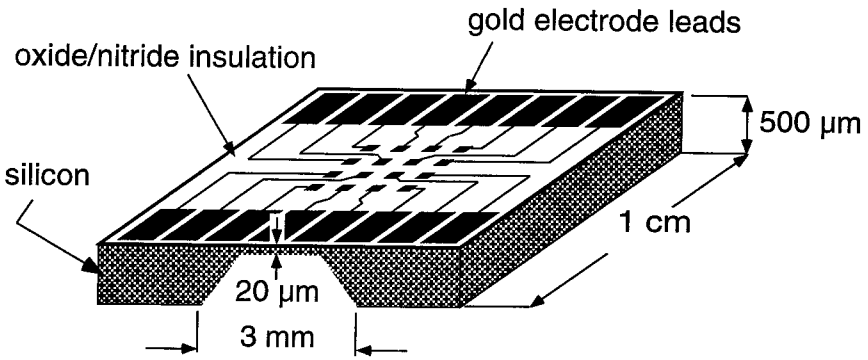

a) Tilted view of a neurochip

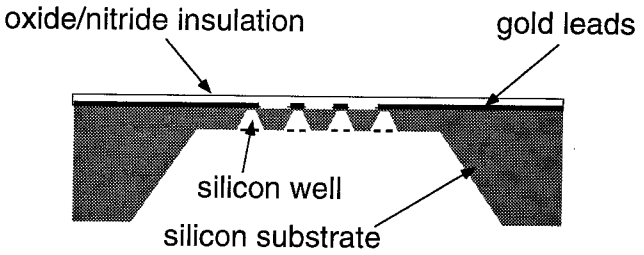

b) Cross section of a neurochip

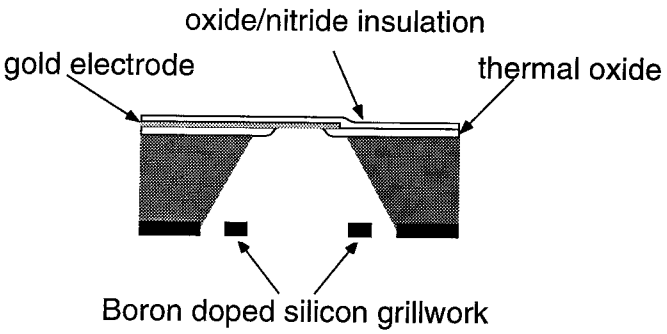

c) Cross section of a neuron well

Figure 2-4: Design and dimensions of a neurochip

	Yield Strength (10^{10} dyne/cm^2)	Knoop Hardness (kg/mm^2)	Young's Modulus (10^{12}dyne/cm^2)	Density (g/cm^3)	Thermal Conductivity (W/cm^{o}C)	Thermal Expansion (10^{-6}/^{o}C)
*Diamond	53	7000	10.35	3.5	20	1.0
*SiC	21	2480	7.0	3.2	3.5	3.3
*TiC	20	2470	4.97	4.9	3.3	6.4
*Al_2O_3	15.4	2100	5.3	4.0	0.5	5.4
*Si_3O_4	14	3486	3.85	3.1	0.19	0.8
*Iron	12.6	400	1.96	7.8	0.803	12
SiO_2 (fibers)	8.4	820	0.73	2.5	0.014	0.55
*Si	7.0	850	1.9	2.3	1.57	2.33
*Steel (max. strength)	4.2	1500	2.1	7.9	0.97	12
W	4.0	485	4.1	19.3	1.78	4.5
Stainless Steel	2.1	660	2.0	7.9	0.329	17.3
Mo	2.1	275	3.43	10.3	1.38	5.0
Al	0.17	130	0.70	2.7	2.36	25

*Single crystal

Table 2.2: The mechanical properties of different materials.

to this the fact that fabrication processes have already been developed by the integrated circuit industry and an unbeatable combination arises. This is the reason that the majority of micromachined structures are based around silicon.

Micromachining technology can be classified as either bulk micromachining or surface micromachining. Bulk micromachining utilizes the etching of single crystal silicon and the obtained structures are made of single crystal silicon and the layers deposited or grown on the silicon [39]. Surface micromachining, however, deposits or grows layers on top of a substrate. The substrate has only a supporting role and is not intentionally altered during the fabrication process.

The micromachining type involved in the neuroprobe and the neurochips fabrication is bulk micromachining.

The fabrication process that has a predominant impact on bulk micromachining is an anisotropic wet etching of silicon. It is crucial for the sculpturing of silicon into different forms. Wet anisotropic etching is a process of preferential directional etching of material (in our case silicon) using a liquid etchant. These etchants attack different crystal planes at different etching rates. The orientation dependence of the EDP etchant rate on a <100> oriented silicon wafer is shown on Figure 2-5.

In Table 2.3. one can find a brief summary of the characteristics of a number of wet silicon etchants [45, 41].

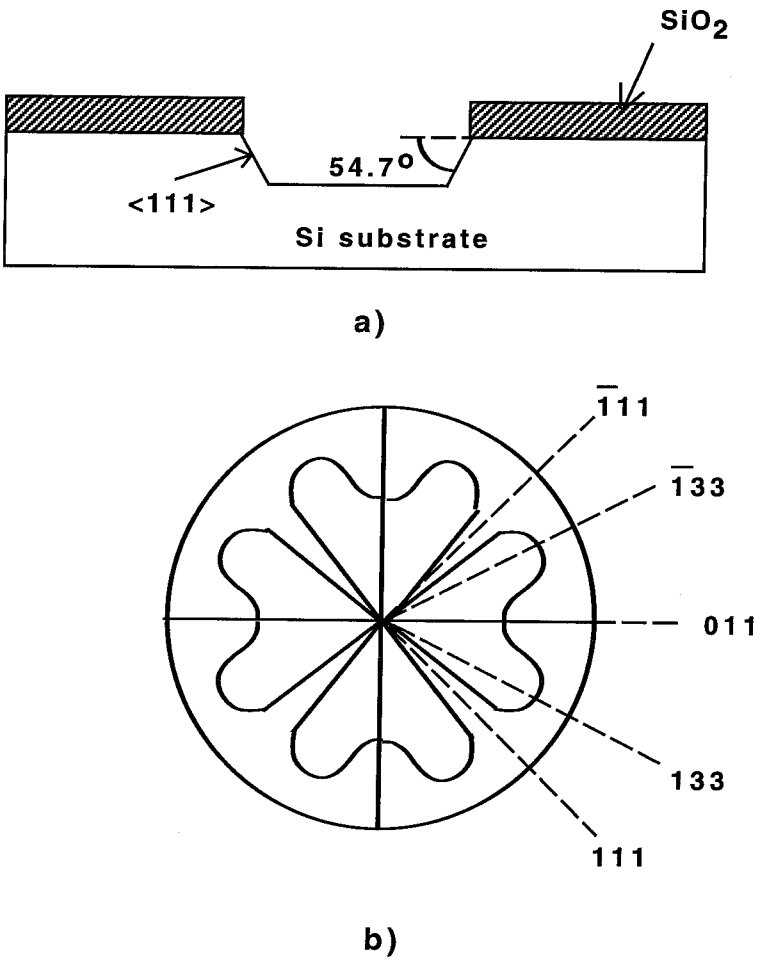

Figure 2-5: (a) Truncated pyramidal pit bounded by silicon<111> crystallographic planes; (b) EDP etch rate dependence on crystallographic orientation in <100> silicon.

Etchant (Diluent)	Typical Compo-sitions	Temp ^{o}C	Etch Rate ($\mu m/min$)	Anisotropic <100>/<111> Etch Rate Ratio	Dopant Dependence	Masking Films (etch rate of mask)
HF **HNO3** **(water,** **CH3COOH)**	10ml 30ml 80ml 25ml 50ml 25ml 9ml 75ml 30ml	22 22 22	0.7-3.0 40 7.0	1:1 1:1 1:1	$<10^{17}cm^{-3}$ n or p reduces etch rate by about 150 no dependence ---------	SiO_2 (30nm/min) Si_3N_4 SiO_2 (70nm/min)
Ethylene diamine Pyrocatechol (water)	750ml 120g 100ml 750ml 120g 240ml	115 115	0.75 1.25	35:1 35:1	$>7x10^{19}$ cm^{-3} boron reduces etch rate by about 50	SiO_2 (0.2nm/min) Si_3N_4 (0.1nm/min) Au,Cr,Ag,Cu,Ta
KOH **(water,** **isopropyl)**	44g 100ml 50g 100ml	85 50	1.4 1.0	400:1 400:1	$>10^{20}$ cm^{-3} boron reduces etch rate by about 20	Si_3N_4 SiO_2 (1.4nm/min)
H_2N_4 **(water,** **isopropyl)**	100ml 100ml	100	2.0	-----	no dependence	SiO_2 Al
TMAH **(water)**	22g 78ml	90	1.0-1.4	20:1	$>4x10^{20}$ cm^{-3} boron reduces etch rate by about 100 (for polysilicon)	Si_3N_4 SiO_2 (0.2nm/min) Al (if some silicon is previously dissolved)

Table 2.3: Properties of different wet etchants.

From this table it can be seen that both of the most common anisotropic etchants — KOH and EDP (Ethylene Diamine Pyrocathecol)— have the slowest etching rate in the <111> direction. Since the exact etching mechanism is not known, one cannot be completely sure, but the anisotropic nature of these etchants seems to be a consequence of the specific crystal properties of a given plane. Namely, a <111> plane is really a double layer bound together by more atomic bonds than are found in other planes.

2.3.1 Dimpled Neurochip Fabrication

The fabrication of the dimpled neurochips starts with epi–wafers with a 16μm thick, lightly–doped layer on top of a 4μm thick, heavily boron–doped layer (for some of the batches we used a boron/germanium doped layer, for reasons that are going to be explained in Section 2.3.6.). First, a composite layer of 180 nm LPCVD silicon nitride on top of 50 nm thermal oxide is formed. Photolithographic steps then pattern the nitride–oxide layer to define openings (6μm in diameter) for the metal electrodes at the bottom of the neuron wells (Fig.2-6.b.)

Plasma and isotropic silicon etching steps then follow to etch through the nitride–oxide composite layer and create a 0.5μm recess into the silicon substrate. Next, a fully recessed LOCOS process planarizes the surface and creates a 1μm oxide step around the openings. The nitride is then stripped, and a 10nm/200nm/10nm Cr/Au/Cr metalization is done using a lift–off process. This process forms the neuron–well electrodes as shown in Fig.2-6.c. Metalization is covered by a composite insulation layer of 0.5μm LTO and 1μm PECVD nitride (Fig.2-6.c.). Next, openings in the insulation layer are made to create bonding pads and to permit etching of alignment marks. The alignment marks are used later to do front–to–back alignment across the membrane that is formed in the subsequent steps, according to the procedure in the Section 2.3.3. An EDP etching then forms the silicon membrane using the heavily boron–doped buried layer as an etch stop (Fig.2-6.d).

Photolithographic steps on the cavity side of the membrane follow, and SF_6 RIE etching is used to form the grilllwork in the heavily boron–doped layer. The neuron wells are formed by EDP etching all the way to the well electrodes on the front side of the wafer. The removal of pad oxide and chromium at the bottom of the wells then finishes the fabrication

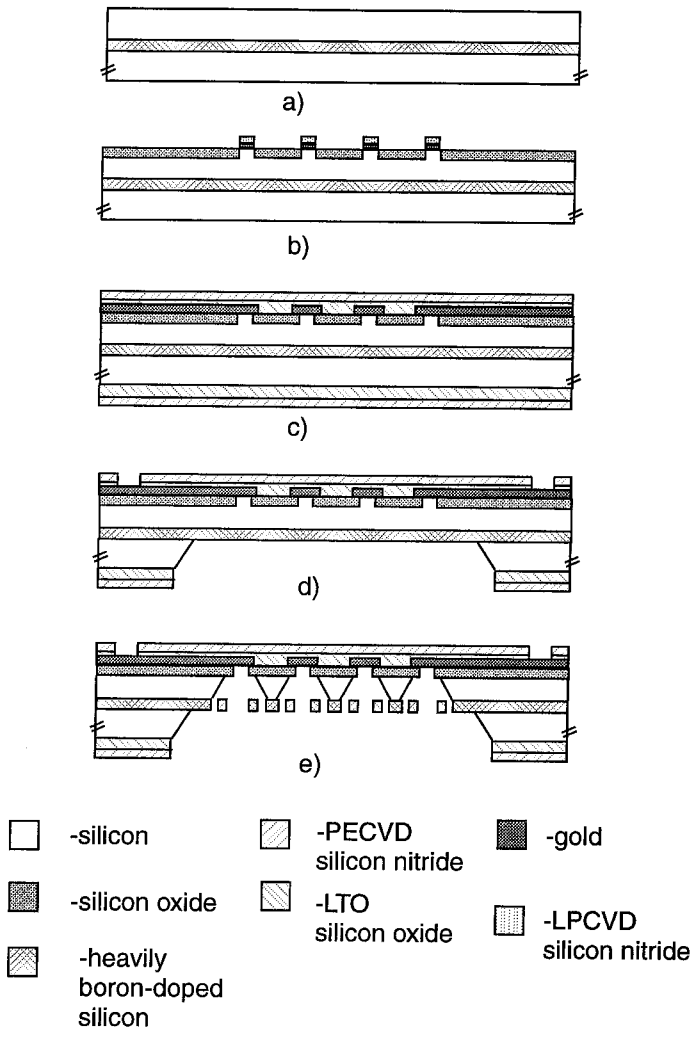

Figure 2-6: Cross section of the neurochip after some fabrication steps

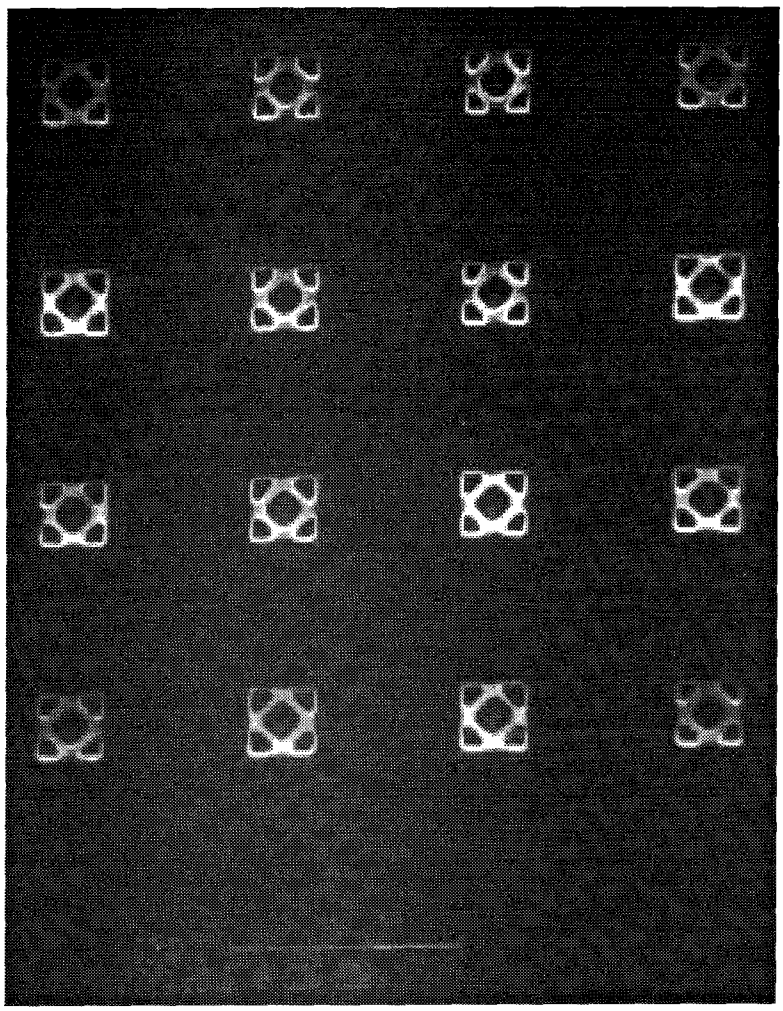

Figure 2-7: SEM of a 4x4 array of neuron wells at the bottom of a neurochip.

(Fig.2-6.e).

Fig.2-7. shows an SEM of a fabricated neuron–well array. Fig.2-8. shows a close–up view of one well. Clearly seen in Fig.2-8. is a 3μm diameter gold, circular electrode at the bottom, defined by the fully recessed LOCOS step. Empirically it is noticed that one needs a big central hole for the implantation of the neuron, whereas neurons usually grow neurites through the corner openings of the grillwork.

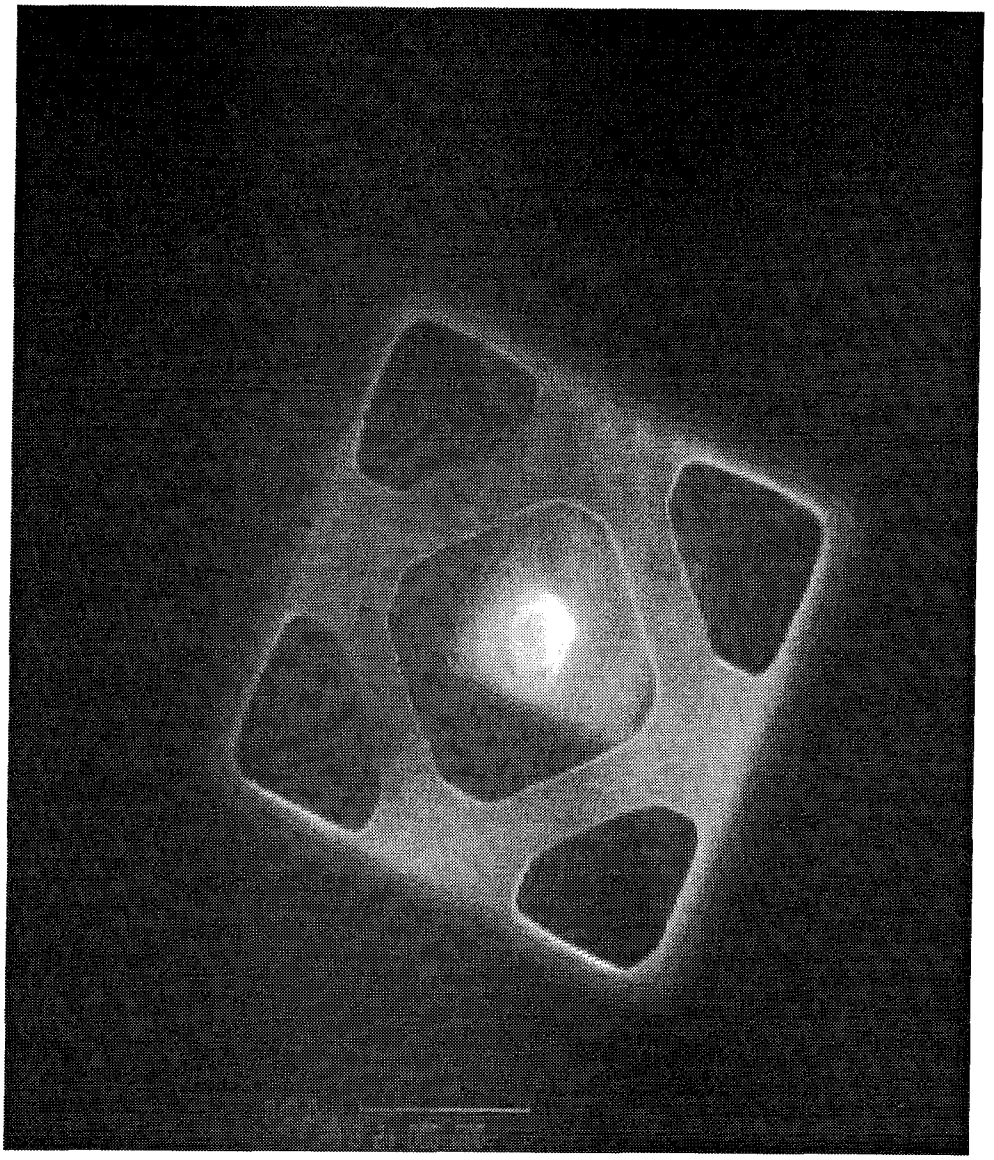

Figure 2-8: SEM of a single neuron well 25x25μm^2 at the top with 3μm in diameter gold circular electrode at the bottom.

2.3.2 Flat–Bottomed Neurochip Fabrication

The starting wafers for the flat–bottomed neurochip fabrication are the same as used for the other devices that were fabricated: commercially available 4" epi–wafers, with a 16 μm thick, lightly doped layer on top of a 4-μm thick, heavily boron–doped layer (Fig.2-9.a). First, double–sided alignment marks are patterned using a special alignment jig. The purpose of these alignment marks is to enable a rough front–to–back alignment (within 50-100μm) of the subsequently formed cavity with respect to the front side pattern.

Then, a thermal oxide 250nm thick is grown at a temperature of 1050C, followed by the deposition of 200nm of LPCVD low–stress nitride (820C, 15.6sccm of NH_3 and 64.7sccm of DCS). The back side of the wafer is patterned using the first mask, which forms 9x3mm open windows in the photoresist. RIE etching by SF_6 plasma (gas flow of 24.4 sccm of SF_6 and power of 1kW) removes LPCVD nitride, and BHF etching removes the thermal oxide from the windows.

Photoresist AZ1350J, 2μm thick is spun on the front side of the wafer, and patterned with the electrode pads mask, which has square openings on the site where neuron well bottoms are going to be. Then RIE SF_6 etching is used to remove nitride from those sixteen well/electrode interfaces. Existing photoresist is stripped using O_2 plasma ashing, and another layer of AZ1350J photoresist, 2μm thick is spun onto the front side of the wafer. The third mask (with fine front–to–back alignment marks) is used to pattern the photoresist, and RIE SF_6 etching is used to etch through the exposed LPCVD nitride,. BHF is again used to etch through the remaining thermal oxide. This layer of photoresist is stripped, and another layer of AZ1350J, 2μm thick is applied on the front side of the wafer. It is patterned with the fourth mask (metal lift–off mask). A thermal evaporation of 10nm/300nm/10nm Cr/Au/Cr is then performed. Lift–off is done using an ultrasonic acetone bath.

Etching by commercially available EDP etchant (Transene Inc.) at 95C is used for the forming of the big cavity in the next step. AZ1350J photoresist is then spun at 3000rpm using a special chuck after the cavity is completed, and the exposure of the neuron well grillwork is done using the GCA4800 stepper. After developing the photoresist, the edges of the cavity are carefully painted, because edge coverage of the big cavity by the photoresist

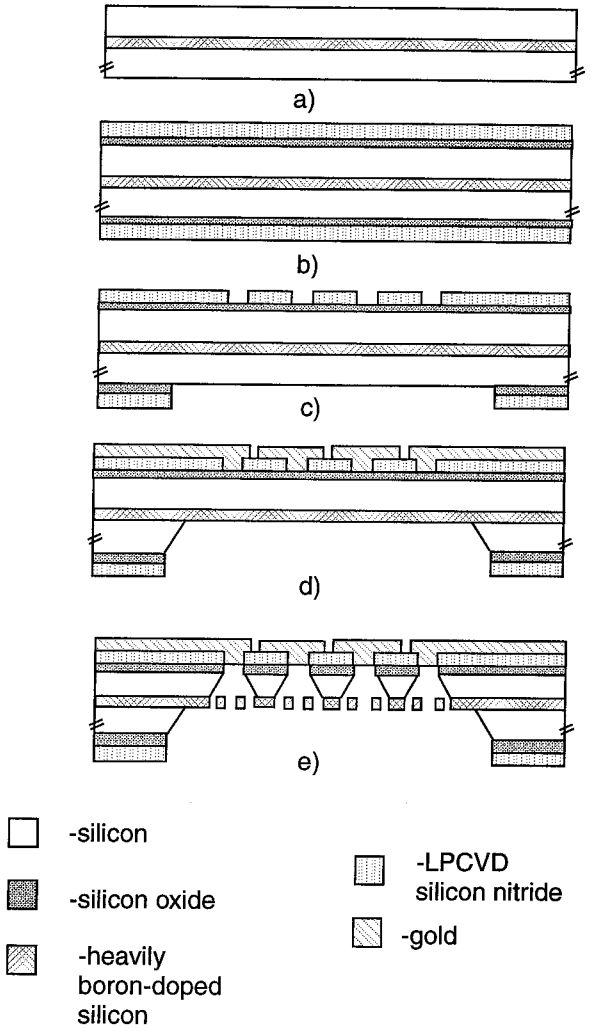

Figure 2-9: The cross section of the flat–bottomed neurochip after some fabrication steps.

is not good enough to prevent damage during RIE etching in subsequent steps.

The grillwork is etched through the B^+ doped layer using RIE SF_6 etching (gas flow 24.4 sccm, power 1kW). The wafer is then diced into individual dies. They are etched in EDP to form the neuron wells. Finally, the SiO_2 pad layer is removed from the bottom of neuron wells with BHF (Fig.2-9.e.).

2.3.3 Novel Extra Accurate Method for Two–Sided Alignment on Silicon Wafers

Accurate double–sided alignment of photolithographic patterns is often crucial in micromachining. Infrared (IR) backside and double–side mask aligners are avilable, although they are expensive. However, typical IR backside aligners have an absolute limit for viewing resolution of about $\pm 6\mu$m , while double side mask aligners have an alignment accuracy no better than $\pm 2\mu$m. Neither is acceptable for many applications which require better-than-two-micron accuracy such as in the case of neurochip fabrication [48].

One possible and inexpensive method to achieve good alignment accuracy is to use sandwiched mask tools to make wafers with pre–aligned marks on both sides before real process begins. For example, White and Wenzel [54] estimated a theoretical alignment accuracy of no more than 1μm across a 250μm thick, 2–inch wafer. However, one disadvantage is that if there is an pre–alignment error between these marks, it is hard to be corrected without major modification of the tool. This error can vary and depend on the design and implementation of the tool [10]. So far, better–than–one–micron accuracy using this method has not been demonstrated in literature and, from our own experience, the best accuracy we obtained so far has only been 5μm.

Finally, Kim et al. [13] described a different front–to–back alignment technique involving the visual alignment of stepper cross bars (alignment keys) to the center of a free diaphragm ($30\text{x}30\text{x}1.6\mu\text{m}^3$) etched from the back of the wafer. Although less than one micron alignment error was claimed, no experimental evidence of this was provided. In addition, it relies heavily on the skill of the operator to perform the alignment to the "membrane center" which is not marked.

For the purpose of the neuroprobe fabrication we developed an improved method by

forming alignment marks on the diaphragm so direct key–to–mark alignment can easily and reliably be performed from both sides of the wafer. The neuron wells are experimental proof which confirms the less–than–two–microns alignment accuracy. In the following sections, two examples involving double–sided alignments using a pre–marked diaphragm in two common cases are presented. The first is double–sided alignment across a thin diaphragm (20μm thick) and the second is across a whole 500μm thick, 4–inch silicon wafer.

Front–To–Back Alignment Across a Thin Membrane

The necessity for double–sided alignment across a thin membrane exists in our project of fabricating micromachined silicon neuroprobes for *in vivo* studies of neural networks.

As previously described, the neuroprobes have 15 neuron wells, which are micromachined in a 20μm thick silicon membrane. Each well is a trapezoidal cavity bulk–micromachined from the membrane. One side of the well is a heavily–doped silicon grillwork and the other side is a circular gold electrode (3μm in diameter) on a thin (1.5μm) free–standing insulating membrane, $7\text{x}7\mu\text{m}^2$. An accurate alignment within two microns between the grillwork and the gold electrode is crucial so that the electrode is positioned at or near the center of the $7\text{x}7\mu\text{m}^2$ diaphragm. In fact, any error of more than 2 microns will cause serious current leakage problems and the neuron well will not work properly.

Fabrication of the neurochips has been described in the previous sections. During the process (See Fig.3-5c.), a composite layer of 0.5μm LTO and 1.0μm PECVD Si_xN_y covering the front side is first patterned with the alignment marks used by the GCA stepper. Then, an etching window for the 9 by 3 mm membrane is opened at the back side of the wafer, followed by the EDP etching to create a 500μm deep cavity which is etch–stopped by a heavily –boron doped buried layer.

The front–side alignment mark on the composite layer is then simultaneously freed into a diaphragm with a small cavity underneath it. During the EDP etching step, the small cavity is formed much earlier than the big one because it is in the thin, (16μm thick) lightly doped epitaxial layer on top of the boron layer. The long overetch of the boron layer from the small cavity side causes the boron layer to be etched away so that a square opening in the membrane is formed by the time the big cavity etching is done. As a result, the front–

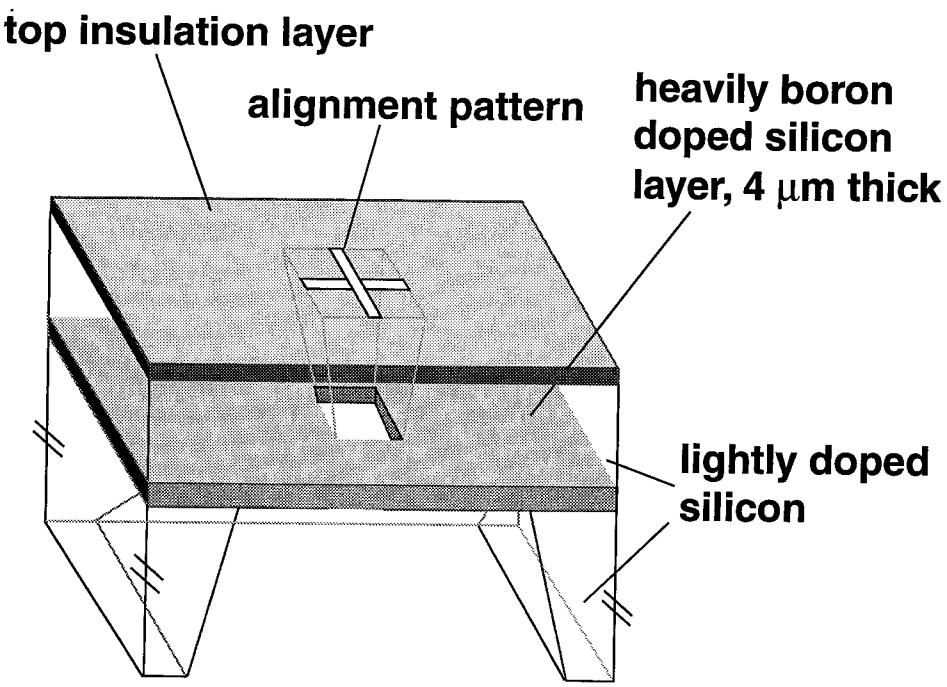

Figure 2-10: Forming the alignment mark for front–to–back alignment across a thin membrane.

side alignment mark on the insulating membrane becomes visible through the opening from the back side of the membrane (See Fig.2-10). Fig.2-11. shows the micrograph with a real alignment mark viewed from the big cavity side.

Photolithography is then performed at the bottom of the 500-μm deep cavity using the alignment marks from the front side to define the heavily boron–doped grillwork. Fig.2-8. shows a finished neuron well. The obtained 1.5μm overall accuracy is clearly seen from the SEM picture.

Front–To–Back Alignment Across a Whole Wafer

The same alignment method can also be used across the whole wafer [48]. We have done this in the following ways. First, the wafer is coated with a 0.5μm low–stress silicon nitride wafer. This layer is patterned with the alignment marks used by GCA stepper. There are two ways to etch the diaphragm free for double–sided alignment as shown in Fig.2-12. @ The first way is to pattern etching channels simultaneously with the alignment marks (Fig.2-12a) on the same side and then etch in EDP or TMAH. The advantage of using this

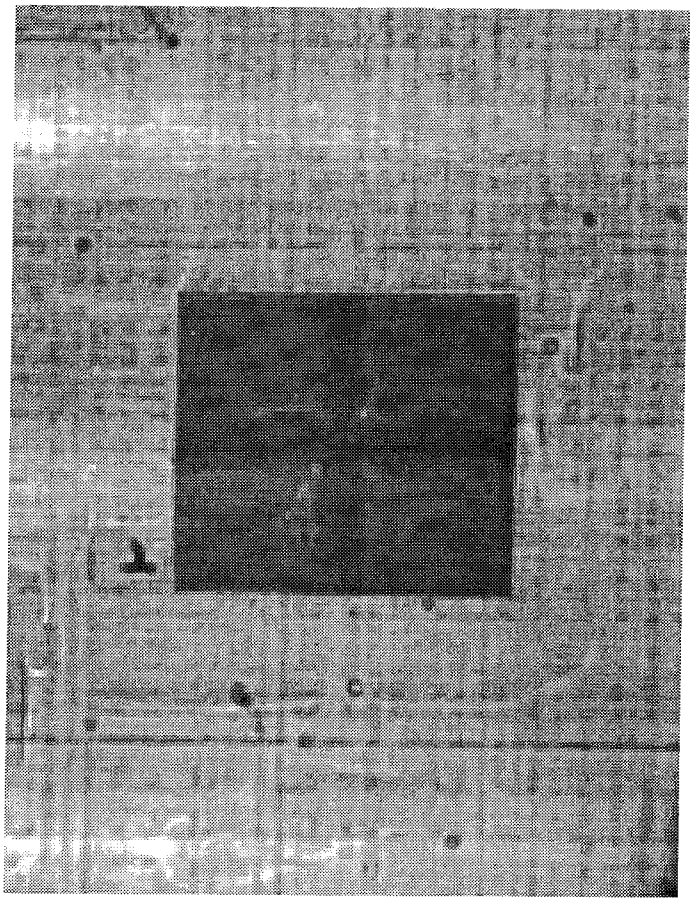

Figure 2-11: Optical micrograph of the alignment mark as it appears in the stepper's field of view (cross bars are 5μm wide).

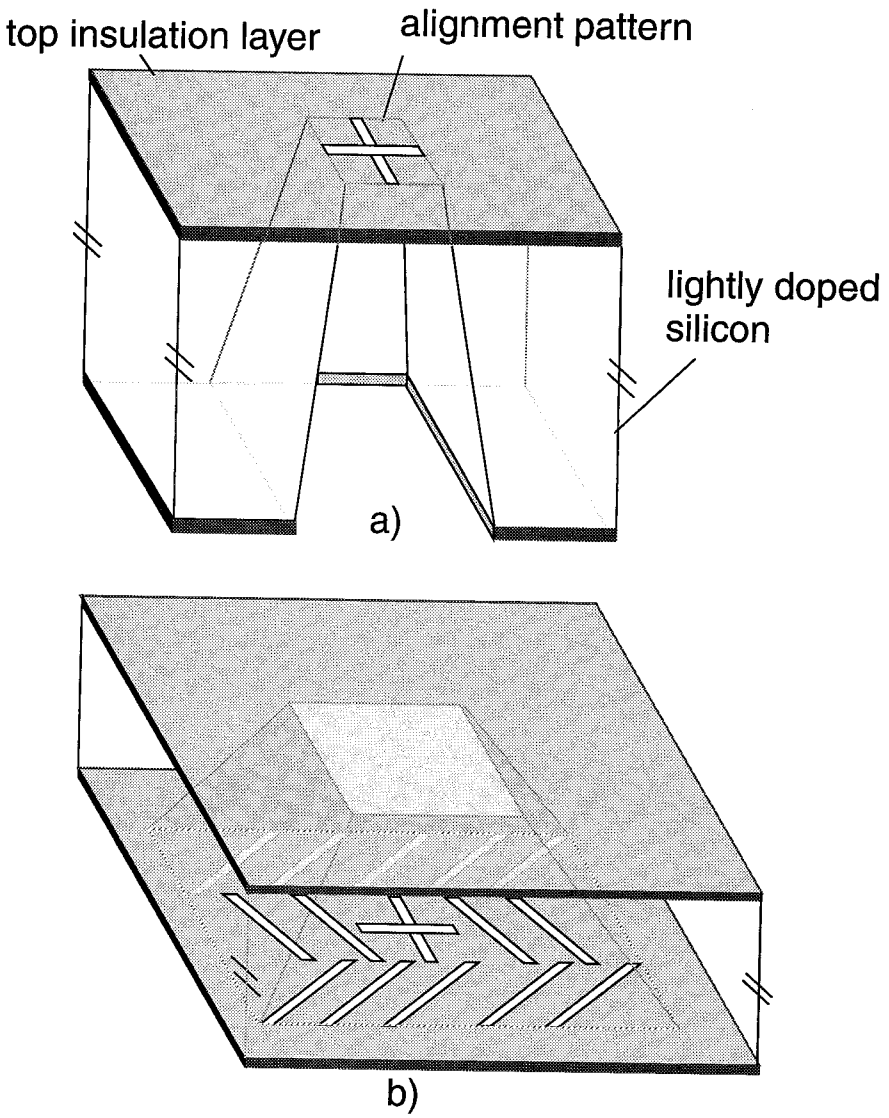

Figure 2-12: Forming the alignment marks for front–to–back alignment across a whole wafer: (a) by patterning etching channels simultaneously with the alignment marks: (b) by opening etching windows on the back side of the wafer and etching up to the front side, with alignment marks already patterned in the insulation layer.

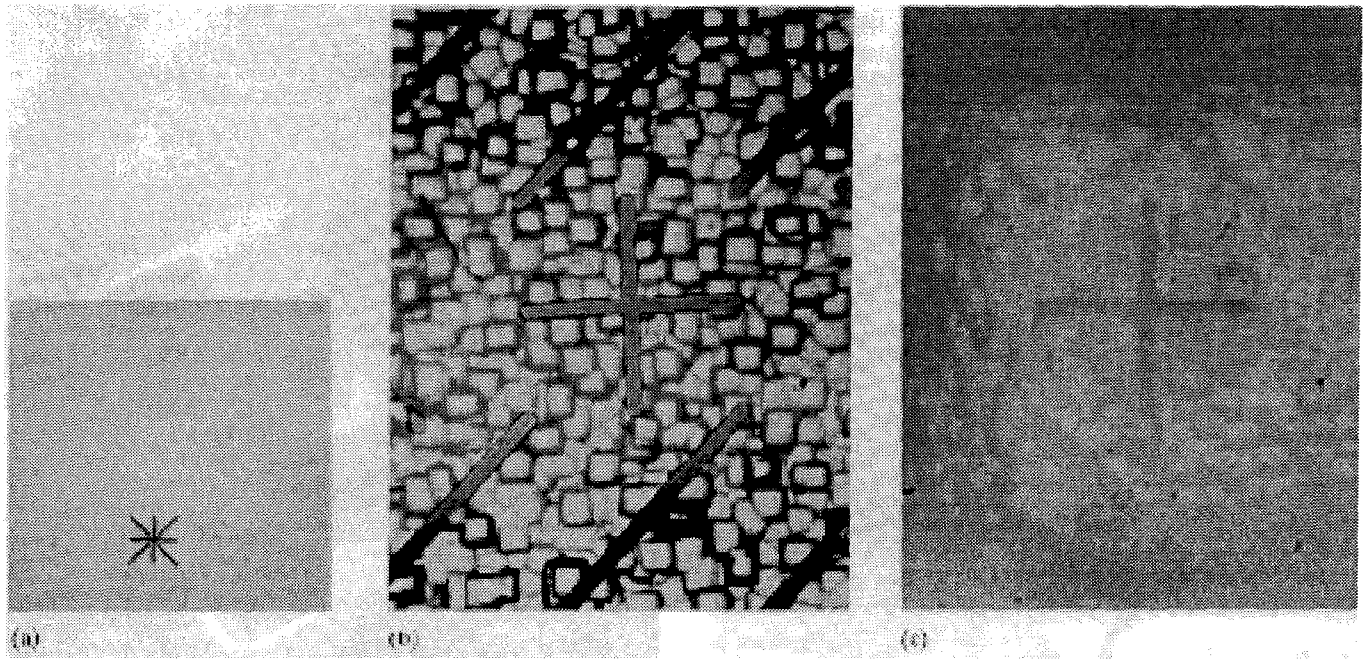

Figure 2-13: Finished membranes with alignment marks: (a) formed by opening etching windows on the back side of the wafer and etching up to the front side; (b) formed by patterning of the etching channels simultaneously with the alignment marks and wet etching (viewed from the rough back side of the wafer); (c) the same as (b), but viewed through the transparent membrane on the front side of the wafer.

method is that only one photolitography is needed; the disadvantages are the loss of device area on the front side and the fragility of the membrane. The second method is to open etching windows on the back side of the wafer (Fig. 2-12b.), and then etch up to the front side. The advantages are opposite to the previous disadvantages. The disadvantages are the need for a second photolithography and for preliminary alignment accuracy.

Fig.2-13. shows the finished membranes with alignment marks. The alignment mark (cross) is 5μm wide, 126μm long, and is shaped like a standard GCA stepper alignment mark, so accurate alignment can be obtained. However, it is difficult to confirm the alignment accuracy in this case because of the lack of accurate calibration methods and equipment.

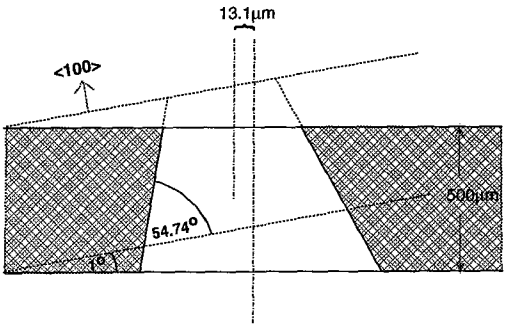

Figure 2-14: Influence on the alignment accuracy of a 1° offset of the wafer with respect to the <100> surface orientation.

Discussion

In analyzing the accuracy of different double–sided alignment methods, most frequently overlooked are the wafer orientation offset and the slice taper across the wafer. Here, we discuss the influence of these two factors on the accuracy of front–to–back alignments.

For <100> single–crystal silicon wafers, the surface orientation offset for 4" wafers is typically ±1° [58]. Assuming the 1° offset of the wafer with respect to the <100> surface orientation, the slopes of walls of the cavity formed by anisotropic etching through the wafer are different as shown in Fig.2-14.

As a result, the center of the small window is not right above the center of the big window. The alignment offset for 4", 500μm thick wafer then is

$$\varepsilon_{orient.} = \frac{1}{2} \cdot \left(\frac{1}{\tan 53.74^\circ} - \frac{1}{\tan 55.74^\circ}\right)[\mu m] = 13.1\mu m. \tag{2.7}$$

Such a big offset implies that the alignment accuracy of the membrane-center alignment

method [13] is very sensitive to the orientation offset. In comparison, our alignment method does not have the orientation offset problems because of visual alignment to the marks.

The second factor that could have an effect on the alignment accuracy is the slice taper across the wafer. The maximum taper across 100mm diameter wafer, according to the silicon slice specifications for <100> orientation [40], can be 10μm.

In fact, this slice taper always affects alignment accuracy for all the alignment methods. Fortunately, it can be shown that the maximum angle of taper is only $5.73 \cdot 10^{-7}\mu$m, which is negligible ($\ll 1\mu$m) even for the state-of-the-art micromachining.

The developed method for double-sided wafer alignment is accurate and inexpensive. It can be applied to an entire wafer, as well as to a thin membrane. The accuracy of this method is not affected by the variation in the surface orientation of the wafer. It could have a wide range of applications for micro-electro-mechanical systems (MEMS).

2.3.4 Photolithography on Bottom of a Cavity

One important step that had to be developed for the neuroprobe fabrication is the exposure of the 500-μm-deep cavity. The first problem is photoresist coverage and the second (which ended up being much more serious) is focusing at the bottom of a cavity.

Photoresist is applied by putting a couple of drops of photoresist in each of the cavities and spinning it using a special non–vacuum chuck (See Fig.2-15). It is nonuniform (variation can be as much as 50%), but it enables usable photolithography, assuming that the membrane is flat and that the focusing system works properly.

The only problem is that coverage of the sharp corners of the cavity is not good, so additional hand painting of the edges is done to protect them during the subsequent RIE etching step.

Focusing at the bottom of the cavity cannot be done using a contact aligner. Attempts have been made, but even at the bottom of the cavities only 100μm deep, resolution better than 7-8μm cannot be achieved. That is much worse than the required 3-4μm lines at the bottom of a 500μm deep cavity which are necessary for the grillwork bars.

Success was achieved using a GCA 4800 projection stepper. First, in order to design the size of the cavity, one should understand the way that the stepper does focusing on the

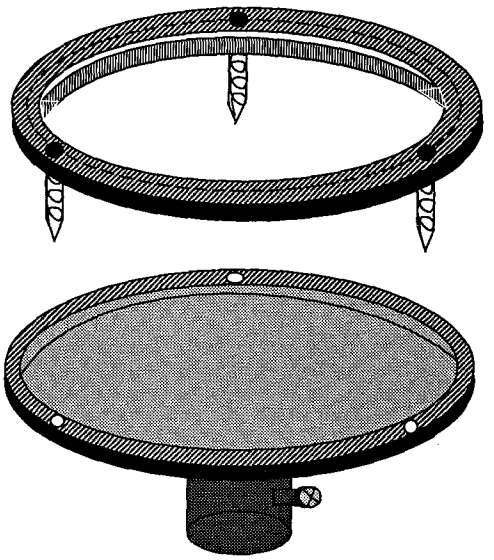

Figure 2-15: The design of the special non–vacuum chuck.

wafer (See Fig.2-16.). The focusing infrared beam hits the middle of each die and bounces from the wafer into the receiving photodiode, which is followed by a preamplifier.

If the output of the preamplifier is as shown on Fig.2-16, the stepper can focus on the wafer. Otherwise, the focusing cannot be done and it means that the bounced beam could not be detected by the photo–diode because the surface is too warped and it didn't bounce in the expected direction or it hit some obstacle on its way out (the walls of the deep cavity, for example). A very important parameter is the size of the focusing beam. By shining a white light through the same set of lenses used by the infrared light beam, and assuming that the optical properties of the system are approximately the same for both infrared and visible light wavelengths, we measured that the size of the light beam is 2x4mm^2 (See Fig.2-17.). The angle Θ at which the beam hits the wafer (See Fig.2-16) for our type of the stepper is 11°. That seems to be a large angle compared with the other types of projection stepper, where it can be as small as 3-4 degrees. This is a fortunate circumstance for this project, because the larger angle makes it easier for the beam to bounce in and out of the cavity (See Fig.2-18.).

The smallest size of the cavity that enabled successful focusing was 9x3mm^2 and this size of cavity was applied for the neurochip fabrication. As for the neuroprobe fabrication which is going to be described later, the size of the cavity is bigger ($\approx$ 9x4mm^2), because

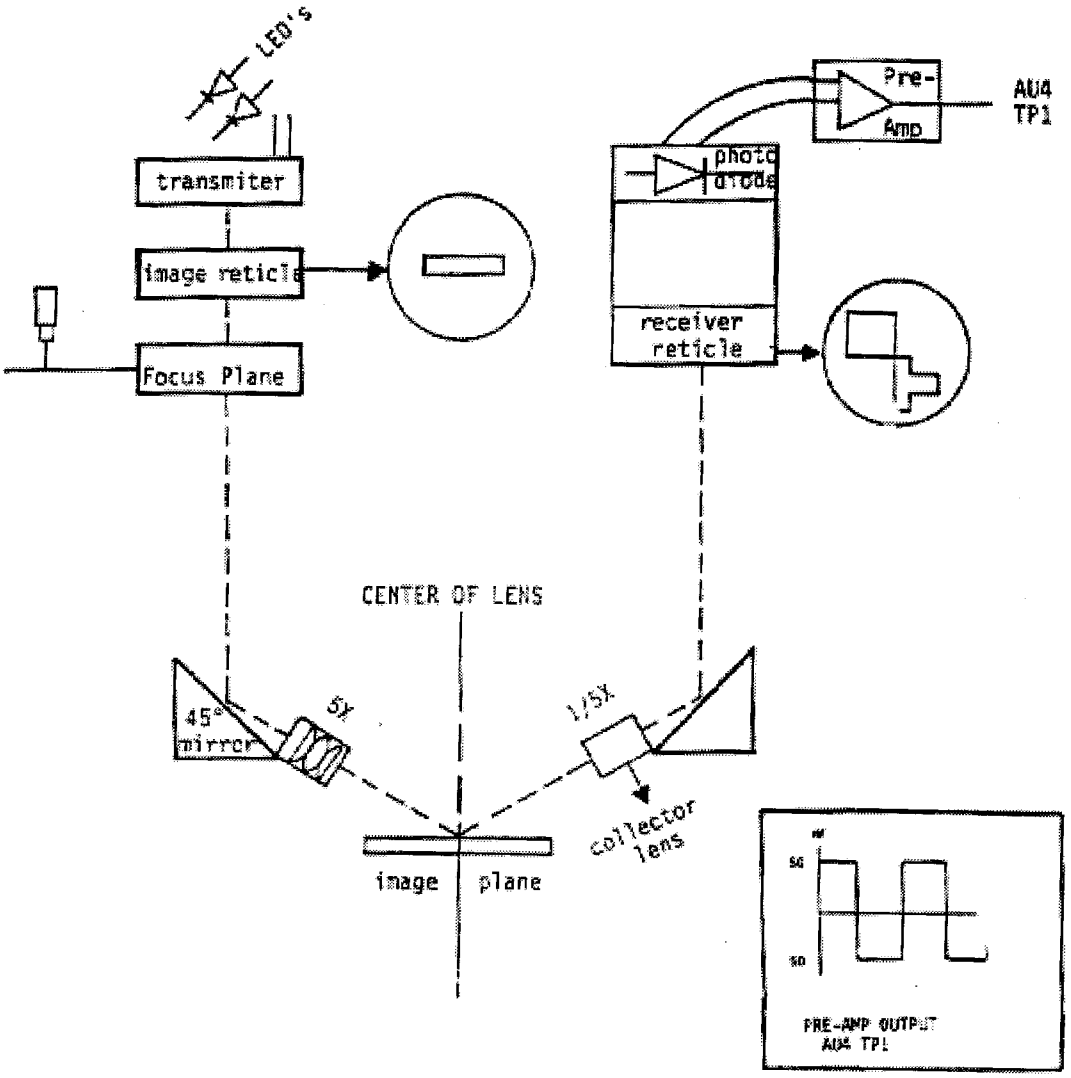

Figure 2-16: Auto–focus illumination path of GCA 4800 stepper.

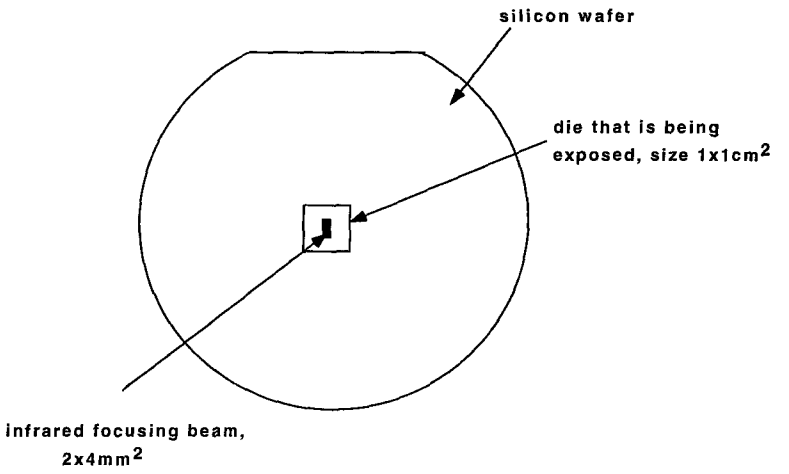

Figure 2-17: The size and the relative position of the infrared focusing beam with respect to the silicon wafer.

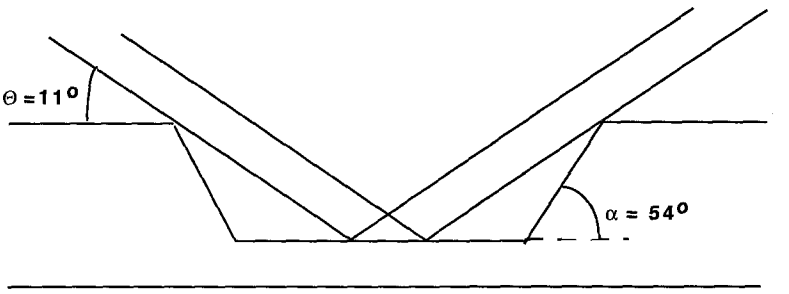

Figure 2-18: The focusing beam bouncing in and out of the cavity formed on the silicon wafer.

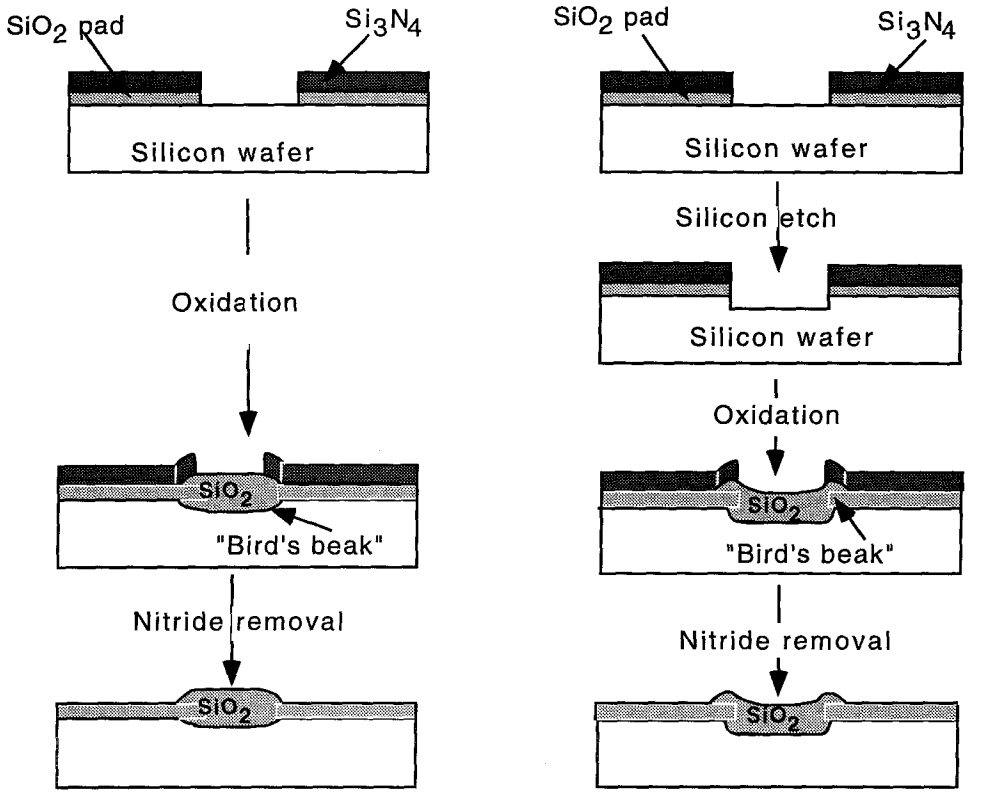

Figure 2-19: Formation of semi–recessed oxide (SEMIROX) and fully–recessed oxide (full ROX) silicon structures using Si_3N_4 as an oxidation mask.

it is dictated by the length of the probe's shank. However, care is taken that the cavity is properly centered, because without it the exposure is not possible.

2.3.5 Bird's Beak Phenomena

One of the most important processes for the isolation of devices in integrated circuits is so–called LOCOS (LOcal Oxidation of Silicon). This technique involves the formation of a semi (or fully) recessed oxide in the nonactive (or field) areas of the substrate. This selective oxidation process was introduced by Appels and Kooi in 1970. [1].

There are two kinds of LOCOS process. One is partially (or semi) recessed isolation oxide process (SEMIROX), where the field oxide is selectively grown without etching the silicon (Fig.2-19). If the silicon is etched to a depth of about half of the desired field oxide thickness after the oxide-preventing layer is patterned, the field oxide can be grown until it

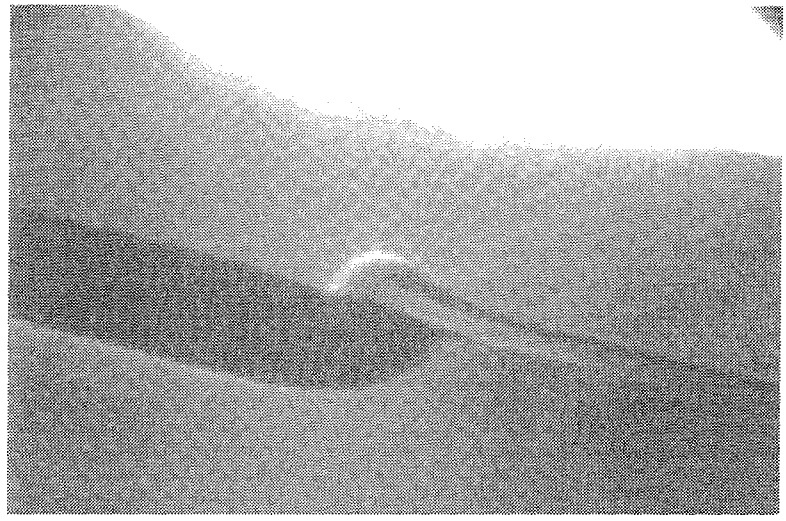

Figure 2-20: Cross section through experimental silicon structure showing full ROX profile. (Courtesy of Mr. Chang Liu).

forms a planar surface with the silicon substrate (See Fig.2-19.). This is so–called full ROX process.

The ideal profiles that are expected are not obtained in practice due to the diffusion of oxygen and the growth of SiO_2 under the edge of the Si_3N_4 during thermal oxidation [3].

Around the perimeter of the Si_3N_4 mask one gets a ridge of thermal oxide above the surface of the wafer. That profile reassembles a bird's head with a "crest" and a "beak" (See Fig.2-20.). Neither of these features is favorable. The crest is a prominent topographic feature that can cause a break or discontinuity in the thin films deposited on top of it. On the other side, bird's beak reduces the nonoxidized area of the wafer. In the integrated circuit industry this means a reduction of the available active area. In the micromachining field, although the size of the active area is not as important as in the integrated circuit industry, it is an annoyance. The reason is that the height of the bird's crest and the length of the bird's beak have to be known in order to do the proper design of structure.

The height of the bird's beak influences the thickness of the thin films that should be deposited on top of it without breakage. The length of the bird's beak has to be taken into account when the micromachined structure is designed, if the dimensions have to be controlled to within microns.

The shape of the bird's beak and crest depend on a number of parameters: (*i*) The

thickness of thermally grown recessed oxide, (*ii*) The thickness of the pad oxide used to alleviate the stress between the silicon substrate and the silicon nitride, (*iii*) The thickness of the Si_3N_4 film used as an oxidation mask, (*iv*) The field oxidation temperature and (*v*) The orientation of the wafer [3, 59] .

The dependence of the ratio between the length of the bird's beak (L_{bb}/T_{ox}) with respect to the field oxidation temperature, the orientation of the wafer, and the pad oxide thickness are shown on the Fig.2-21.

From this empirical data, it seems that to shorten the length of the bird's beak, it is better to operate at a higher temperature and shorter oxidation period rather than to operate at a lower temperature. Also, <111> wafer have smaller bird's beak than <100> wafers. Unfortunately, bulk micromachining usually deals with <100> wafers, so this information is not very applicable there.

In Fig.2-22, one can see the selected features of the bird's beak and crest of full ROX structures plotted as the ordinate vs. the thickness of Si_3N_4 used as the oxidation mask.

It comes out that the thicknesses of the nitride layer and of the oxide pad have opposing effects on the size of the bird's beak and crest. The oxide pad thickness determines the ease of oxidation between the nitride film and the silicon substrate. On the other hand, if the nitride thickness is increased, the growth of the bird's beak and crest are more effectively suppressed due to the increased rigidity of the nitride film [3].

The last parameter to worry about is the influence on the field oxide thickness on the bird's beak length. The length is the bird's beak increases with a thicker field oxide (See Fig.2-21.b).

Knowing these bird's beak properties, we decided that for the neuroprobe fabrication we are going to use a 50nm thick pad oxide, a 180 nm thick Si_3N_4 and an $\approx 1\mu$m thick field oxide. From Fig.2-21b, our prediction was that the length of the bird's beak is going to be 0.9μm. Consequently, the nitride circles formed by the first mask that ought to define the area of the subsequently deposited gold electrodes encircled by an oxide ring are designed to be 6μm in diameter, knowing that after the field oxidation the unoxidized portion will be only 4μm in diameter. The height of the bird's crest ended up being 350nm, which can be estimated from Fig.2-23. This scan of the bird's beak is taken before the nitride stripping,

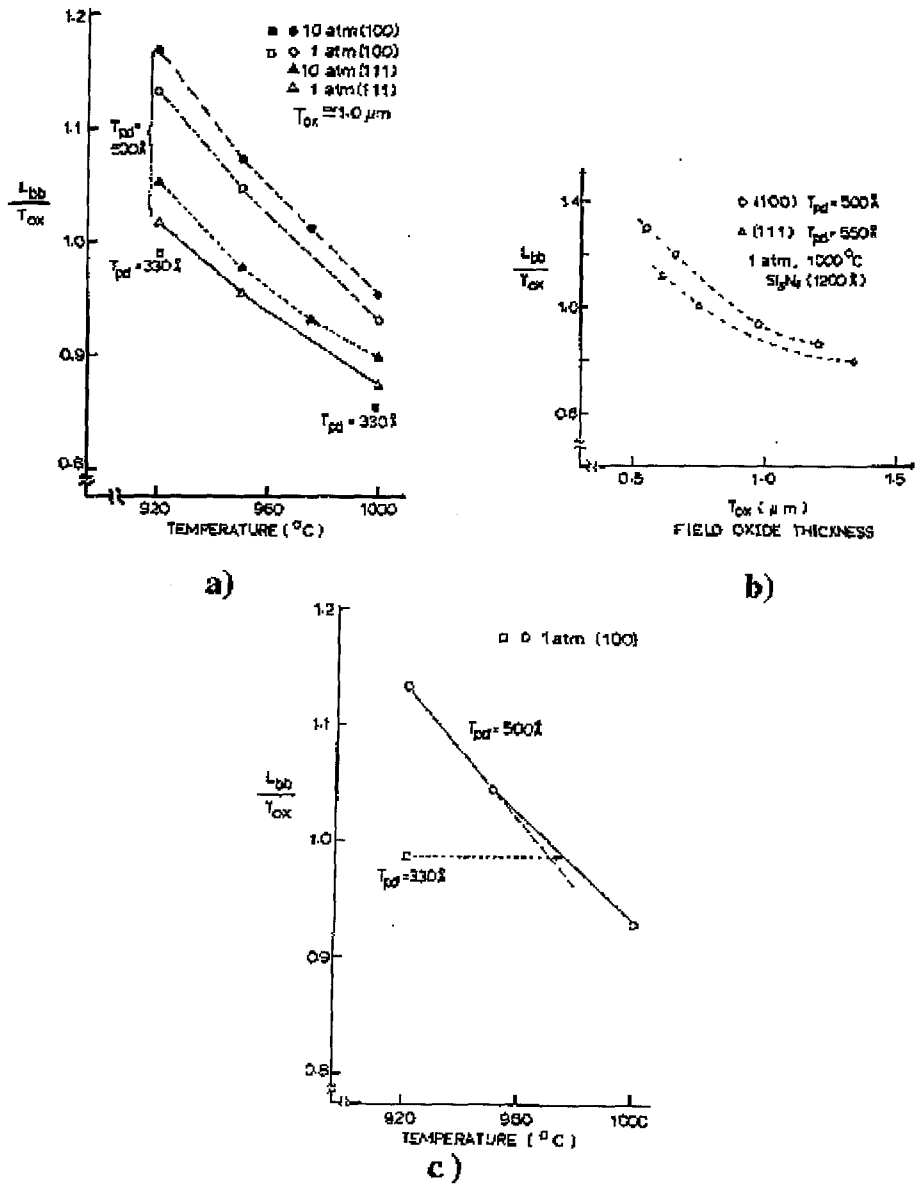

Figure 2-21: Experimental results of the effect of different processing parameters on (L_{bb}/T_{ox}): (a) The effect of the processing temperature and the orientation of the wafer; (b) The effect of the field oxide thickness,(c) The comparison between the effects due to temperature and thickness of the pad oxide layer [58].

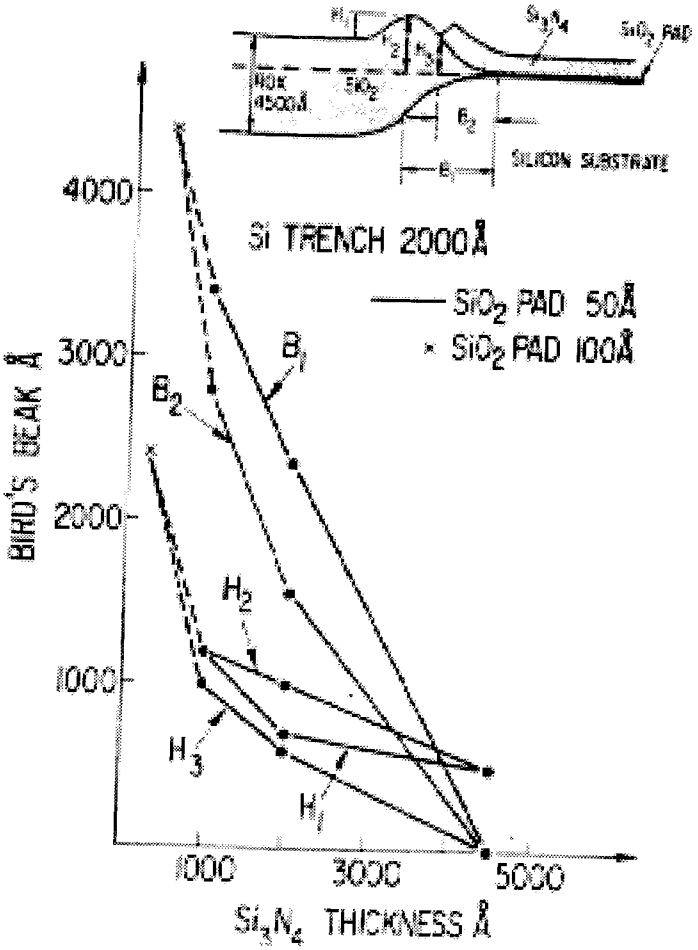

Figure 2-22: Selected features of the bird's beak and crest of full ROX structures plotted as a function of the thickness of Si_3N_4 used as the oxidation mask [3].

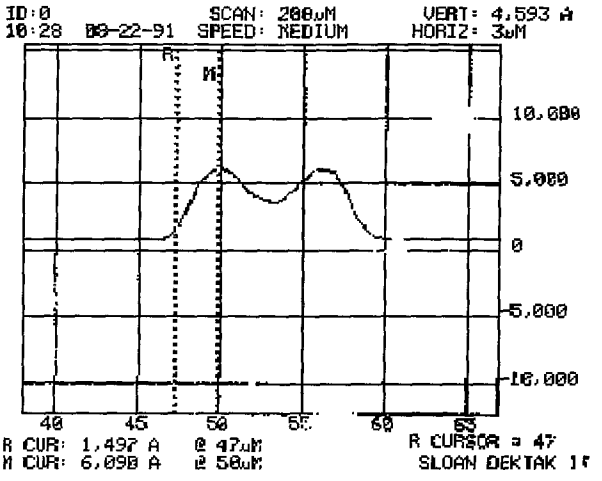

Figure 2-23: The profile of the bird's beak occurred during the neuroprobe fabrication on the electrode site. The scan is taken before the 160nm thick LPCVD nitride removal.

so from the shown height one should subtract 160nm, which is the thickness of the LPCVD nitride layer. The metalization layer that was sufficient to do proper step coverage was 200nm.

2.3.6 The Properties of the Boron–Doped Etch–Stop Layer

The initial thickness of the boron–doped etch–stop layer is determined from the targeted thickness of the grillwork and the duration and temperature of the high–temperature processes previously applied on the wafer. Namely, during high–temperature processes an outdiffusion of the boron dopant into the lightly–doped silicon occurs. Consequently, the starting thickness of the boron–doped layer is decreasing during the fabrication, predominantly during the oxidation process which is done at 1050C for three hours. Knowing these parameters, as well as the thickness of the grillwork that we want to have at the end of the processing (2μm), it is possible to roughly calculate the initial thickness of the B^+ doped epi–layer that is necessary.

Fick's second law of diffusion is

$$\frac{\delta C(x,t)}{\delta t} = D\frac{\delta^2 C(x,t)}{\delta x^2}, \tag{2.8}$$

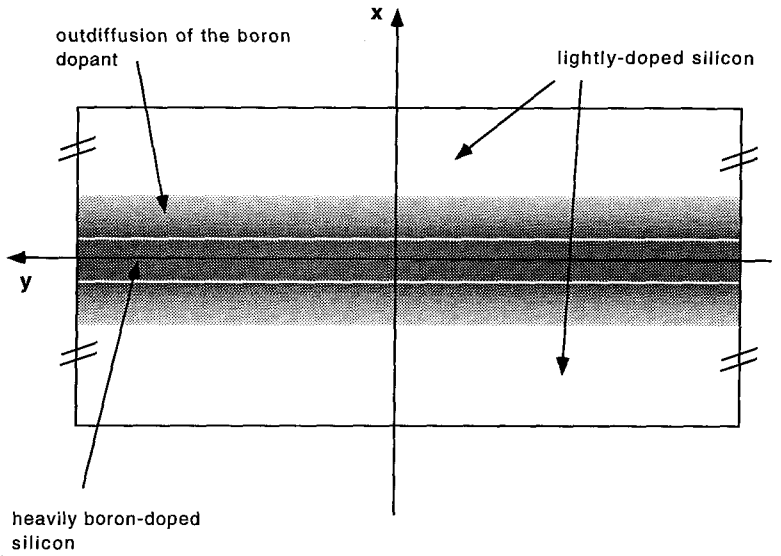

Figure 2-24: A schematic presentation of the etch–stop epi–layer dopant outdiffusion.

where C is the concentration of solute (which is assumed to be a function of x and t only), x is the coordinate axis in the direction of the solute flow, t is the diffusion time, and D is the diffusivity (sometimes called the diffusion coefficient or the diffusion constant) [44].

In our case, with the heavily boron–doped etch–stop layer buried, there is a fixed total amount of dopant per unit area Q_T, and the dopant diffuses only into the silicon (all of dopant atoms remain in silicon). The initial condition is C(x,0) = 0, and the boundary conditions are ${}_0\int^{\infty}$C(x,t)dx = Q_T and C(∞,t) = 0.

The solution that satisfies the above conditions is

$$C(x,t) = \frac{Q_T}{\sqrt{\pi Dt}} exp(-\frac{x^2}{4Dt}). \tag{2.9}$$

The other data we need to calculate the initial thickness is the minimum concentration of the boron that can stop EDP etching (C$\geq$5 x 10^{19}at/cm^3) and the initial concentration of the dopant in the B^+ layer (C=2x10^{20}at/cm^3). Since we have a symmetric problem (our buried layer is outdiffusing in both directions), we can place the coordinate system in the middle of the etch–stop layer, and from the targeted half–thickness of the grilllwork (1μm) calculate the initial thickness of the epi–layer that has to exist (See Fig.2-24.).

The diffusion coefficients depend exponentially on temperature and follow the Arrhenius

behavior [12]:

$$D = D_0 exp(-\frac{E_A}{kT}). \tag{2.10}$$

For boron as an impurity, $D_0 = 10.5\ cm^2/sec$ and $E_A = 3.69$eV. Keeping in mind that the fabrication process performed at the highest temperature is the oxidation process done at 1050C, we can calculate that for C(x=1μm, t=10800s) the total amount of dopant per unit area is $Q_T = 3.246$ x $10^{16} at/cm^2$. The total initial doping level for the epi–layer is p = 2x10^{20} atoms/cm^3, so the initial thickness of the epi–layer if one wants to have 2μm thick grillwork at the end has to be:

$$X_0 = 2\frac{2.346x10^{16} atoms/cm^2}{2x10^{20} atoms/cm^3} = 3.32\mu m. \tag{2.11}$$

Considering that we have the other processes at high temperatures as well (for example, LPCVD nitride deposition is performed at 800C), it was decided that the heavily boron–doped etch–stop layer of 4μm thickness would be used for the neurochip and the neuroprobe fabrication.

The purely boron–doped etch–stop layer showed very good etch–stop properties in EDP. However, its surface finish had a peculiar pattern on it, which we call a "linen pattern." It is believed to be caused by stress dislocations in the heavily tensile–stressed boron–doped layer (Fig.2-25.).

We have tried and succeeded to solve that problem by using a boron/germanium–doped etch–stop layer. The reason behind the tensile stress in boron–doped etch–stop layer is that boron atoms are smaller than silicon atoms. So, if one dopes the etch–stop layer simultaneously by electrically inactive atoms that are larger than silicon atoms (for example, germanium), it is possible to achieve zero stress in doped layer [31]. Fortunately, the boron/germanium doped layer has even better etch–stop properties in EDP than a boron–only doped layer. What's more, it has a mirror–like surface which is indispensable for our neurochips. For *in vitro* experiments all observations are performed by microscope, and it is important to have a nice and smooth surface finish in order to see the neural processes (See Fig. 2-10).

However, there is one side–effect. It was found out that boron diffuses with a lower

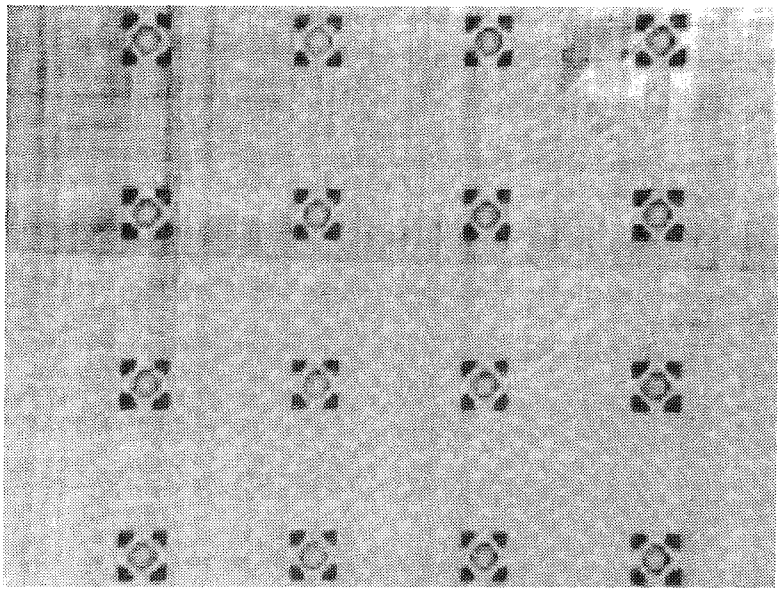

Figure 2-25: The appearance of the surface of the purely boron–doped etch–stop layer.

diffusivity during field oxidation in the presence of implanted germanium. Namely, the grillwork made of boron/germanium–doped silicon tended to be much thicker than the purely boron–doped layer (See Figs.2-26. and 2-27.).

Later on, it showed up that this effect has already been noticed by the integrated–circuit industry and is used to improve electrical isolation in high–density CMOS circuits [30]. In the case of the neurochip, it has a two–fold positive effect: grillwork can be made much stronger and thicker, or (if so strong grillwork is found out to be not essential) a thinner etch–stop layer can be used which results in cheaper wafers.

2.4 Preparation of Neurochips

Several things are required before conducting the electrophysiological experiments with the neurochips. First, the neurochip must be mounted on a printed circuit board (PCB) and its bond pads connected to the PCB traces. Then, the neurochip surface has to be treated chemically in order to promote adhesion and growth of neurons. Finally, the neurochip is loaded with neurons. (For an explanation of the last two procedures, see Appendix D).

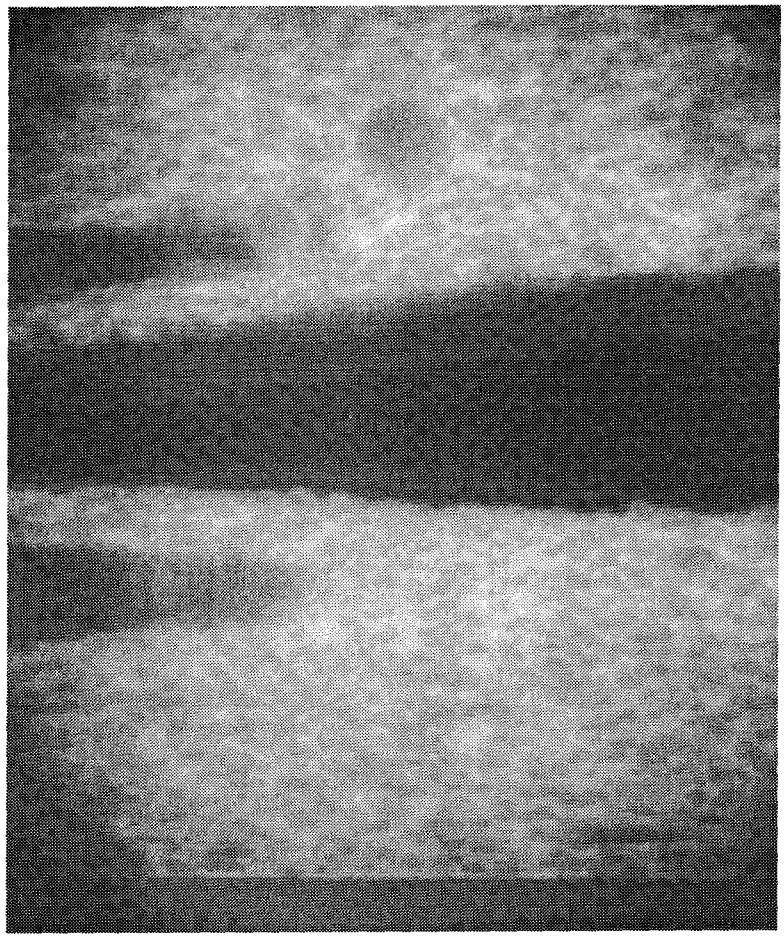

Figure 2-26: A side view on the purely boron–doped grillwork after the completed fabrication.

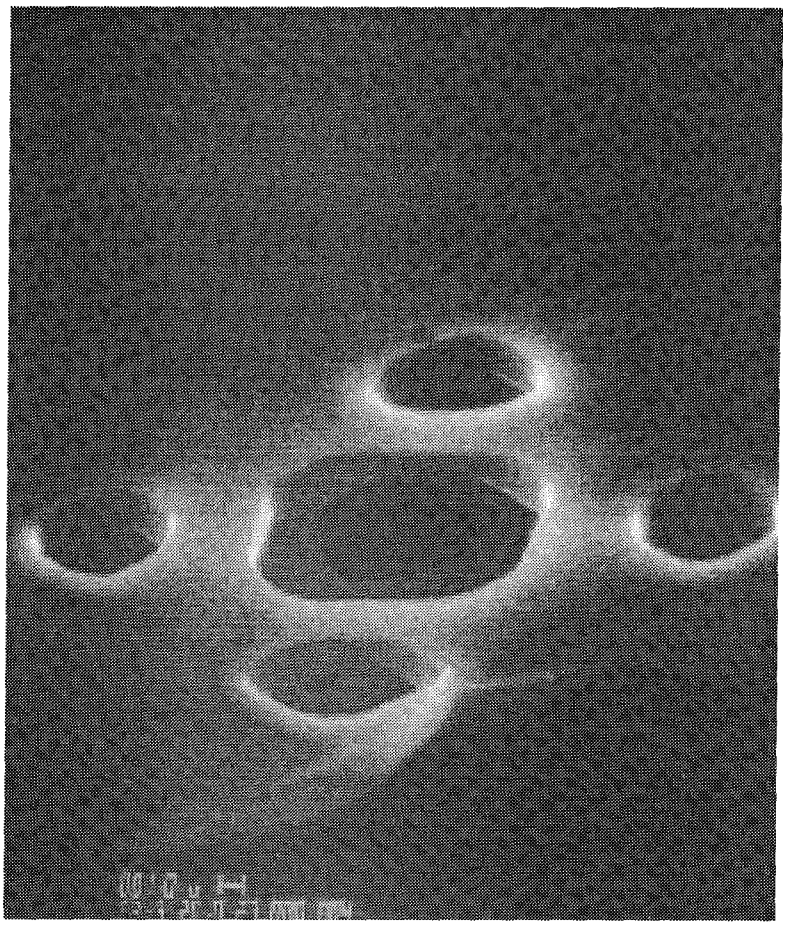

Figure 2-27: A side view on the boron/germanium–doped grillwork after the completed fabrication.

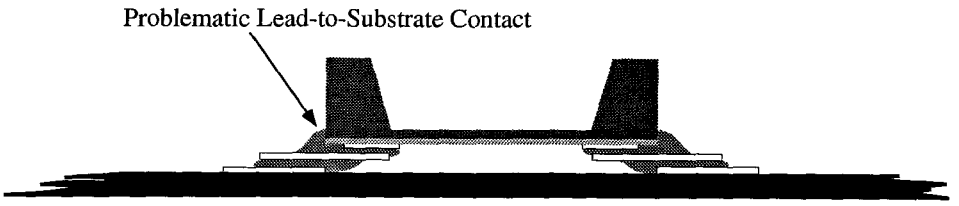

Mounting Problem

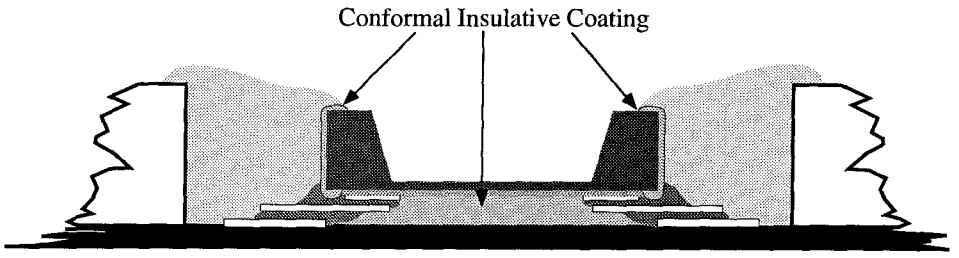

Mounting Solution

Figure 2-28: The mounting of the neurochip.

2.4.1 Mounting of Neurochips

The electrical connections to the neurochip cannot be done by standard procedures (for example, lead bonding) because the bond pads of the neurochip must face the PCB. The orientation of the neurochips makes it impossible for a lead bonder to attach a wire to the chip and then to the PCB. Consequently, the bonding has to be done by hand.

A procedure was developed using conductive epoxy to attach wire "legs" to the neurochip, which are then connected to the bond pads of the PCB. It is very important that the sides of the neurochip are previously coated with some kind of conformal insulating material. This prevents possible later contact of the silver conductive epoxy with the bare sides of the neurochip, which caused numerous problems in the past (See Fig.2-28).

A petri dish is then glued to the PCB surrounding the petri dish and the area between

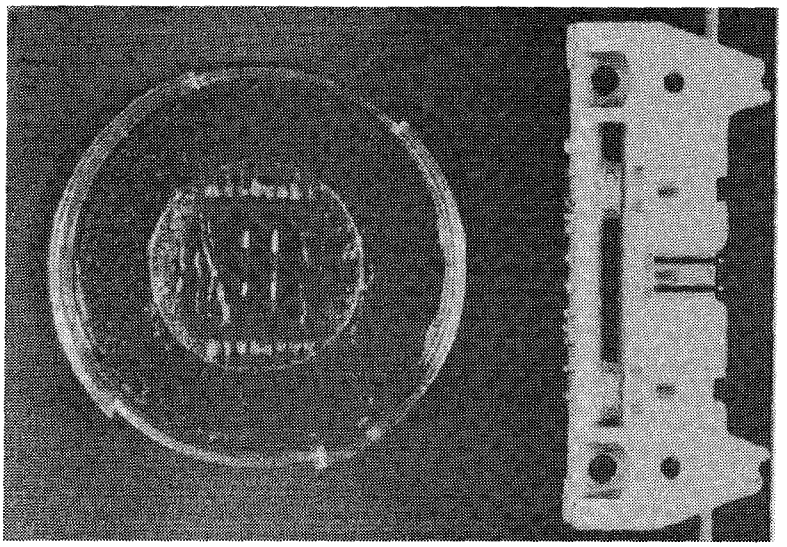

Figure 2-29: The neurochip mounted onto a printed circuit board and sealed at the bottom of petri–dish.

the chip and the petri dish is sealed with silicon rubber so that the neurochip can be immersed in the cell medium. The product of this mounting process is shown in Fig.2-29.

2.5 The Use of Neurochips

After the neurochip is mounted and its surface adequately treated to promote the adhesion of the subsequently implanted neurons and their processes, the cells are moved into the neuron wells according to the procedure described in Appendix D. Since the embryonic neurons are very delicate and fragile, moving them into the wells has been a major difficulty in our physiological experiments. Our process shows a survival rate of 75%, i.e., as much as three quarters of the neurons pushed into the wells can grow neurites out of the wells, which is accepted as the only evidence that they survive the implantation.

The biocompatibility of the neurochip is evident in that these implanted neurons grow into live neural networks. As an example, Fig.2-30 shows a developed neural network cultured in Dr. Pine's lab in Caltech's Biology Department using rat SCG neurons. Currently, electrophysiological experiments, including stimulation and recording of the cultured neural networks, are underway. .

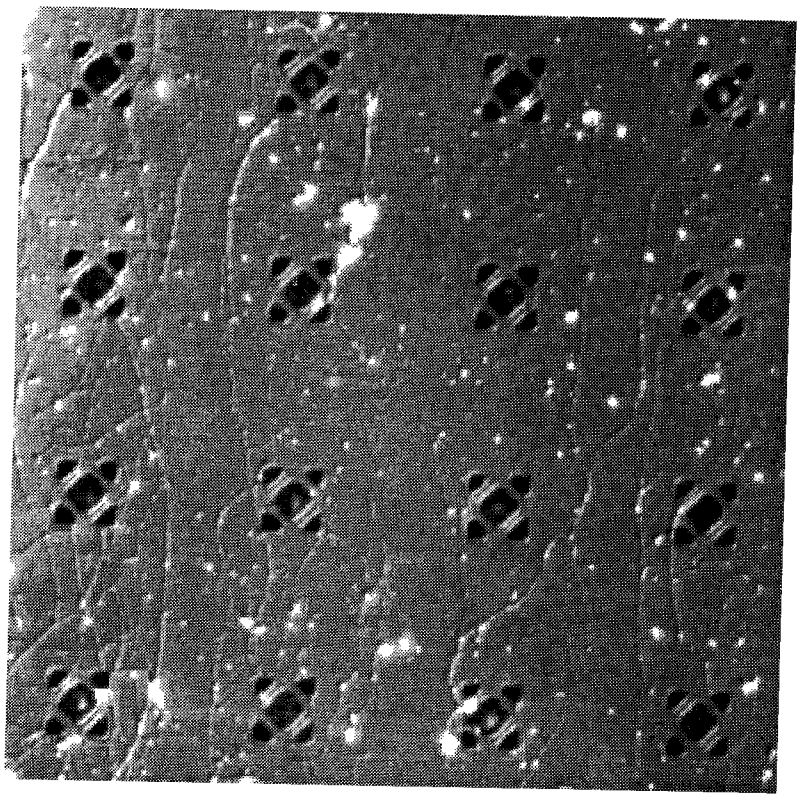

Figure 2-30: A live neural network formed by rat superior cervical ganglion neurons. Clearly seen are the processes growing out of the wells.

Chapter 3

Cultured Neuroprobe for *In Vivo* Studies of Neural Networks

3.1 Basic Concept Of the Neuroprobe

As mentioned previously, the major breakthrough in *in vivo* studies of neural networks were silicon-micromachined probes with metal electrodes, first demonstrated by Wise et al. at the University of Michigan. However, some problems remained unsolved with their devices. For example, metal electrodes which are the basis of present neural prosthesis devices indiscriminately (with respect to cell type) stimulate or record all nearby neurons. Furthermore, with chronic stimulation the non-specific inputs may introduce unintended and undesirable changes in the stimulated nervous system (so-called "rewiring"). Another serious problem is that the insertion of any probe into the nervous system (Fig.3-1.) causes local tissue damage (Fig.3-2.) which creates a layer of damaged/dead cells in the vicinity of the probe.

This can significantly reduce the signal–to–noise ratio as healthy neurons are not in immediate contact with the electrodes. Also, possible variations in the position of the probe makes reliability of long–term usage of these devices questionable.

Here, we propose a new approach which uses "linking neurons" incorporated into an inserted probe. In this way, highly specific connections can be made with specific neurons. The "linking neurons" are implanted within a "neural probe" structure which enables them to be inserted into a host's brain. We are attempting to study whether implanted probe

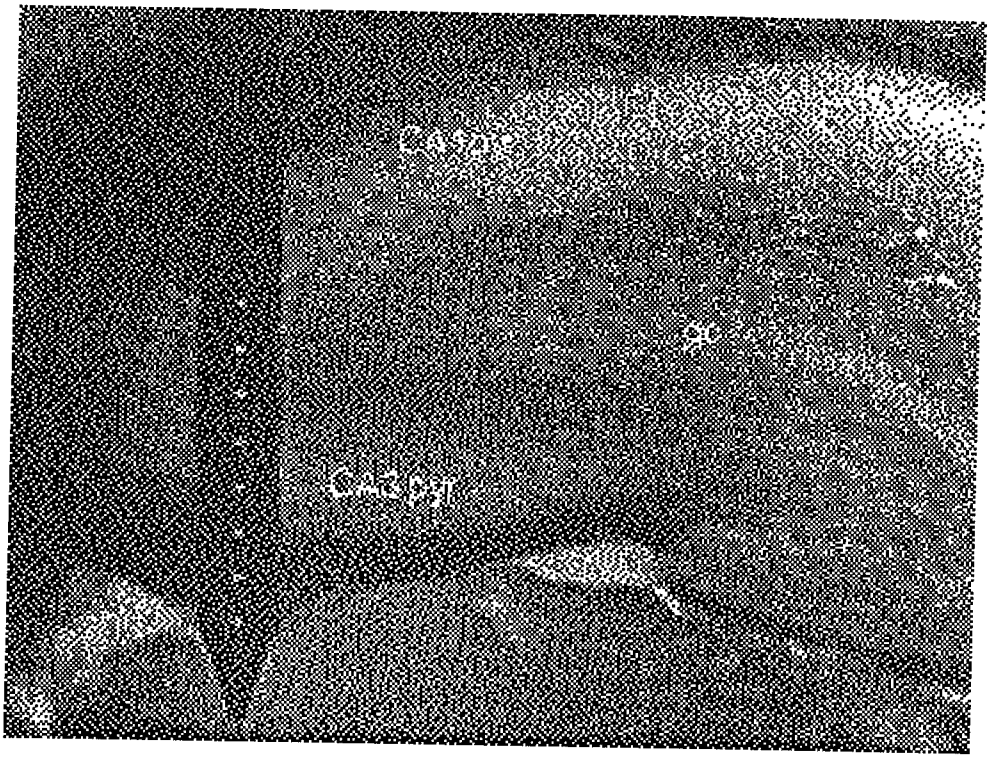

Figure 3-1: Probe inserted in a rat's brain for studies of brain damage by the probe.

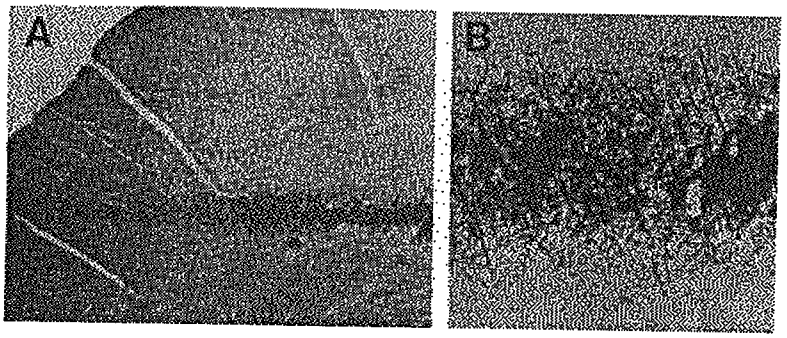

Figure 3-2: Local damage of the brain tissue caused by probe insertion. Damage is visible as "dark neurons" obtained by staining

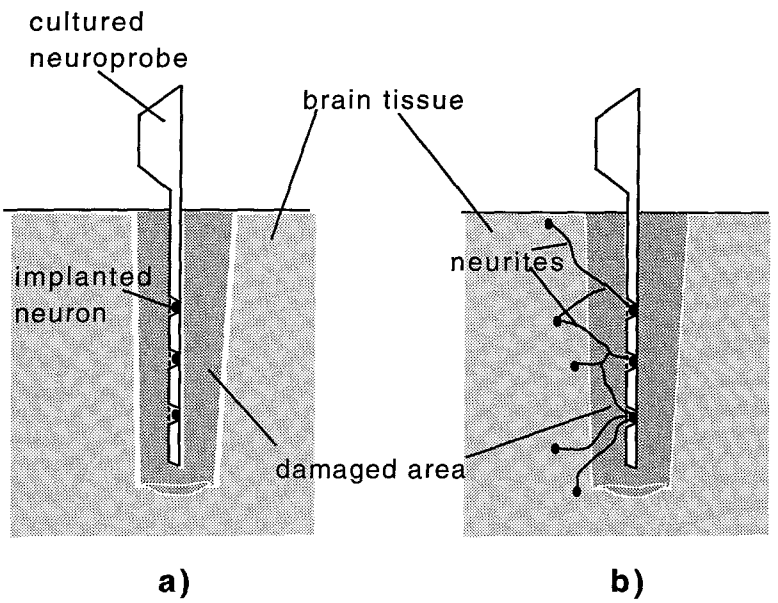

Figure 3-3: The schematic use of the cultured neuroprobe a) Cross section of the brain immediately after insertion of the probe; b) Cross section after formation of synaptic connections.

neurons will establish functional synaptic connections with the host's brain, in which case they can serve as an interface between the recording electrodes and the nervous system in which they are implanted. This bridge would then completely eliminate the problem related to neuronal damage around the probe and poor signal–to–noise ratio because even though this damage still exists, connections are established by the healthy neurons (Fig.3-3).

Problems arising from possible probe motion would be less significant, since the intermediate "captive" neuron between the electrode and nervous system would be a physical connection, which is more difficult to damage. Linking neurons would enable long–term, reliable devices for prosthetic applications. The linking cultured neurons are implanted in the silicon neuron wells that were previously described (See Fig.1-8). The proposed basic structure of the cultured neuroprobe is shown at Fig.1-13.

3.2 Neuroprobe Design

The cultured probe is designed so that it can successfully stimulate and record in the rat hippocampus, which is the region of the brain that we decided to explore. The reason for

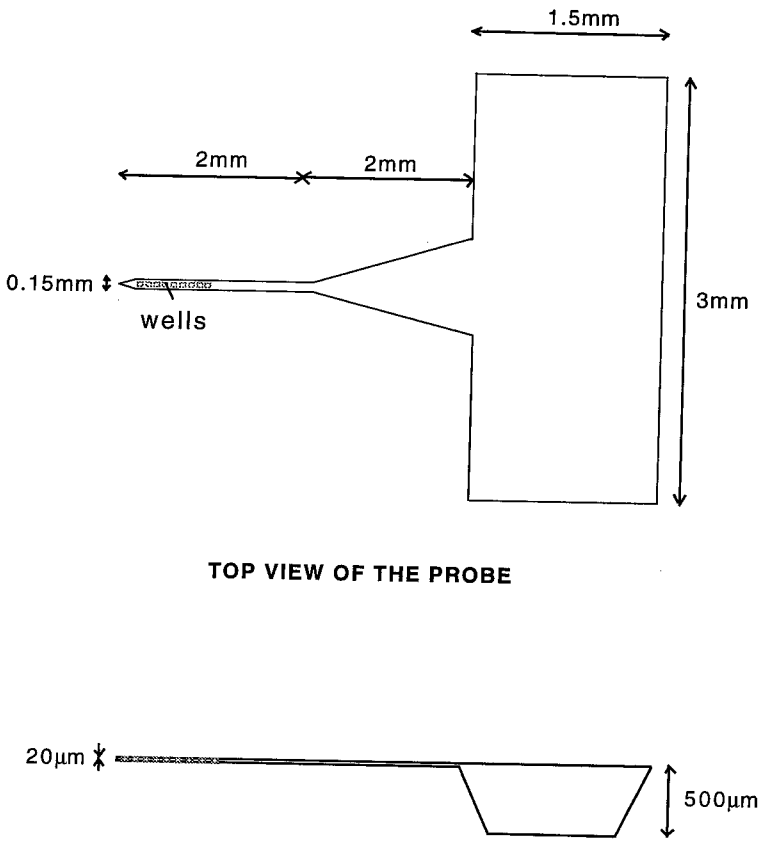

Figure 3-4: Design and dimensions of a neuroprobe.

this choice is that the rat hippocampus is the tissue in which the most evidence of the successful synaptic integration has been obtained. The hippocampus has a well–defined cytoarchitecture, physiologically identifiable cell types, large field potentials and powerful behavioral influences. Our collaborators from Rutgers University in New Jersey have a lot of experience with hippocampal studies on live rats.

Considering the location of the rat hippocamus, it was decided that the needle portion of the probe should be 4mm long. Fifteen neuron wells and one control electrode extend about 1mm from the tip towards the handle. (See Fig.3-4). The neuron wells are 50μm apart in one design, and 100μm in another. Their depth (controlled by the thickness of the top epi–layer) is 16μm for the implanted hyppocampal pyramidal cells, so that they can

fit snugly inside the wells. The shank width is determined by the lead width and spacing. Our current design has 4μm leads with 8μm pitch. The shank is 150μm wide, with a 2mm straight section and a 2mm tapered section ending at the 500-μm-thick handle. There are two designs of the handle: 3x3mm^2 and 3x1.5mm^2. In both cases contact pads are 200x200μm^2.

3.3 Neuroprobe Fabrication

The fabrication starts on epi–wafers with a 16μm, lightly–doped layer on top of a 4-μm, heavily boron–doped layer [47](Fig.3-5a). First, 50nm of thermal oxide is grown on wafer by dry oxidation on 1050C. The following LPCVD silicon layer is deposited at 800C, using gas flows of 120sccm of ammonia and 40sccm of dichlorosilane. Photolithography is then performed, using KTI 27cs photoresist spun at 3000rpm for 30sec. Photolithographic steps pattern the nitride–oxide layer to define openings (6μm in diameter) for the metal electrodes at the bottom of the neuron wells (Fig.3-5b).

Plasma etching using SF_6 gas at 200 mTorr is done to etch through the nitride layer. BHF is used to remove the pad oxide, followed by an isotropic etching (HNO_3:H_2O:HF=50:20:1) to etch 0.4μm down into the silicon substrate. Next, a fully recessed LOCOS (LOcal Oxidation of Silicon) step planarizes the surface. This thermal oxidation is performed at 1050C, and the oxide thickness grown is 0.8μm. After the LOCOS process, the initial size of the openings shrinks from 6μm to 4μm, which is precalculated and taken into account (See Section 2.3.5.). This local oxidation of silicon creates a 0.8μm oxide step around the gold electrode. The purpose of this step is to ensure good electrical insulation of the electrode and to provide a tight seal with the cultured neuron in the well. It is actually simulating a loose–patch electrode. The LPCVD nitride is then stripped, using H_3PO_4 heated at 150C. A metal layer consisting of 10nm/200nm/10nm Cr/Au/Cr is then evaporated on top of patterned AZ1350J photoresist, 1.7μm thick. The composite metal layer is patterned using lift–off which is very suitable in this case for two reasons. First, it is rather difficult to etch, controllably, 4μm lines with 8μm pitch. Second, whenever one has multiple metal layers, a lift–off process is favored, because different metal etchants don't have to be applied to

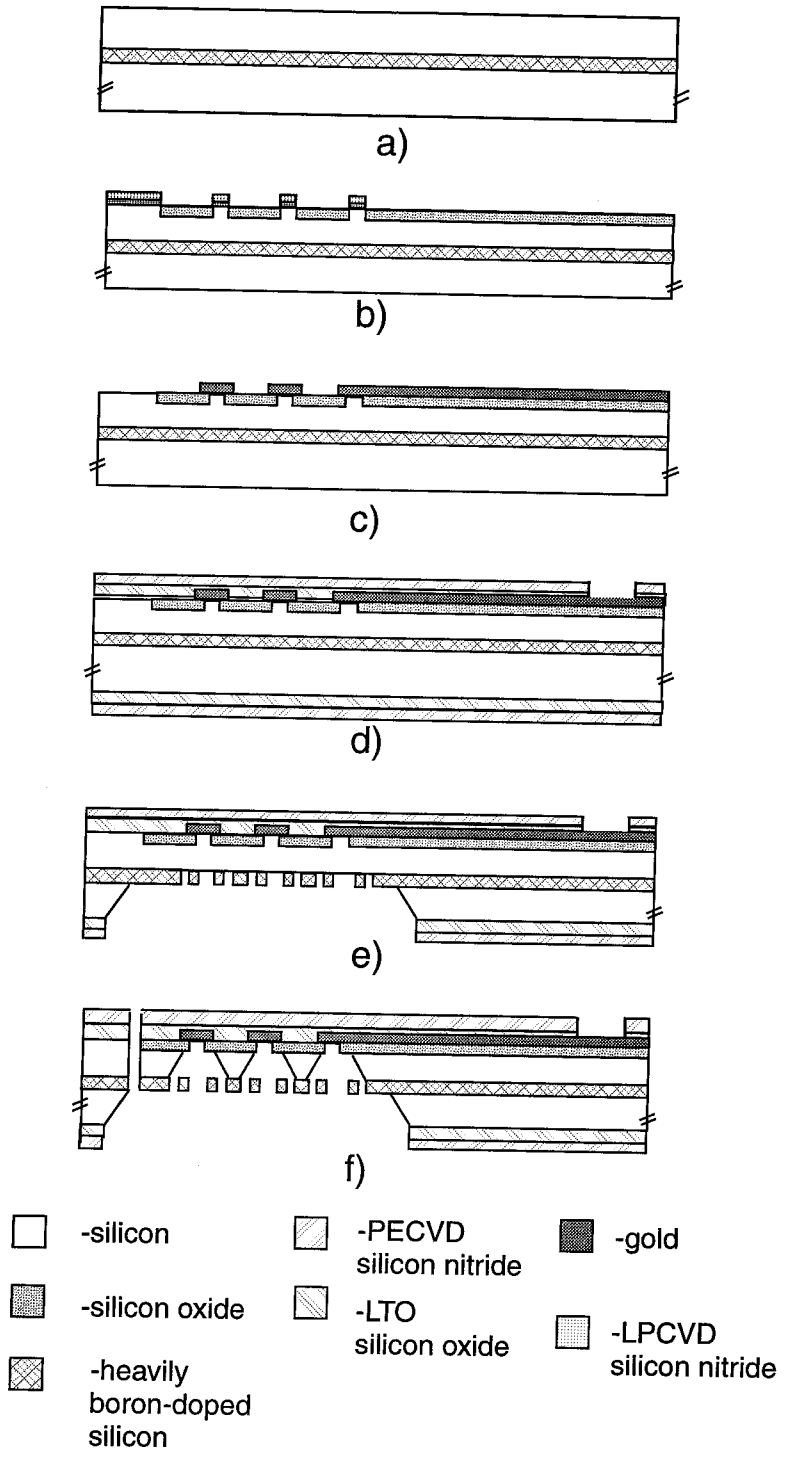

Figure 3-5: The fabrication process for the cultured neuroprobe.

remove the unwanted metal. This process forms the neuron well electrodes as shown in Fig.3-5c. Metalization is covered by a composite insulation layer of 0.5μm LTO and 1μm of PECVD nitride. By using this combination, optimal stress compensation is achieved. It is very important for the photolithography that is performed on a membrane in a subsequent step. There is one reason more to use PECVD nitride as the outer layer. Namely, it is believed that a hydrophilic insulation layer immersed in saline solution tends to swell and it is inappropriate for long–term applications [9].

Next, opening of the bonding pads and etching of the alignment marks in the insulation layer is performed. This is achieved by a combination of SF_6 plasma etching for the PECVD nitride removal, and CHF_3/O_2 plasma etching followed by BHF etching for the oxide removal. The alignment marks are used later to do front–to–back alignment across a membrane that is micromachined in the subsequent steps. The details of the double–sided alignment process are described in the Section 2.3.3.

Windows on the back of the wafer are opened, using the same dry and wet etching steps used for the opening of the alignment marks and the bonding pads. The following EDP etching (we used ethylenediamine-pyrocathecol-water solution that is commercially available from the Transene Company as an anisotropic silicon etchant PSE-300) is performed at 95C. This forms the silicon membrane using the heavily boron–doped layer as an etch–stop (Fig.3-5e.).

Photolithographic steps on the cavity side of the membrane follow. The wafer, which already has huge, fragile membranes, should not be exposed to vacuum from the cavity side so the special chuck is used (See Fig.2-15.). Using this special chuck, KTI 27cs photoresist is spun on the wafer at 3000rpm. The wafer is exposed using a GCA4800 projection stepper (See Section 2.3.4.).

Reactive Ion Etching (RIE) is used to form the grillwork in the heavily boron–doped layer. The neuron wells are formed by EDP etching all the way to the well electrodes on the front side of the wafer. This is followed by the removal of the pad oxide and chrome at the bottom of the well by BHF and chromium etchant respectively.

The remaining steps are devoted to the definition of the probe shape. First, 500nm of chromium is evaporated on the top side of the wafer. Next, the chromium layer is patterned

by performing the last photolithography and etching.

The fabrication continues with RIE etching all the way through the membrane, using the patterned chromium as the masking layer. Finally, the chromium is etched away using chromium mask etchant. The probes are released by snapping them off the substrate. The SEM micrograph of the tip portion of the probe is shown on Fig.3-6., and a close–up view on the probe's neuron wells is shown on Fig.3-7.

3.3.1 Dummy Probe Fabrication

During preliminary experiments, it was crucial to prove that neurons are growing out of the wells and into the animal's nervous system. Stimulation and recording from the neurons was not the main focus. For these applications, a special process was developed to fabricate so–called "dummy probes." They have the shape of the real probes and neuron wells in the shank that have grillwork on top. However, these neuron wells don't have electrodes at their bottom. In that phase of our experiments, electrodes were not that important, and the proposed process for making "dummy probes" was much simpler using only three masks.

The starting wafer is a 4" epi–wafer with 16 μm of lightly doped silicon on top of a 4-μm thick, heavily boron–doped layer (Fig. 3-8.a.). First, double–sided alignment marks for rough front–to–back alignment are patterned on both sides of the wafer using a special alignment jig. Next, 0.5μm of low–stress LPCVD nitride is deposited on the wafer (820C, 15.6sccm of NH_3 and 64.7sccm of DCS). Photoresist KTI 27cs is spun on the back side of the wafer at 2500rpm, and patterned using the first mask for the big cavity opening. The exposed low–stress LPCVD nitride is etched away using SF_6 plasma etching (200mTorr, 200W). The following step is EDP etching at 95C (Fig.3-8b.) until the heavily boron–doped silicon etch–stop layer is reached.

The subsequent steps are performed on the top side of the wafer. Knowing that it is very fragile at this point, one should use the specially designed chuck for photoresist spinning (See Section 2.3.1). Also, during the exposure on the stepper, the back side of the wafer should be protected by dicing tape so the vacuum does not break the membranes.

Photolithography with the second mask which defines the grillwork is done on the front

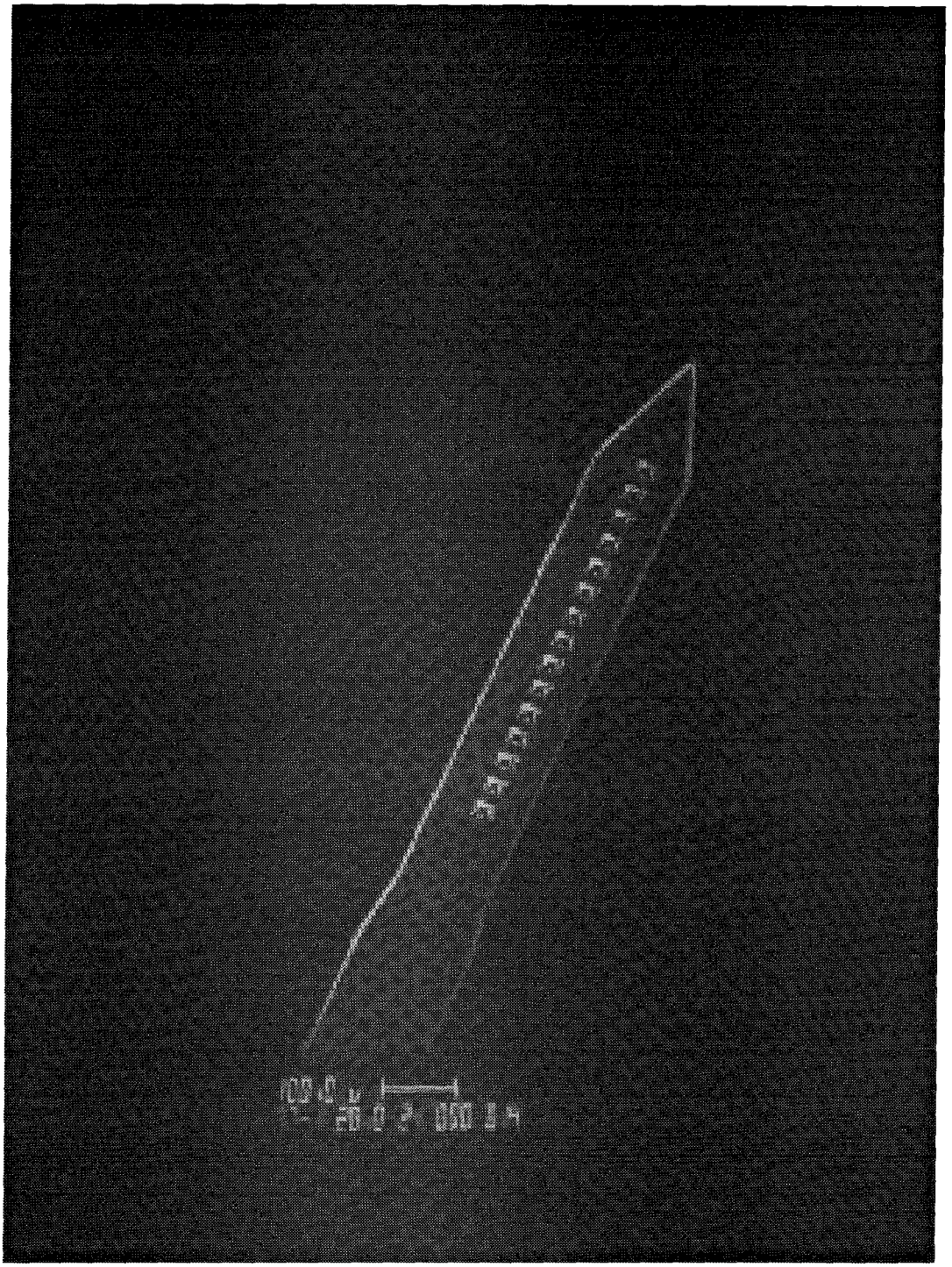

Figure 3-6: SEM of the tip portion of the probe. Fifteen neuron wells are situated along the probe.

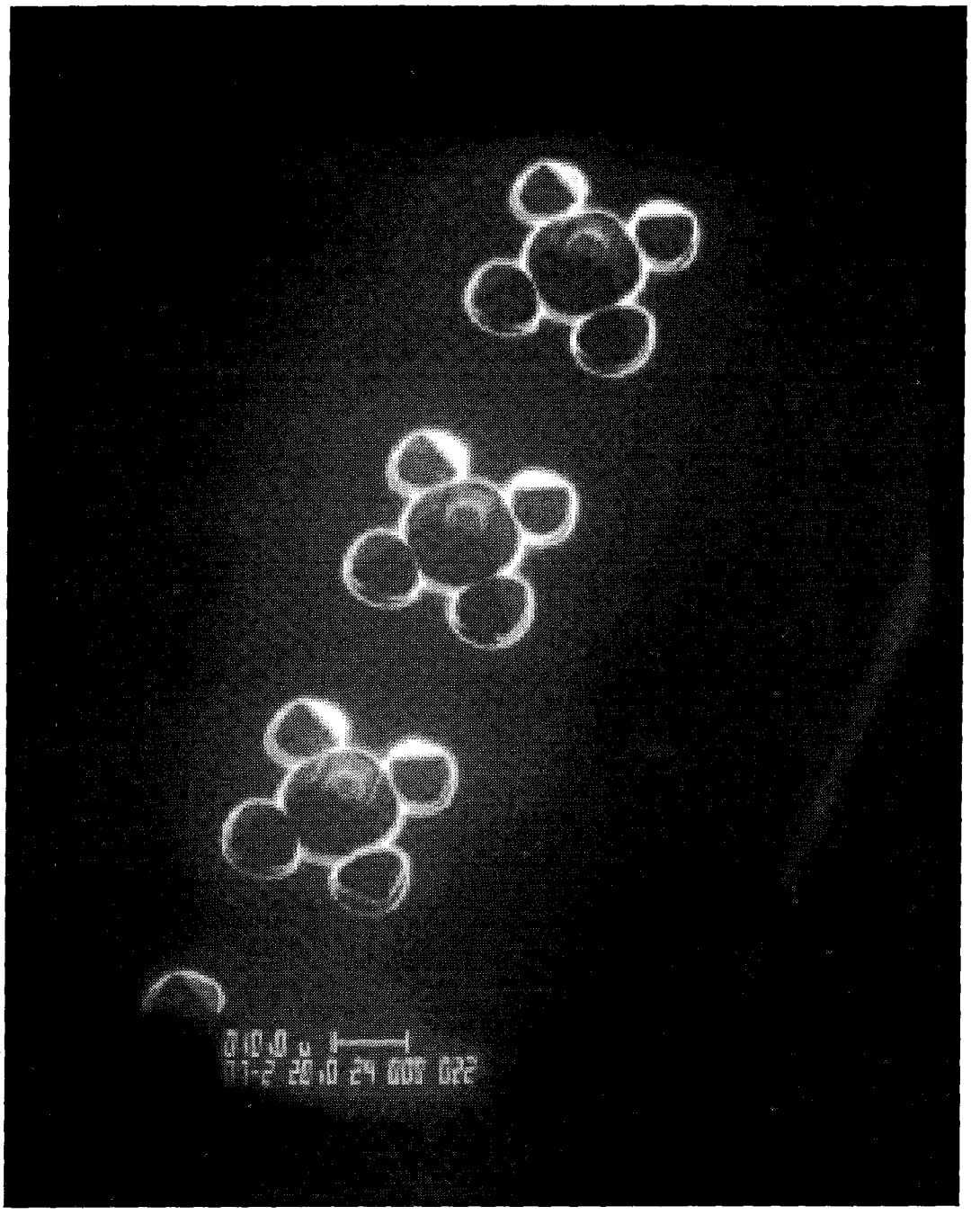

Figure 3-7: The close–up view on the neuron wells. Gold circular electrodes 3μm in diameter can be seen at the bottom of the neuron wells.

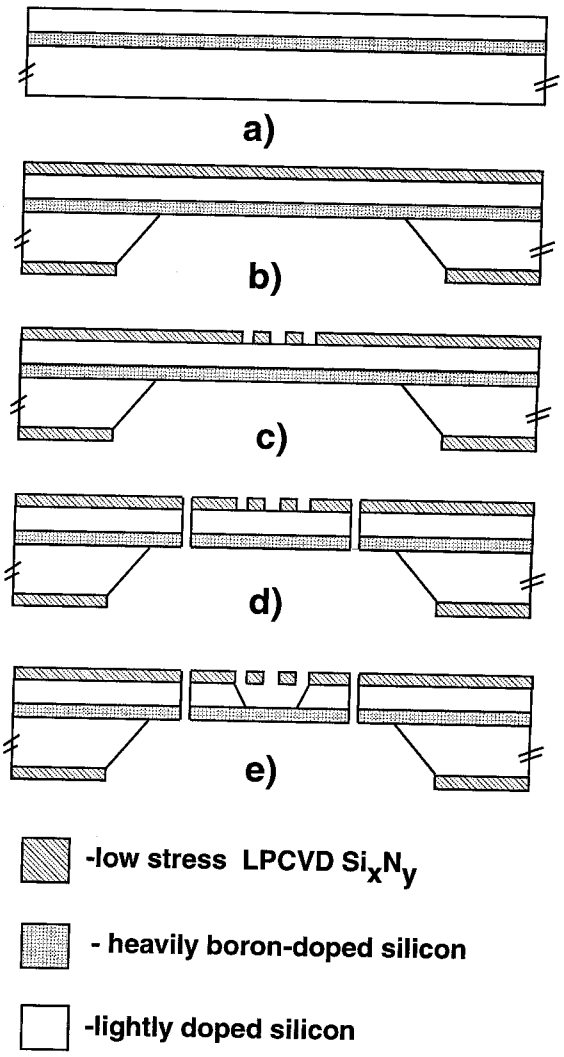

Figure 3-8: Some of the cross sections of the shank of the dummy probe in the different phases of the fabrication process.

side of the wafer using photoresist KTI 27cs, spun at 2500rpm. Etching of the grillwork is done in the RIE with gas flows of 17sccm of SF_6 and 15 sccm of O_2 at a power of 1kW. Pumping down the RIE machine with the diffusion pump before the RIE etching seems to be very important for nitride removal. When the diffusion pump is not used one does not get any etching at all. It is also necessary to mention that the depth control is crucial here. One should not etch too deeply into the silicon, or a bubble problem occurs (it will be described later).

Next, the remaining photoresist is removed by O_2 plasma ashing. A layer of chromium 150nm thick is evaporated on the top surface of the wafer. A new layer of photoresist KTI100cs, spun at 2000rpm, is then applied to the front side of the wafer and soft baked for 30min at 90C. This photoresist is exposed using the third mask, which defines the shape of the probe. After hard–baking the photoresist at 120C for 30min, the chromium is patterned using chromium etchant. Then a long RIE etching is performed (15sccm of O_2, 17sccm of SF_6, power 1kW) to etch all the way through the membrane.

After the shape of the probes are defined, another EDP etching at 95C is done to etch the neuron wells in the lightly doped silicon layer. Their bottom is, in this case, the heavily boron–doped silicon layer, whereas their grillwork is made of low–stress LPCVD silicon nitride.

Dummy probes are dipped in hot water, KOH solution and hot water respectively to remove all traces of the EDP which is potentially harmful to cells. Finally, the dummy probes are snapped from the substrate. In Fig.3-9 one can see SEM micrographs of the tip of the dummy probe and of a single neuron well.

The RIE Masking Problem

The dummy probe fabrication process that was originally developed used the 10μm thick photoresist for the masking layer during the RIE process. This thickness of photoresist was quite sufficient to serve during the approximately 60 minutes of RIE etching, since the etching rate of the photoresist in SF_6/O_2 plasma was only 100 nm/min. However, it turned out that it was impossible to achieve good step coverage with a thick layer of photoresist. Air bubbles formed above the grillwork and below the layer of photoresist, visible to the

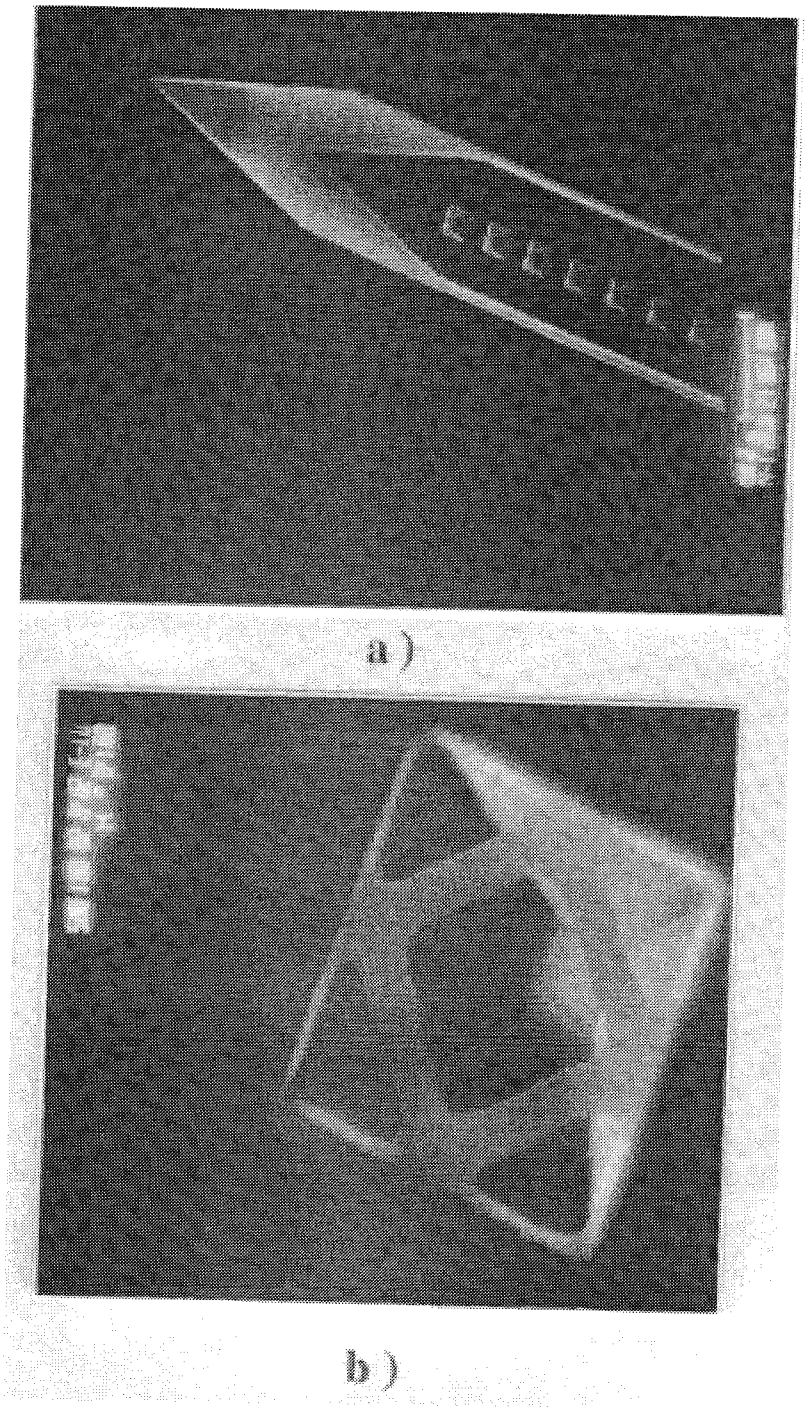

Figure 3-9: a) SEM of the tip of the dummy probe, b) SEM of the single neuron well in the dummy probe.

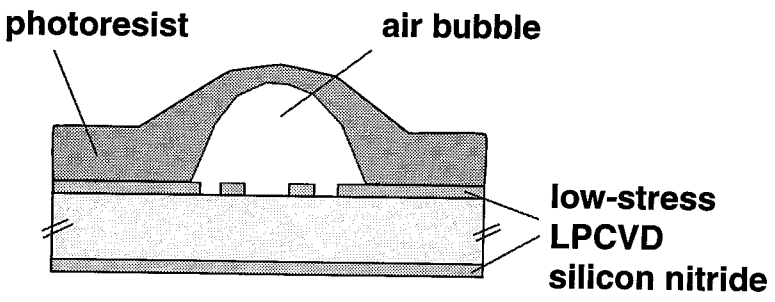

Figure 3-10: The schematic presentation of the bubble formed during the spinning of photoresist.

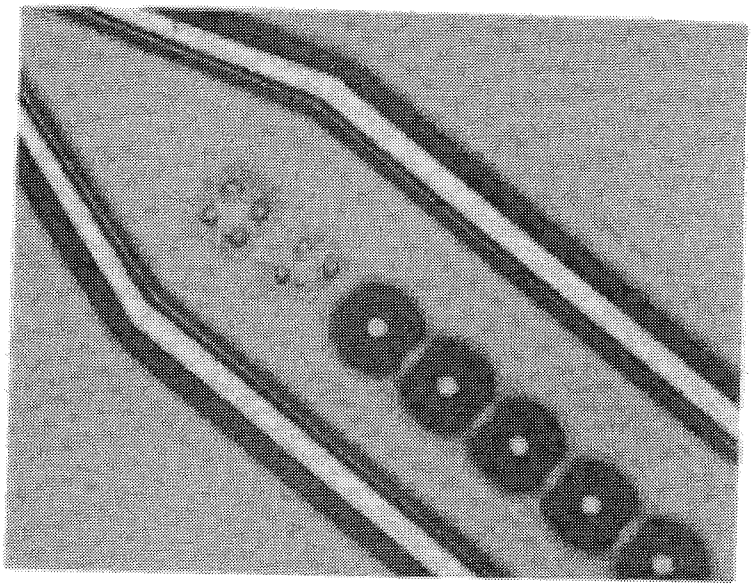

Figure 3-11: The photograph of the bubbles obtained after photoresist hard baking.

naked eye immediately after spinning photoresist, and becoming even larger after hard baking (See Figs.3-10. and 3-11). These air bubbles were fatal for photoresist protection of the grillwork area during the subsequent RIE etching. Instead of a dummy neuroprobe we ended up having a micromachined sewing needle as shown in the Fig.3-12.

This problem was finally solved by using a patterned chromium layer as the protective material during the RIE etching. The etching was performed under pure SF_6 plasma, because the mixture SF_6/O_2 causes oxidation and deterioration of the chromium layer, which is not a suitable masking material in SF_6/O_2 plasma. Apparently, the chromium improved the step coverage and adhesion of the photoresist, because the bubbles did not

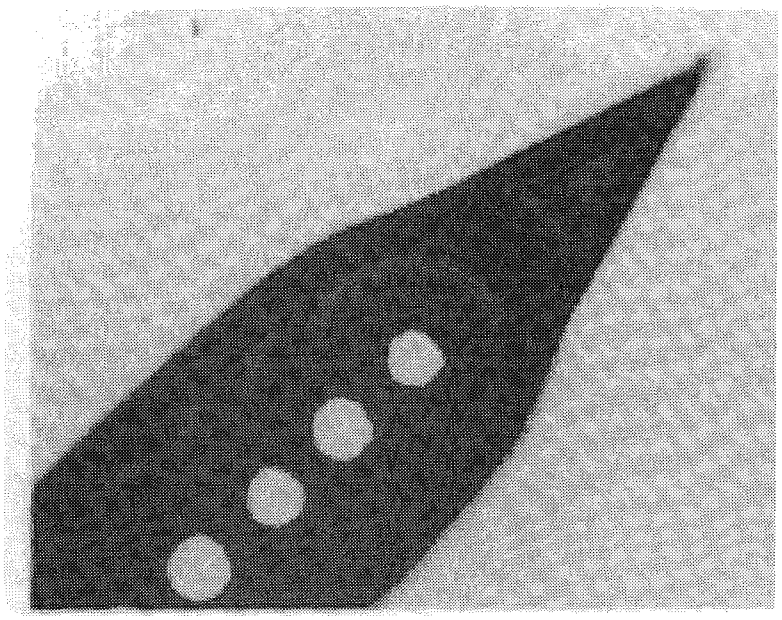

Figure 3-12: The micromachined sewing needle.

appear anymore, and the dummy probe was completed with no additional problems. The same masking layer is successfully utilized during the neuroprobe fabrication.

3.3.2 Compensating Corner Undercutting of Anisotropically Etched <100> Silicon

It is known that all anisotropic etchants used nowadays undercut convex corners during the etching of <100> silicon, if the mask edge is parallel to the <110> direction. Depending on the kind, concentration and the temperature of the etchant used, bigger or smaller under–etch is present. The under–etch can have detrimental effects on the structure if sharp corners are needed. Fortunately, it is possible to add certain compensation structures to the corners of the structures to avoid this problem. Compensation structures are etchant–dependent, because crystal planes are etched at different speeds by different etchants. Beveling planes at undercut convex corners, which are rounding the corners of the etched mesa if the compensation structures are not added, are <212> planes. That is determined by the angle measurement of the octagonal mesa obtained from a square mask (Fig.3-13). The suggested design of the compensation pattern [60] is to add star–like protrusions at the corners of the

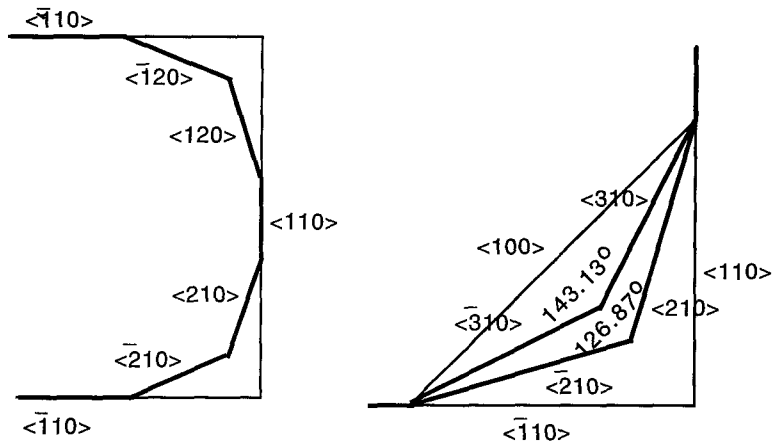

Figure 3-13: Analysis of included angles of the bevel. (Adapted from [59]).

square mask. Undercutting is planned to etch the silicon below these protrusions, but to leave the square mesa untouched. In Fig.3-14 one can see the proposed design for the mask compensation. The blow–up of one corner of the compensated mask is shown in Fig.3-15. Basically, one should etch an uncompensated mesa and measure the extent of undercut, **du**, from the designed mesa corner to the mesa corner obtained after etching. As $\delta_c = \delta_u$, all the other parameters can be obtained: $d_c = \sqrt{5}\delta_c, d_u = \frac{\sqrt{5}}{2}\delta_u, d_c = 2d_u, \overline{OP} = \sqrt{2}d_c$ This compensation structure is very good, but it requires a lot of space. Fortunately, we could accomodate it for cultured neuroprobes having handles of 3x3mm^2 without any problem (See masks given in Appendix A). This compensation method gave very good results (Fig.3-16.).

On our other probes, which have 3x1.5mm^2 handles, we did not have enough room for this kind of compensation, so we ended up using a rectangular pattern [35].

3.4 Strength Characterization of Silicon Microprobes

Silicon probes are used to penetrate a variety of biological tissues, and they should be designed in such a way to withstand that penetration without breaking. Fortunately, even though silicon probes are extremely thin and fragile, it ends up that miniature silicon structures with a cross section smaller than 2x10^{-5}cm^2 have a maximum fracture strength which is six times larger than the fracture strength of bulk silicon [28].

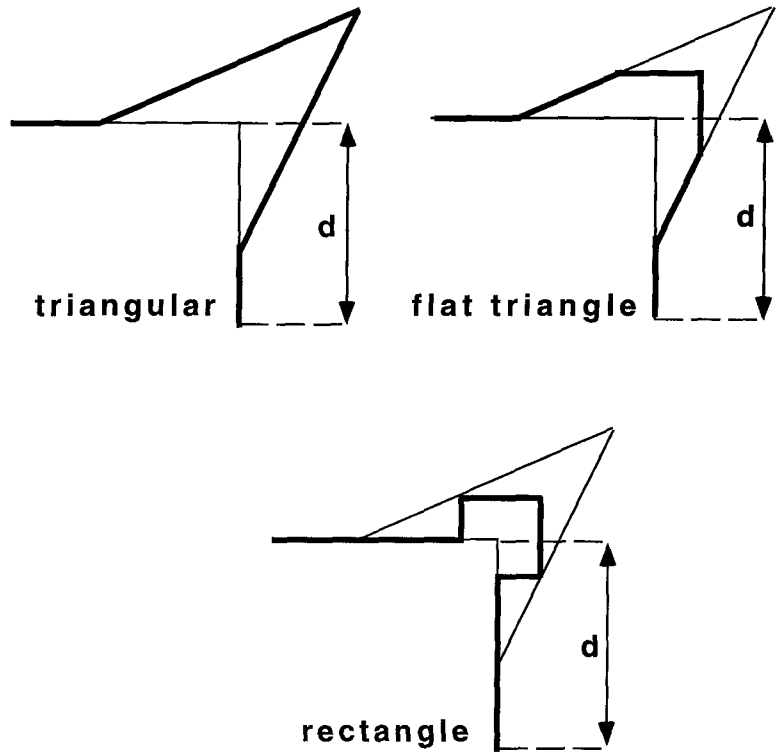

Figure 3-14: The design of the mask compensation.

Cultured neuron probes were exposed to bending and buckling tests to study their strength in order to evaluate whether they can survive the insertion process. The influence of the neuron wells on the fragility of the probes was not clear, so it was extremely important to perform the mechanical testing of the probes and to prove that they are as strong as neuron probes of the same dimensions without neuron wells. The bending test was performed on the static testing set–up assembled at Caltech (Fig.3-17.). Basically, it consists of a load cell on which the probe can be mounted, and that measures the force exerted on a fixed stylus positioned above the sample. The corresponding displacement with respect to the initial position is measured by a Linear Voltage Differential Transformer (LVDT).

The typical loading curve obtained using such a setup is shown in Fig.3-18.

The stiffness of the probe shank in the z–direction, calculated as the ratio of the force and the corresponding displacement, is 1.15 N/m. The testing showed that the cultured probe is very compliant in z-direction (Fig.3-19.). This bending picture is taken just before the probe broke. In reality, during the penetration of the brain tissue, two situations can

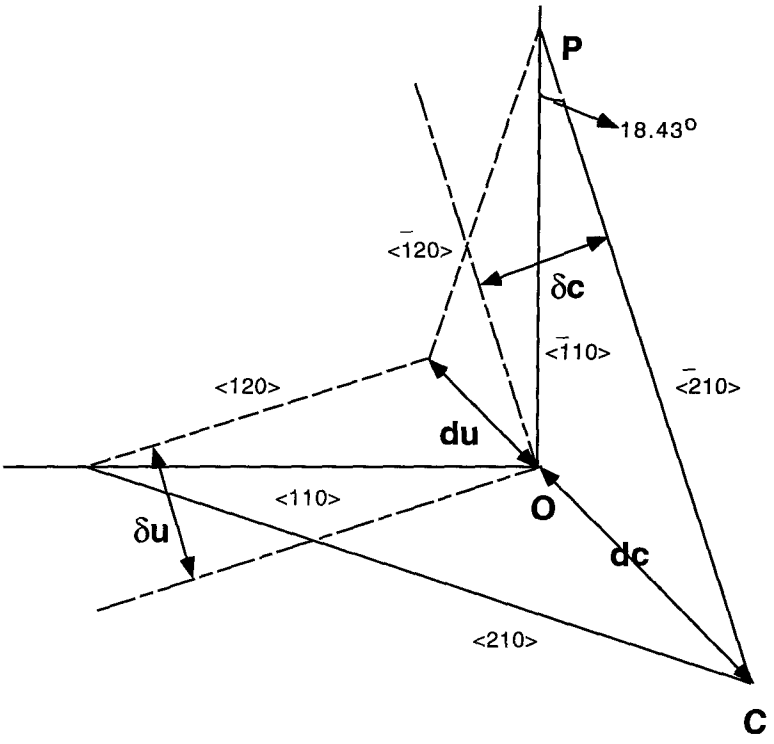

Figure 3-15: The blow–up of one corner of the compensated mask. (Adapted from [59].

occur: a) the shank can be deflected in a quarter-circle, or b) the shank can buckle and form a semicircle (Fig.3-20.).

In case (a), the maximum stress on the shank (at the bottom of the shank) and the average stress (in the middle of the shank) are given by [52]

$$\sigma_{max} = \frac{3E_t y_A}{2L^2} \tag{3.1}$$

$$\sigma_{ave} = \frac{3E_t y_A}{4L^2}, \tag{3.2}$$

where L is the shank length, t is the thickness, E is silicon's modulus of elasticity (Young's modulus) and y_A is the maximum deflection of the probe tip.

In case (b), although it is more common in most neural applications, the deriving of the stress equation is much more complicated. However, Najafi and Hetke from University of Michigan found that, based on experimental measurements, case (b) can be treated exactly like case (a), with the only difference being the effective length of the probe shank [22]. The

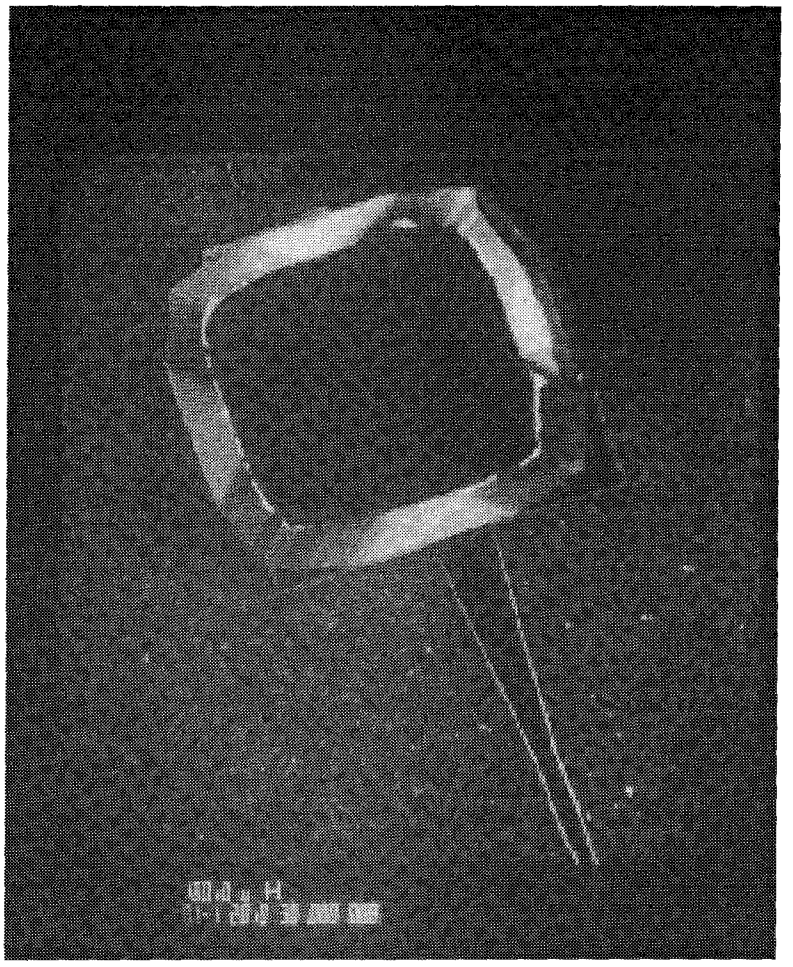

Figure 3-16: The handle part of the cultured neuron probe obtained using the triangular compensation

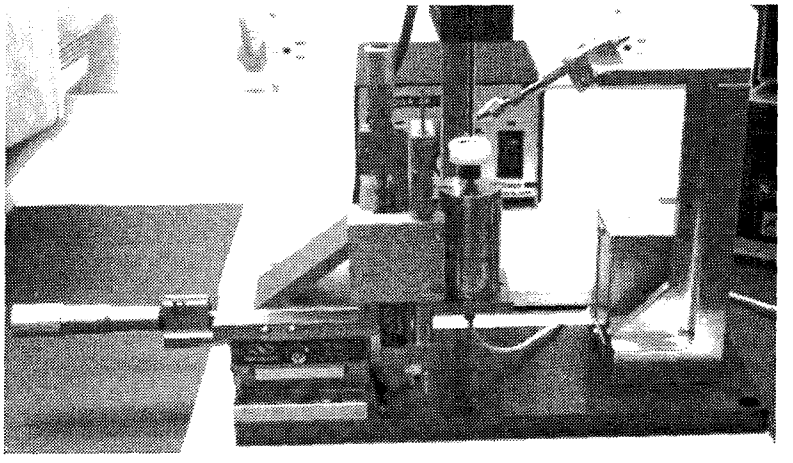

Figure 3-17: Static testing set–up

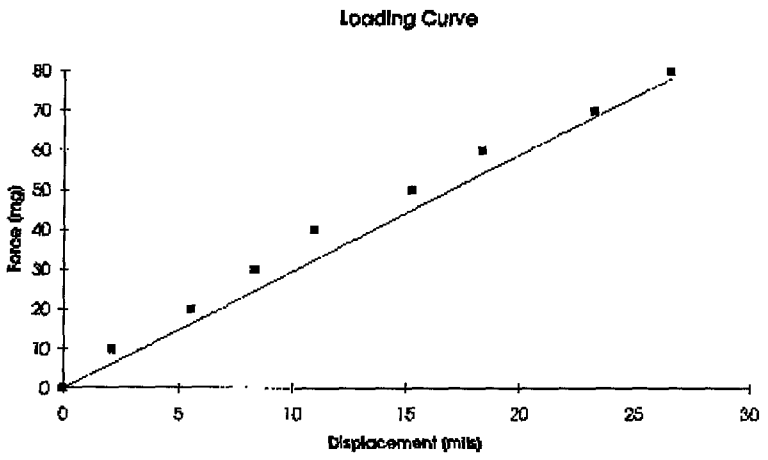

Figure 3-18: The loading curve of the cultured neuron probe.

effective length of the shank, L_{eff}, is only one half of the actual shank length, which then causes the deflection to be 1/4 of what is expected.

On the basis of the bending test, since our static setup measures the deflection of the shank with remarkable accuracy ($\pm 2.5\mu$m), one can calculate the fracture strength of the silicon on the basis of [12] and compare it with the other results obtained in literature.

Our probe broke when the loading point of the shank, which is 2.92mm down the shank, was deflected 1.7mm down. It comes out that the fracture stress of silicon is $1.14\text{x}10^{10}$ dynes/cm^2, which is in extremely good agreement with the results obtained in [28] and [22]. (See Fig.3-21.).

From Fig.3-21 one can see that fracture stress is a function of the area of the cross section. It is approximately constant for cross sections $\leq 2\text{x}10^{-5}$cm^2, and then it drops exponentially until the cross section is $2\text{x}10^{-4}$cm^2. After that, the fracture stress is constant and has the same value as bulk silicon ($3.5\text{x}10^9$dynes/cm^2). In order to increase the fracture strength, it seems that it is beneficial to decrease the width of the probe while keeping the thickness of the probe constant. In our case, the thickness of the probe is 20μm (determined by the size of the neuron), so the width of the probe should be designed to be less than 100μm in order to achieve the maximum fracture strength.

Buckling tests have been performed as well (Fig.3-23), since that is the most likely deformation of the probe during the insertion. The typical loading curve is shown in Fig.3-22.

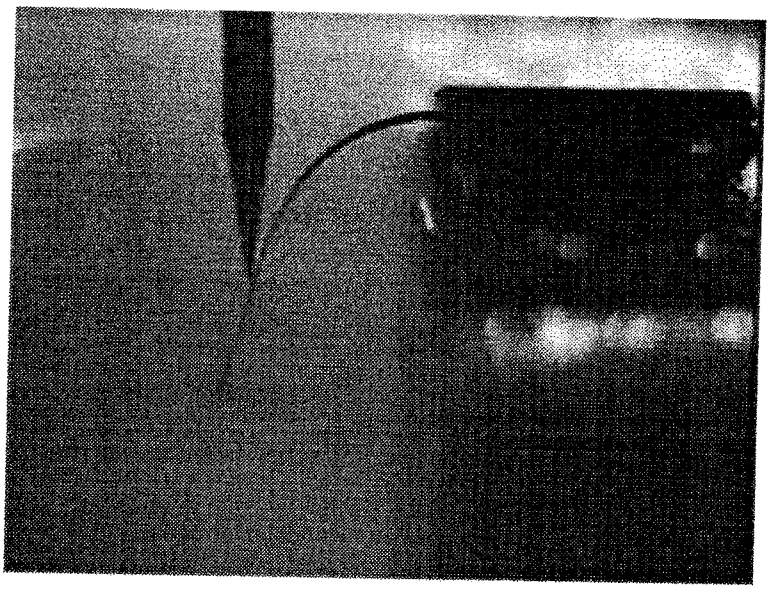

Figure 3-19: Bending of the probe shank. Flexibility is demonstrated, but in real case the probe will never be bent as much.

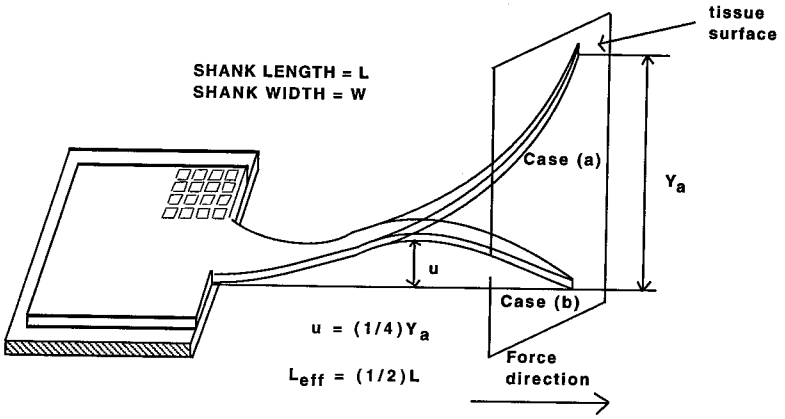

Figure 3-20: Diagram of silicon probe shanks under two deflection conditions: (a) the probe tip is allowed to freely move parallel to tissue surface and the shank is deflected in a quarter circle; and (b) the probe is pressed against the tissue causing the shank to buckle forming a semicircle.(Adapted from [21]).

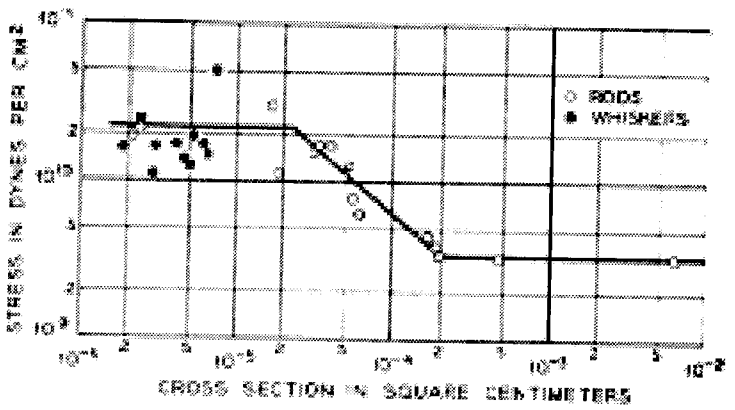

Figure 3-21: Effect of size on room-temperature fracture strength [27].

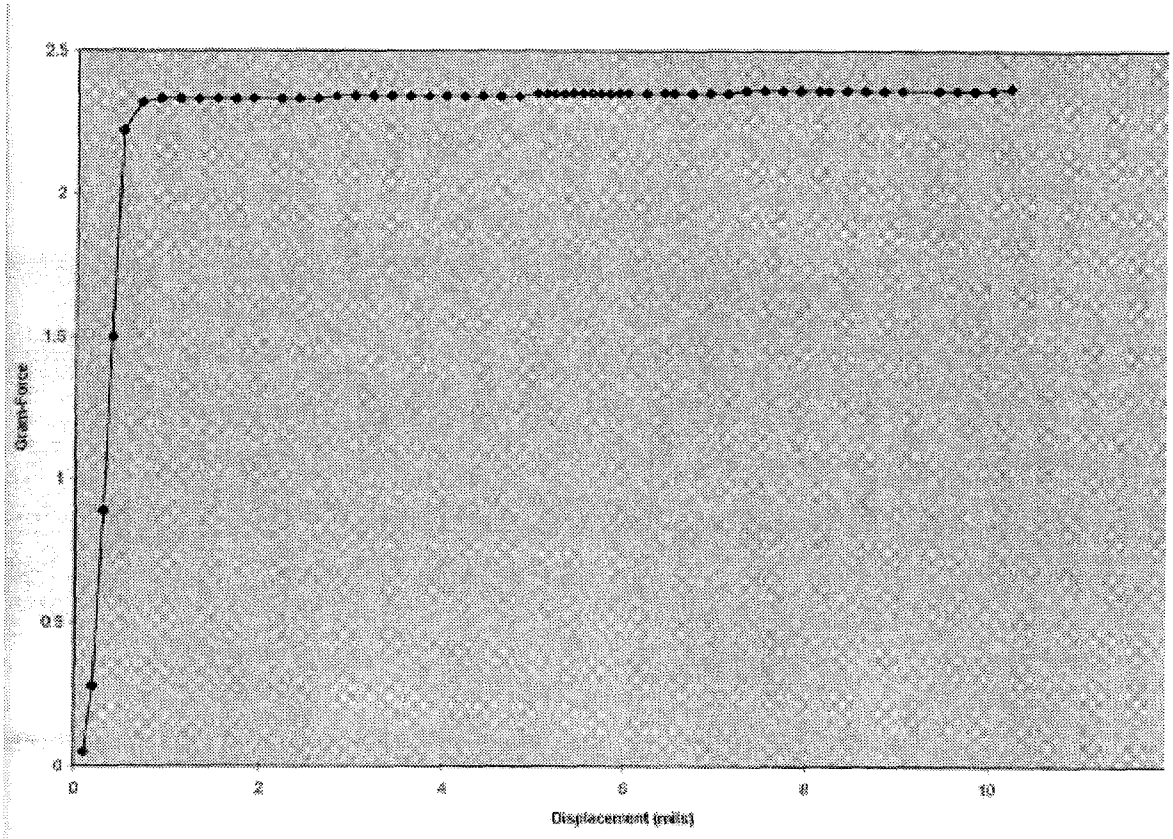

Figure 3-22: The buckling loading curve of the cultured neuron probe.

By measuring the maximum deflection of the probe just before breaking, the maximum stress at that moment is calculated as 8.7×10^9 dynes/cm^2, which is strong enough for the penetration of the rat pia arachnoid and dura layer surrounding the brain tissue (See Table3.1) [22].

3.5 Use of the Cultured Neuroprobes

This part of the experimental work is performed at Rutgers University, NJ by Dr. Gyuri Buszaki and his collaborators. The focus is to demonstrate the long–term survival and outgrowth of neurons from the implanted silicon probe because that is the assumption and the foundation of the entire project.

Probes with cultured septal cells incorporated in the neuron wells were implanted in the rat hippocampus. After the probes have been inserted into the hippocampus, the handle

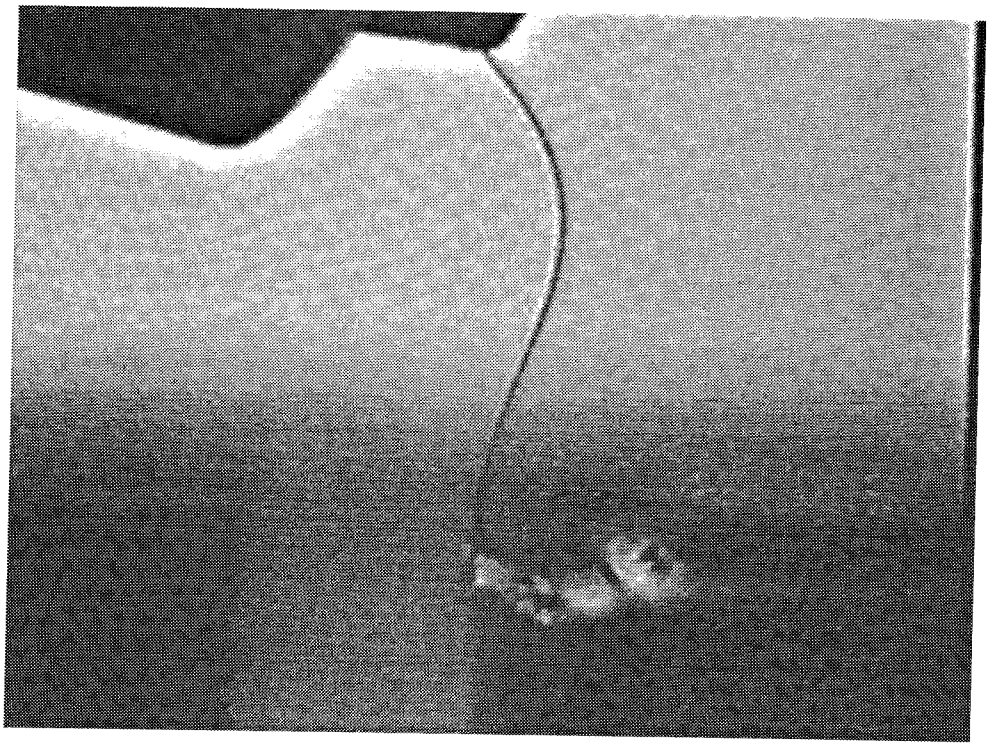

Figure 3-23: The maximum buckling of the probe shank, obtained just before its fracturing.

Probe Thickness	Guinea Pig Pia Penetration Stress Dynes/cm^2	Guinea Pig Dura Penetration Stress Dynes/cm^2	Rat Pia Penetration Stress Dynes/cm^2	Rat Dura Penetration Stress Dynes/cm^2
15μm	5×10^8	1.7×10^{10}		
30μm	Small	3.5×10^9	4×10^8	2×10^9
40μm	Small	4.2×10^9	1.2×10^7	3.7×10^8
60μm	Small	6.5×10^8		

Table 3.1: Summary of maximum stress penetration levels for different probes in guinea pig and rat pia arachnoid and dura layers.

area was broken and the opening was covered with paraffinized wax [34]. The rats were perfused 1 to 2 months after the probe placement. Brain slices 200 to 400μm thick were cut by a vibrotome, making sure that the section contained a large part of the probe. After photographing, these sections were thinned down to 60μm and stained to reveal AChE-positive fibers (the neural processes that could have originated only from the septal cells implanted in the probe; visible by using a special staining method).

In one out of five rats, clear evidence of AChE-positive fiber outgrowth from surviving neurons in the wells was found (Fig.3-24). These results prove that the theoretical foundation of the neuroprobe project is sound and that cultured neurons do grow from the probe into the animal's brain.

Further *in vivo* experiments, including improving the repeatability of the results, as well as the electrophysiological experiments, will be performed at Rutgers University.

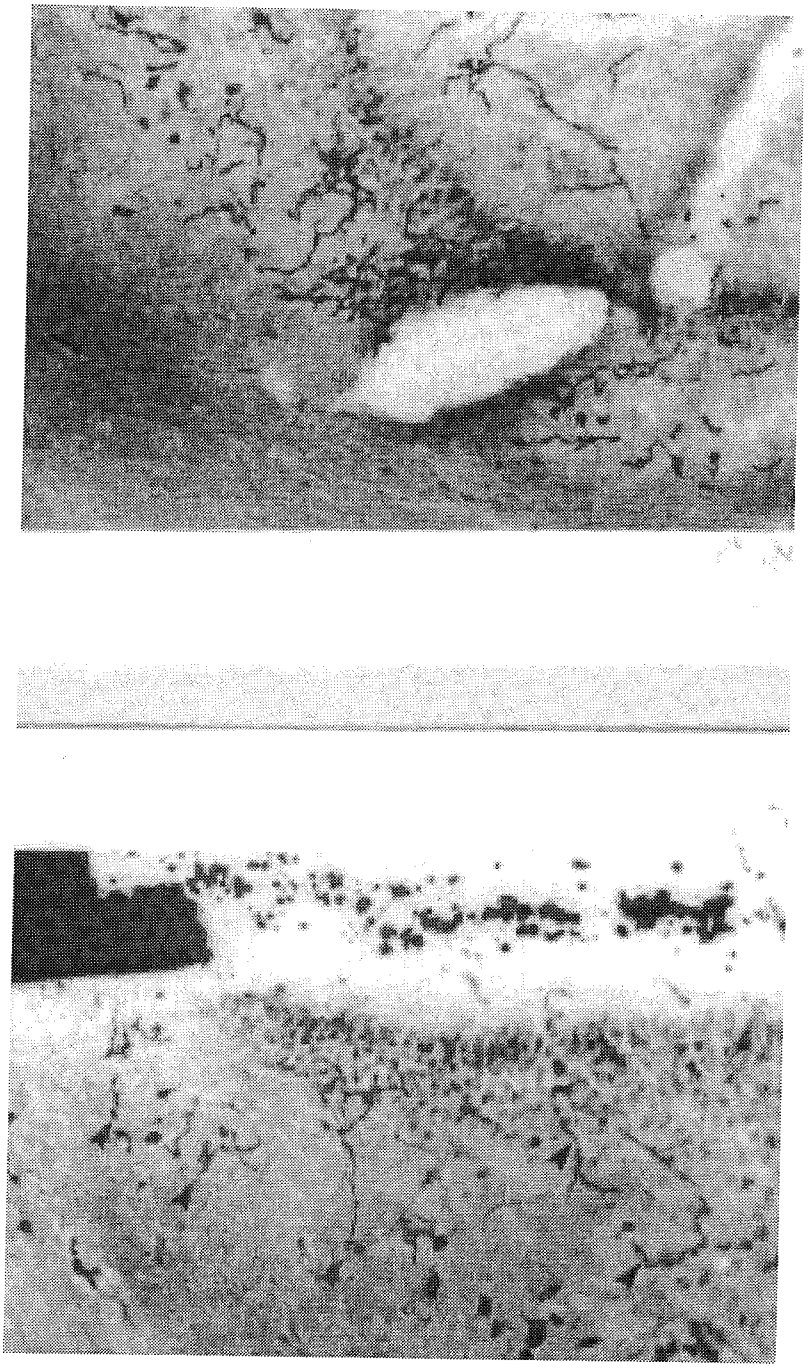

Figure 3-24: The clearly identifiable network of stained axons in the vicinity of two probes.

Chapter 4

Conclusion and Suggestions for Future Work

4.1 Summary

In summary, the next generation of the devices for *in vivo* and *in vitro* studies of neural networks has been designed and fabricated. These devices are based on a neuron well structure where individual cultured neurons can be implanted and cultivated. This approach can significantly improve the poor signal–to–noise ratio characteristic of the majority of contemporary devices for the extracellular stimulation and recording from neurons. In order to confirm this assumption, preliminary electrophysiological experiments have been conducted. The biocompatibility of our devices for periods up to a couple of weeks has been demonstrated. Equally important, the growth of the cultured neurons implanted in neuroprobes for *in vivo* studies into the host's brain has been confirmed. Finally, mechanical testing of neuroprobes has been done by bending and buckling tests to examine their mechanical strength and its sufficiency for the survival during the insertion process.

Further physiological experiments are necessary in order to confirm the validity of the neuron well approach. Since this project is very complex from the point of views of both biologists and electrical engineers this is going to require some time and a lot of patience. However, the possible achievment is definitely worth the effort. If this concept proves to be as promising as the preliminary results indicate, a new generation of neural prosthetic devices based on the concept of neuron well can be born.

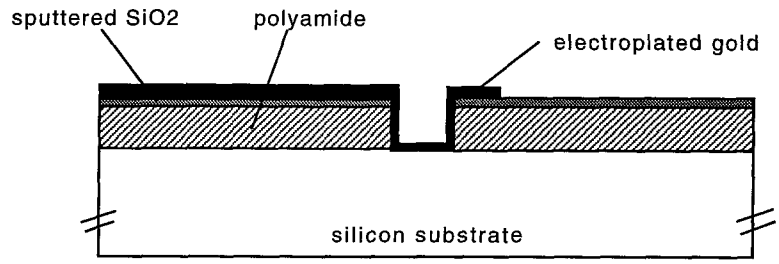

Figure 4-1: A neuron well formed by the gold electroplating.

4.2 Future Work

The neuron well structure is, as previously mentioned, very valuable in the development of new structures for *in vivo* and *in vitro* studies of neural networks. Currently, the main drawback of the existing devices based on this concept is a complicated and elaborate fabrication procedure, which is very unforgiving. The most crucial steps have to be done at the end of the process (exposure at the bottom of a 500μm-deep-cavity and an extra–accurate front–to–back alignment). At that point the wafers are already very fragile, having large and thin membranes. Consequently, the yield is unfortunately small and unpredictable. Once the wafer is finished, it can be as high as 70-80% . However, some of the wafers break during the process and cannot be finished, which has a bad effect on the overall fabrication efficiency.

All of this indicates that the preferable way is to invent a one–sided fabrication process in order to make the neuron wells. My suggestion is to use a gold electroplating process to form "golden cups" where neurons could be implanted (Fig.4-1.). If the cup is deep enough to confine the neuron, grillwork might not be necessary. Another way to do one–sided processing for forming of the neuron well is to etch the pyramidal opening in silicon by means of EDP, evaporate gold under different angles (to cover the wells and the entire flat surface of the wafer completely) and pattern the gold into the lead shape, keeping all the gold that coats the well in silicon. This also produces a "golden cup" approach. The above suggestions are applicable for neurochips only, because the neuron wells for the cultured neuron probes do need a grillwork to keep neuron in place during the insertion process.

Another possible variation of the neurochip could employ the technique of voltage-sensitive dye recording [5]. This method stains the neurons with a dye that changes its

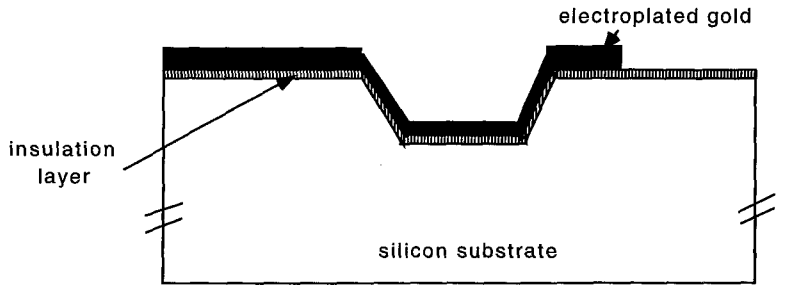

Figure 4-2: A neuron well formed by EDP etching and gold evaporation.

fluorescence by an amount proportional to the intracellular voltage change. These neurochips would still have neuron wells to lock target neurons in position but the grillwork of these wells should be transparent to enable as strong an optical signal as possible. Nitride or oxide grillworks seem to be suitable for that task. A new process for the fabrication of the neurochip with the transparent grillwork is proposed (see Fig.4-3.).

To provide for larger and more intricate studies of *in vivo* neural network studies, cultured neuron probes could be fashioned into two– and three–dimensional structures. At present, our cultured nueral probe is a one-dimensional array of neuron wells. These probes could easily be made into two-dimensional arrays by creating a multi-pronged structure, similar to a "hair comb" (Fig.4-4.a.). These "combs" could then be stacked to create a single probe, similar to a "hair brush," capable of stimulating and sensing a three-dimensional region in a host's nervous system. Both of the structures could significantly increase the area of the brain involved in an experiment.

Also, as mentioned in Section 3.4., to increase of the fracture strength of the probe, if we want to keep the present total thickness of 20μm, the width of the shank of the probe should be less than 100μm. It means that, in order to still have sixteen neuron wells, one should reduce the lead width to 2μm with 4μm pitch. This could be achieved by improving the existing lift–off process.

However, neuroprobes and neurochips in their present shape have yet to be used to their full potential. Slight changes in the thickness of the top epi–layer can be used to change the size of the neuron wells and therefore enable different kind of neurons to be implanted. Experiments that change environmental parameters could also be done.

It has to be said that due to the sensitive and long fabrication process, mass production of

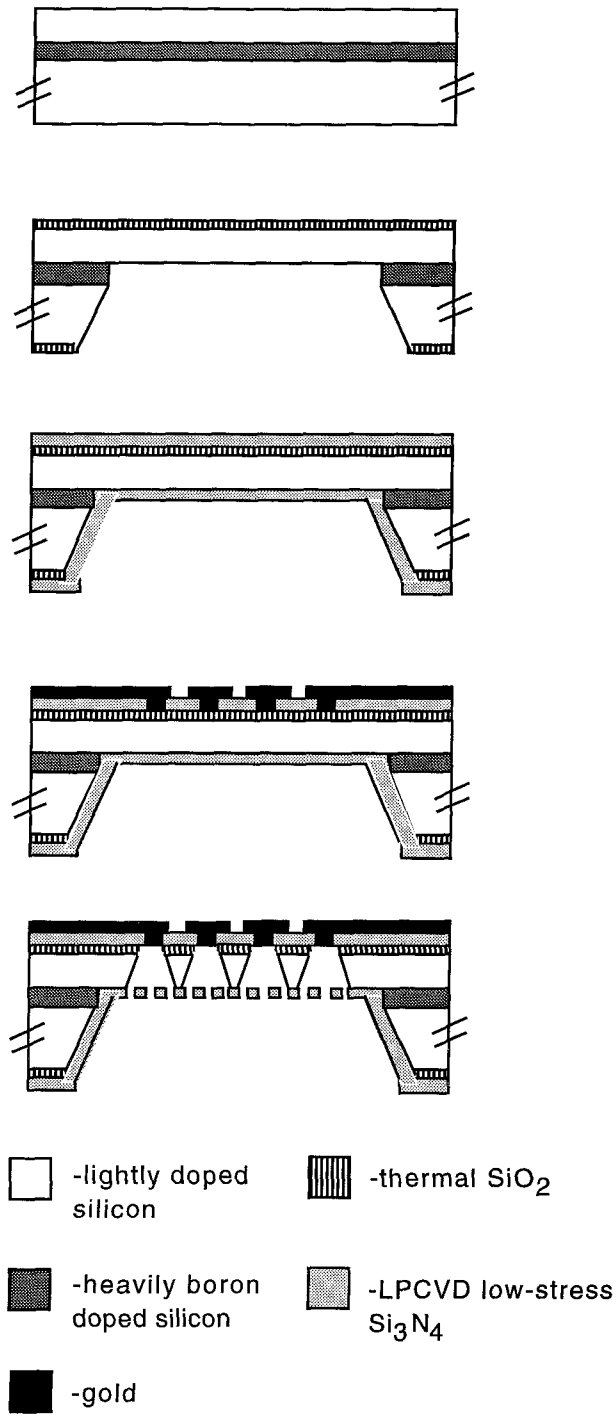

Figure 4-3: Cross section of a neurochip with transparent grillwork after some fabrication steps.

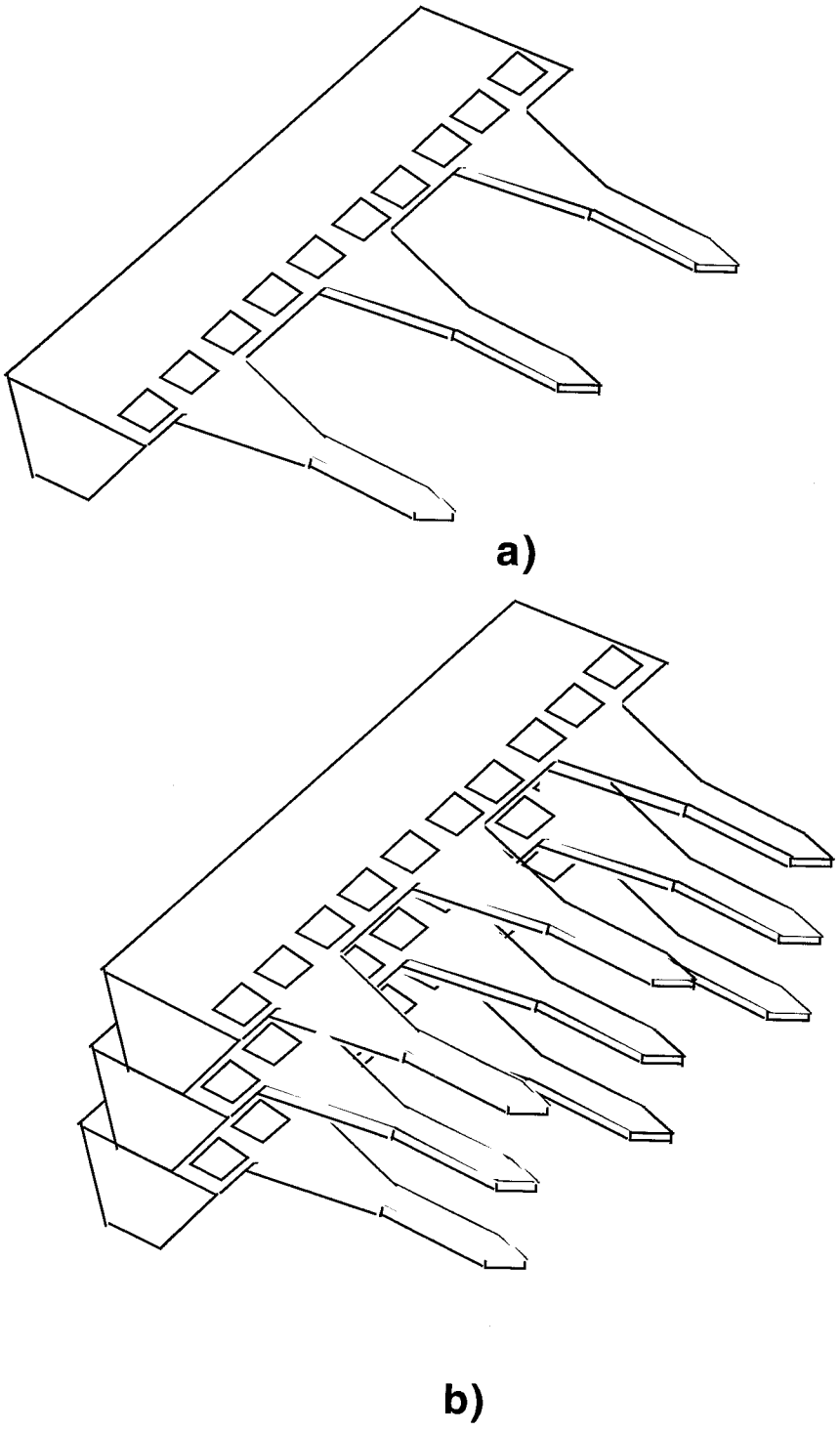

Figure 4-4: a) Multi–prong cultured neuron probe, b) Three–dimensional stack of cultured neuron probes.

devices containing neuron wells for more than a couple of bio–laboratories is not reasonable if the production is done in a university environment. It could be taken over by a private enterprise company, assuming that it has a projection stepper and LPCVD furnaces, without which the fabrication of the neurochips and the neuroprobes would be impossible.

I am hoping that some day one of the relatives of the cultured neural probe will be successfully used as the neural prosthesis for the repair of the damaged nervous system of some paraplegic or quadruplegic person... It would be such a gorgeous day!

A

The Detailed Fabrication Process for Cultured Neuroprobes

The fabrication process for the cultured neuroprobes requires eight masks. Figure A.1. shows the set of masks that are used in the fabrication.

Use <100> epi–wafers, substrate N<100> 1-10Ωcm, layer #1 10^{20} A/cc B (optional:added 2% of Ge for the stress reduction), 4μm thick; layer #2 1-10Ωcm, 16μm thick. Wafers do not have to be double polished.

1. Clean the wafers

a) Do piranha etch cleaning (80% H_2SO_4, 20% H_2O_2, 120C) for 15min.

b) Rinse in water until the resistivity of the DI water is >10 Ωcm.

c) Spin dry.

2. Form front–to–back alignment marks for the rough alignment

a) Prime the wafer using HMDS vapor, spin KTI100cs on the back side of the wafer, 3500rpm.

b) Soft bake at 100C for 30min.

c) Cool the wafer, prime it by HMDS vapor and spin KTI on the front side of the wafer, 3500rpm.

d) Soft bake at 100C for 30min.

e) Do double-side contact printing with front and back alignment mark fixture. Exposure dose 50mJ/cm^2, use test wafer to optimize the exposure.

f) Hard bake at 120C for 30min.

g) Etch front side alignment marks, SF_6 plasma, 300mTorr, 400W, 1.5μm to 2.5μm down in silicon.

h) Etch back side alingment marks, SF_6 plasma, 300mTorr, 400W, 3 to 4μm down in silicon.

i) Do oxygen plasma ashing of photoresist, 300mTorr, 400W, 10min/side.

j) Rinse the wafer in acetone, isopropanol and DI water respectively.

3. Form the oxide steps at the bottom of the neuron wells

a) Do dry thermal oxidation, temperature 1000C, target thickness 45-50nm.

b) Do LPCVD nitride deposition, DCS flow 40sccm, NH_3 flow 120sccm, temperature 800C, target thickness 180-200nm.

c) Prime the wafer by using HMDS vapor and spin on KTI 27cs photoresist at 4000rpm.

d) Soft bake 15min at 90C.

e) Pattern photoresist (mask#1, nitride dots), exposure dose 100mJ/cm^2.

f) Hard bake for 30min at 120C.

g) Do oxygen plasma descumb, 1 min, 50W, 300mTorr.

h) Do plasma etching of LPCVD nitride, SF_6 plasma, 200mTorr, 200W.

i) Do BHF etching for 40sec to remove pad oxide.

j) Strip photoresist by oxygen plasma (300W, 300mTorr).

k) Etch 0.4μm down in silicon (isotropic wet etch HNO_3:H_2O:HF = 50:20:1)

l) Do wet oxidation, 1050C, 1drop/4sec H_2O, target thickness 0.8μm.

m) Strip nitride from the bith sides of the wafer, H_3PO_4 at 150C, duration 8-9hrs (the duration is very dependent on the number of the wafers).

n) Do BHF etching for 40sec to remove the pad oxide which was located below the LPCVD nitride.

4. Form the metal pattern

a) Prime the wafer by HMDS abd spin AZ1350J, 30s, 3400rpm.

b) Soft bake 30min at 90C.

c) Expose (mask#2–metal pattern) using dose 360mJ/cm^2.

d) Do oxygen plasma descumb, 1min, 50W, 200mTorr.

e) Evaporate metal (10nm Cr, 200nm Au and 10nm Cr).

f) Do lift–off by sonicating in acetone, isopropanol and water, 5min each.

g) Rinse in water.

h) Spin dry.

i) Clean in oxygen plasma, 300mTorr, 300W, 15min.

5. Deposit the insulation layer

a) Deposit LTO, temperature 450C, SiH_4 flow 42.4sccm, O_2 flow 62.1sccm, target thickness 0.5μm.

b) Deposit PECVD nitride on both sides of the wafer, temperature 300C, power 50W, gas flow SiH_4 9.1sccm, NH_3 flow 25.9sccm, target thickness 1.5μm.

6. Pattern the insulation layer

a) Prime the wafer by HMDS and spin KTI100cs, 3500rpm, 30s.

b) Softbake 15min at 90C.

c) Expose (mask #3 for opening the contact pads), exposure dose 315mJ/cm^2.

d) Expose (mask #4 for defining the alignment marks), exposure dose 315mJ/cm^2. Expose only 8 dies with this mask.

e) Develop in KTI 934 1:1 developer.

f) Do oxygen plasma descumb, 1 min, 50W, 200mTorr.

g) Hard bake 30min at 120C.

h) Etch nitride by SF_6 plasma, 200mTorr, 200W.

i) Etch LTO by BHF. Check the etch completion under the microscope.

j) Remove photoresist by oxygen plasma etching, 300mTorr, 300W.

7. Form the big cavity

a) Prime the wafer by HMDS and spin photoresist KTI 100cs, 3500rpm on the back side of the wafer.

b) Soft bake 15min at 90C.

c) Expose (mask#5–defining the big cavity), exposure dose 315 mJ/cm^2.

d) Develop in KTI 934 1:1 developer.

e) Hard bake 30min at 120C.

f) Etch nitride by RIE SF_6/O_2 plasma, gas flow SF_6 17sccm, O_2 15sccm, power 600W.

g) Etch LTO by BHF etching until the surface is hydrophobic.

h) Remove photoresist by oxygen plasma etching, 300mTorr, 300W.

i) Etch in EDP at 95C for 11hr, visually check the end of the etching.

j) Remove etch–stop layer from the alignment dies using isotropic etchant CH_3COOH:HNO_3:H=8:3:1. This step is optional and is used only for B/Ge doped etch–stop layer.

k) Rinse wafer in DI water and dry it.

8. Form the neuron wells

a) Prime the wafer by HMDS and spin on the back side of the wafer photoresist AZ1350J, 3500rpm for 30s, using special non–vacuum chuck.

b) Softbake 30min at 90C.

c) Expose (mask#7-grillwork mask), exposure dose 315mJ/cm^2.

d) Develop in AZ1350J 1:1 developer. Check visually the end of the development.

e) Hard bake for 15min at 120C.

f) Prime the wafer by HMDS and paint the edges of the cavity by AZ1350J photoresist, using the soft brush.

g) Hard bake for 30min at 120C.

h) Etch in RIE, SF_6/O_2 plasma, power 600W, gas flow 17sccm of SF_6 and 15sccm of O_2 4.5μm down in silicon.

i) Etch in EDP, temperature 95C, time 40min.

j) Dip in hot water, warm solution of KOH and hot water again to remove the remnants of EDP.

k) Dip in chromium etchant for 1min, followed by 2% H_2SO_4 solution and DI water respectively to remove the chromium from the bottom of the wells.

l) Dry the wafer.

9. Define the shape of the probe from the top

a) Evaporate 150nm of chromium.

b) Prime the wafer by HMDS and spin KTI 100cs at 1000rpm.

c) Soft bake 30min at 90C.

d) Expose (mask#8-definition of the shape of the probe), exposure dose 600mJ/cm^2.

e) Develop KTI 934 1:1 developer, 2min.

f) Rinse and dry the wafer.

g) Hard bake 30 min at 120C.

h) Etch exposed chromium with chromium etchant followed by 2% H_2SO_4 solution, rinse the wafer in DI water and dry it.

i) Etch PECVD nitride by RIE etching, SF_6 plasma, gas flow 24.4sccm of SF_6, power 600W.

j) Etch LTO until teh exposed surface if hydrophobic, rinse in DI water and dry.

k) Etch in RIE, SF_6 etching, gas flow 24.4sccm of SF_6, until the membrane is etched all the way through.

l) Etch chromium by using the chromium mask etchant.

m) Rinse in DI water and dry the wafer.

n) Dip in EDP for 10 min to smoothen the edges.

o) Dip in hot water, weak solution of KOH and hot water to get rid of the EDP remnants.

p) Snap the probes from the substrate.

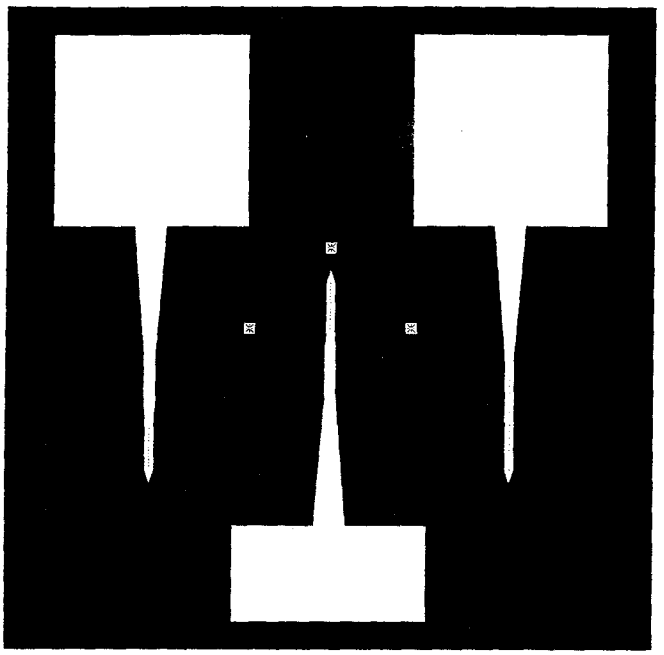

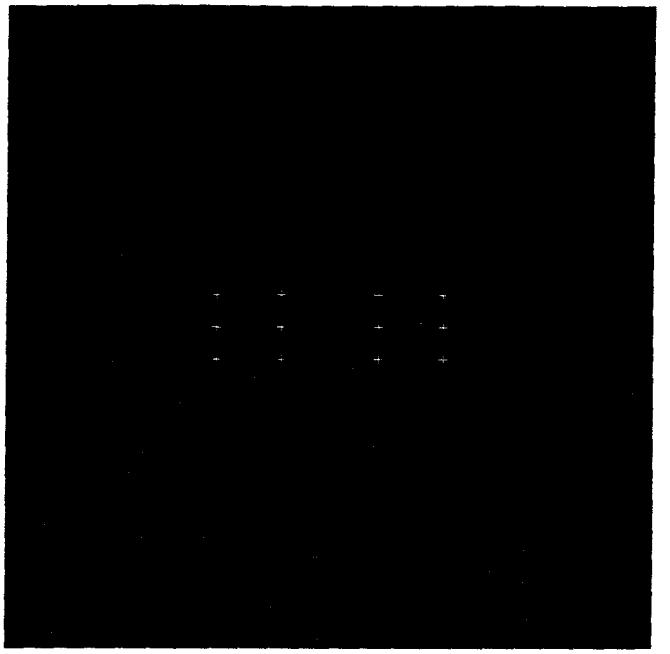

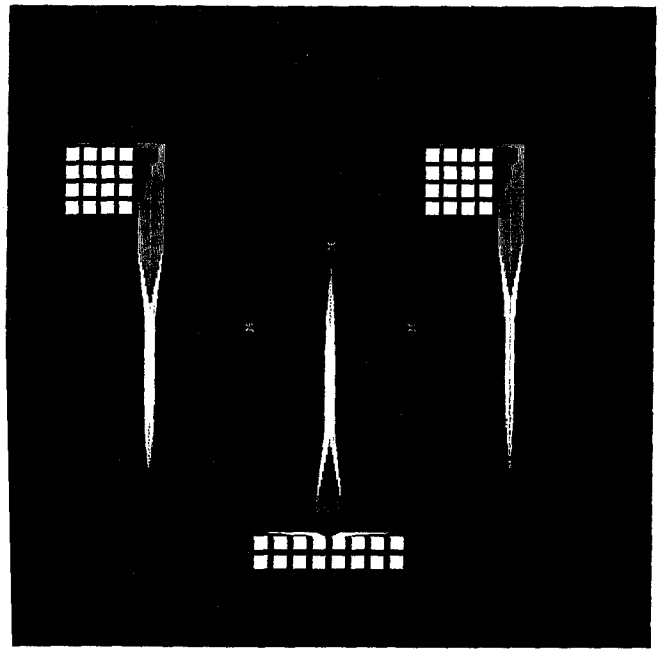

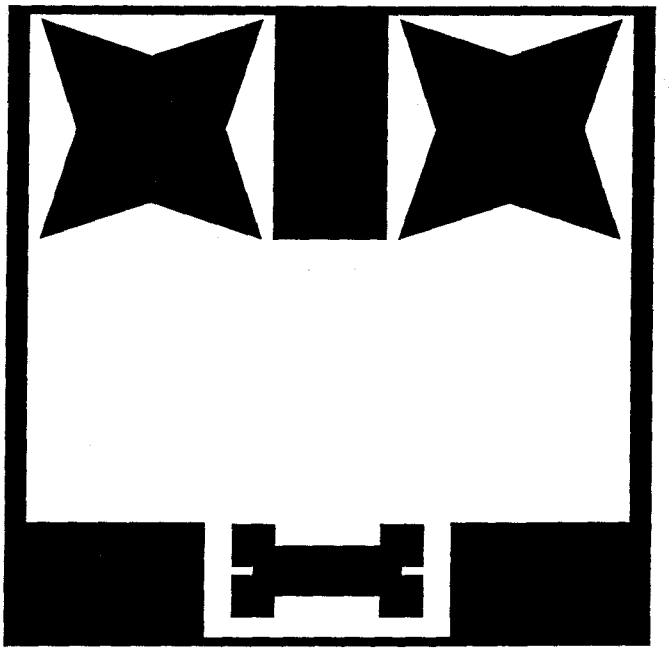

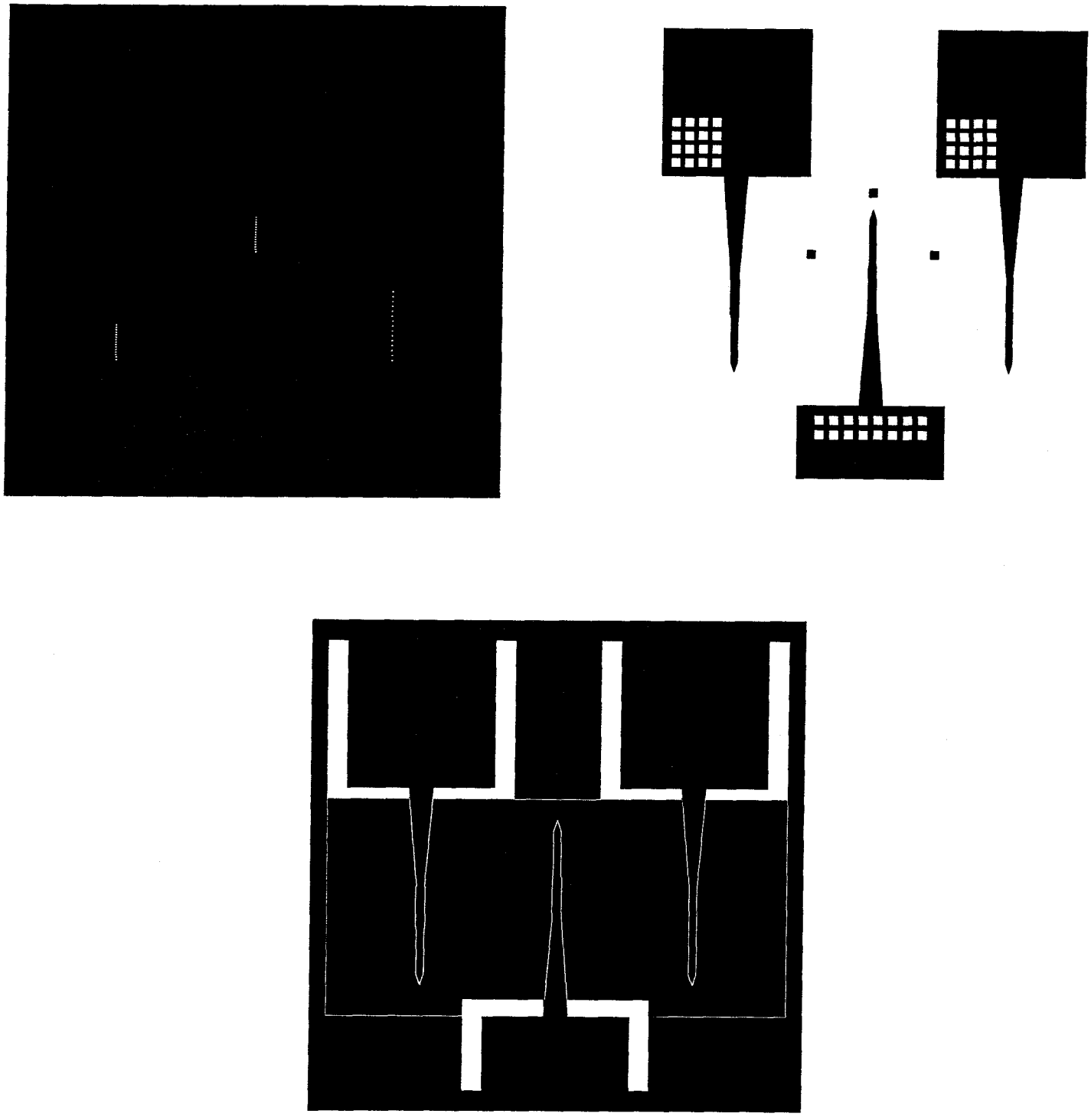

Figure A-1: The set of masks used for cultured neuroprobe fabrication.

B

The Fabrication Process for Neurochips

The fabrication process for the neurochips requires six masks. Figure B.!. shows the set of masks that are used in fabrication. For the opening of the 9x3mm^2 large cavity at the back side of the wafer, instead of the separate mask we used the blank mask and opened exposure shutter 90x30mm^2.

Use <100> epi–wafers, substrate N<100> 1-10Ωcm, layer#1 10^{20} A/cc B (optional: added 2% of Ge for the stress reduction), 4μm thick; layer# 2 1-10Ωcm, 16μm thick. Wafers do not have to be double polished.

The fabrication sequence is very similar to the fabrication sequence for the cultured neuroprobe. The fine details of this farbication process will be specifically mentioned only if different from the corresponding steps in the cultured neuroprobe process:

1. **Clean the wafers**
2. **Form front–to–back alignment marks for the rough alignment**
3. **Form the oxide steps at the bottom of the neuron wells**
4. **Form the metal pattern**
5. **Deposit the insulation layer**
6. **Pattern the insulation layer**
7. **Form the big cavity**
8. **Form the neuron wells**

a) Prime the wafer by HMDS and spin on the back side of the wafer photoresist AZ1350J, 3500rpm for 30s, using special non–vacuum chuck.

b) Softbake 30 min at 90C.

c) Expose (mask #7 -grillwork mask), exposure dose 315mJ/cm^2.

d) Develop in AZ 1:1 developer. Check visually the end of the development.

e) Hard bake for 15min at 120C.

f) Prime the wafer by HMDS and paint the edges of the cavity by AZ1350J photoresist, using the soft brush.

g) Hard bake for 30min at 120C.

h) Etch in RIE, SF_6/O_2 plasma, power 600W, gas flow 17sccm of SF_6 and 15sccm of O_2 for 4.5μm down in silicon.

i) Dice the wafer on 1x1cm^2 dies, cutting the wafer from the front side not to damage the membrane by putting it on the dicing tape.

j) Etch in EDP, temperature 95C, time 40min.

k) Dip in hot water, warm solution of KOH and hot water again to remove the remnants of EDP.

l) Keep in chromium etchant for 1min, followed by 2% H_2SO_4 solution and DI water respectively to remove the chromium from the bottom fo the wells.

m) Dry the dies.

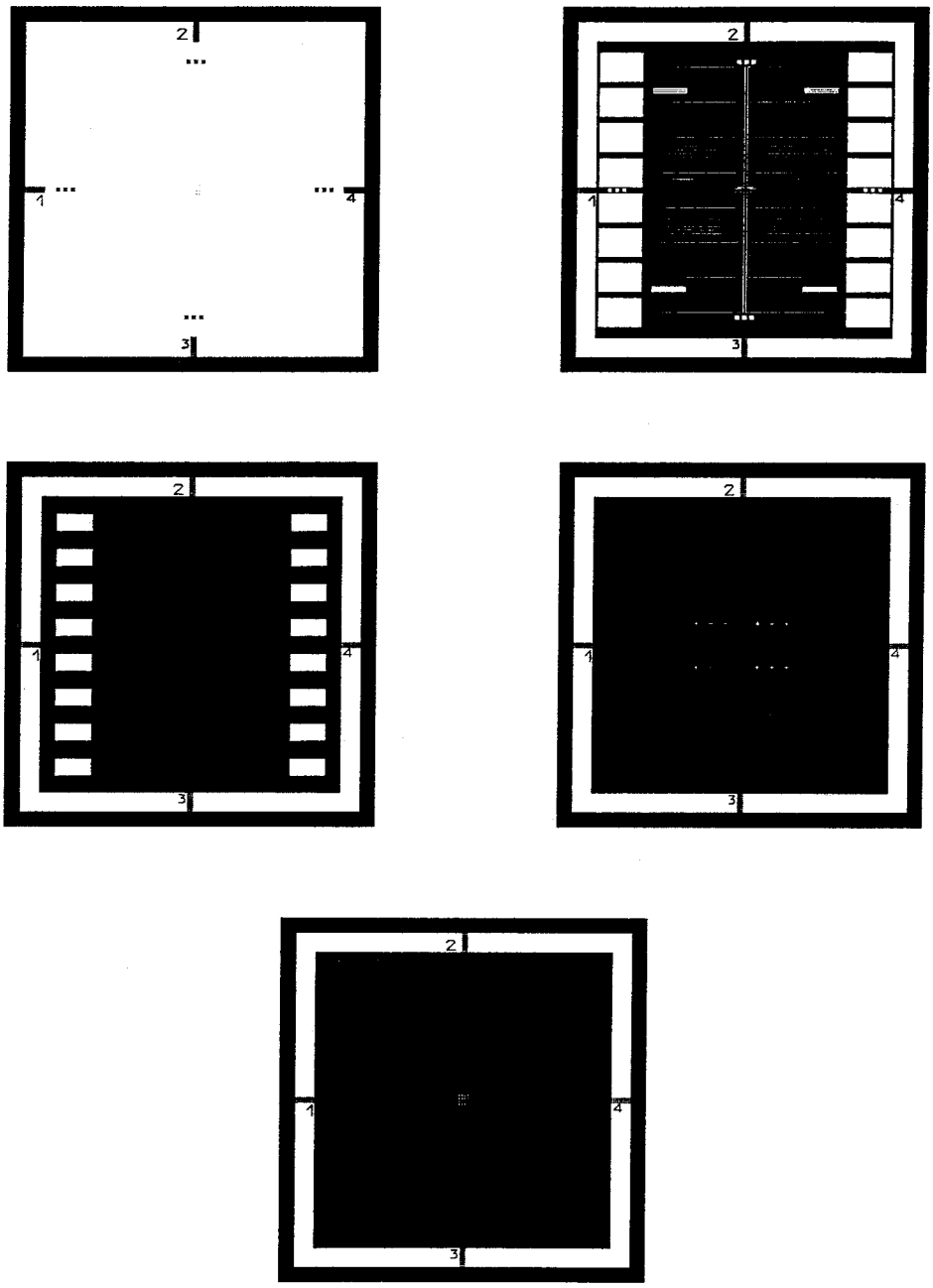

Figure B-1: The set of masks used for neurochip fabrication.

C

The Detailed Fabrication Process for Flat–Bottomed Neurochips

The fabrication process for the flat–bottomed neurochip requires four masks. The nitride mask is slightly modified with respect to the corresponding mask shown in Fig.B.1. and the mask for the opening of contact pads can be omitted, because no insulation is deposited on the flat–bottomed neurochips. Use <100> epi–wafers, substrate N<100> 1-10Ωcm, layer #1 10^{20} A/cc B (optional: added 2% of Ge for the stress reduction), 4μm thick; layer #2 1-10ωcm, 16μm thick. Wafers do not have to be double polished.

1. Clean the wafers

a) Do piranha etch cleaning (80% H_2SO_4, 20% H_2O_2, 120C) for 15min.

b) Rinse in water until the resistivity of the DI water is > 10Ωcm.

c) Spin dry.

2. Form front–to–back alignment marks for the rough alignment

a) Prime the wafer using HMDS vapour, spin KTI100cs on the back side of the wafe r, 3500rpm.

b) Soft bake at 100C for 30min.

c) Cool the wafer, prime it by HMDS vapor and spin KTI on the front side of the wafer, 3500rpm.

d) Soft bake at 100C for 30min.

e) Do double-side contact printing with front and back alignment mark fixture. Exposure dose 50mJ/cm^2, use test wafer to optimize the exposure.

f) Hard bake at 120C for 30min.

g) Etch front side alignment marks, SF_6 plasma, 300mTorr, 400W, 1.5μm to 2.5μm down in silicon.

h) Etch back side alingment marks, SF_6 plasma, 300mTorr, 400W, 3 to 4μm down in silicon.

i) Do oxygen plasma ashing of photoresist, 300mTorr, 400W, 10min/side.

j) Rinse the wafer in acetone, isopropanol and DI water respectively.

3. Form the bottom of the neuron wells

a) Do wet oxidation, 1050C, 1drop H_2O/4sec, target thickness 250nm.

b) Do LPCVD deposition of the low–stress nitride, DCS flow 64.7sccm, NH_3 flow 15.6sccm, temperature 820C, target thickness 200nm.

c) Prime the wafer by using HMDS vapor and spin on KTI 27cs photoresist at 4000rpm.

d) Soft bake 15min at 90C.

e) Pattern photoresist (mask#1, nitride squares), exposure dose 100mJ/cm^2.

f) Hard bake for 30min at 120C.

g) Do oxygen plasma descumb, 1 min, 50W, 300mTorr.

h) Do plasma etching of LPCVD low–stress nitride, SF_6 plasma, 200mTorr, 200W.

4. Form the metal pattern

a) Prime the wafer by HMDS abd spin AZ1350J, 30s, 3400rpm.

b) Soft bake 30min at 90C.

c) Expose (mask#2–metal pattern) using dose 360mJ/cm^2.

d) Do oxygen plasma descumb, 1min, 50W, 200mTorr.

e) Evaporate metal (10nm Cr, 200nm Au and 10nm Cr).

f) Do lift–off by sonicating in acetone, isopropanol and water, 5min each.

g) Rinse in water.

h) Spin dry.

i) Clean in oxygen plasma, 300mTorr, 300W, 15min.

5. Pattern the alignment marks

a) Prime the wafer by HMDS and spin KTI100cs, 3500rpm, 30s.

b) Softbake 15min at 90C.

c) Expose (mask #3 for defining the alignment marks), exposure dose 315mJ/cm^2. Expose only 8 dies with this mask.

d) Develop in KTI 934 1:1 developer.

e) Do oxygen plasma descumb, 1 min, 50W, 200mTorr.

f) Hard bake 30min at 120C.

g) Etch nitride by SF_6 plasma, 200mTorr, 200W.

h) Etch thermal oxide by BHF. Check the etch completion under the microscope.

i) Remove photoresist by oxygen plasma etching, 300mTorr, 300W.

6. Form the big cavity

a) Prime the wafer by HMDS and spin photoresist KTI 100cs, 3500rpm on the back s ide of the wafer.

b) Soft bake 15min at 90C.

c) Expose (blank mask, shutter opened 90x30mm^2), exposure dose 315 mJ/cm^2.

d) Develop in KTI 934 1:1 developer.

e) Hard bake 30min at 120C.

f) Etch nitride by RIE SF_6/O_2 plasma, gas flow SF_6 17sccm, O_2 15sccm, power 600W.

g) Etch thermal oxide by BHF etching until the surface is hydrophobic.

h) Remove photoresist by oxygen plasma etching, 300mTorr, 300W.

i) Etch in EDP at 95C for 11hr, visually check the end of the etching.

j) Remove etch–stop layer from the alignment dies using isotropic etchant CH_3COOH:HNO_3:HF=8:3:1. This step is optional and is used only for B/Ge doped etch–stop layer.

7. Form the neuron wells

a) Prime the wafer by HMDS and spin on the back side of the wafer photoresist AZ 1350J, 3500rpm for 30s, using special non–vacuum chuck.

b) Softbake 30min at 90C.

c) Expose (mask#5-grillwork mask), exposure dose 315mJ/cm^2.

d) Develop in AZ1350J 1:1 developer. Check visually the end of the development.

e) Hard bake for 15min at 120C.

f) Prime the wafer by HMDS and paint the edges of the cavity by AZ1350J photoresist,

using the soft brush.

g) Hard bake for 30min at 120C.

h) Etch in RIE, SF_6/O_2 plasma, power 600W, gas flow 17sccm of SF_6 and 15 sccm of O_2 4.5μm down in silicon.

i) Dice the wafer on 1x1cm^2 individual dies.

j) Etch in EDP, temperature 95C, time 40min.

k) Dip in hot water, warm solution of KOH and hot water again to remove the remn ants of EDP.

l) Dip in BHF for 1 min to remove the thermal oxide from the bottom of the wells.

m) Rinse the die in DI water.

n) Dip in chromium etchant for 1min, followed by 2% H_2SO_4 solution and DI water respectively to remove the chromium from the bottom of the wells.

o) Dry the neurochips.

D

Preparation of Rat Superior Cervical Ganglion (SCG) Neurons and Their Implantation in the Neuron Wells

D.1 Preparation of Rat Superior Cervical Ganglion (SCG) Neurons

The preparation of the cultured neurons and their implantation are done in the laboratory of Dr. Jerome Pine at Caltech's Biology Department by Hannah Dvorak and Michael Maher. Dissection and culture procedures are as described in [7]. Briefly, newborn ($\leq$ 3 days old) Wistar rat pups are anesthetized, the SCG removed and incubated in 0.25% trypsin at 37°C for 25 minutes in an air environment, then rinsed in serum–containing, modified Leibovitz's L-15 air medium (L-15–air), mechanically triturated, and plated onto the neurochip. Twelve drops of medium are used in triturating every whole ganglion.

The media used for SCG culture are two forms of a modified version of L-15, based on that described in [20] as ""growth medium." Basal L-15 medium (Irvine Scientific) is purchased in a liquid form and the additives described in [20], with the omission of Methocel and bovine serum albumin, and 2.5S NGF (Boehinger Mannheim) is used at 100ng/mL. L-15–air is identical to L-15–CO_2 except that sodium bicarbonate is omitted; this medium is used when cultures are exposed to air (as, for example, on the microscope stage during electrophysiology experiments). For some electrophysiology experiments, high-Ca^{2+} L-15 is

used; this is simply L-15 with no additives except for 5mM $CaCl_2$.

Cultures are generally kept in L-15–CO_2 medium in a humidified 5% CO_2 atmosphere at 37°C. One–half of the medium is replaced with fresh medium (which is allowed to equilibrate in the CO_2 incubator before feeding) every 2-3 days. To prevent proliferation of non–neuronal cells, uridine and the antimitotic agent 5–fluoro–2–deoxyuridine (FUdR) (Sigma) are added at a concentration of 10μmM one day after plating, then are diluted out with subsequent feedings.

D.2 Neurochip Preparation

The exposed silicon and silicon oxide surfaces of the neurochip must be treated chemically in order to promote adhesion and growth of neurons. On order for any aqueous solution to get into the wells, the neurochip must first be wetted with a liquid of lower surface tension, generally 95% ethanol. The ethanol is then rinsed out with water, which can now diffuse into the wells; and the water is then replaced with the solution of interest. To prepare a neurochip for culture, it is wetted in this way, and then allowed to sit in a 1 mg/mL solution of poly-L-lysine (MW 20,000) in Dulbecco's phosphate–buffered saline (DPBS) overnight. The poly-L-lysine is then rinsed out by soaking in water for an hour and the neurochip is then allowed to dry. It is sterilized by exposure to UV light for 25 minutes and all subsequent operations are carried out aseptically in a laminar flow hood. The chip is then wetted again and then soaked with a 20μmg/mL solution of laminin in DPBS for at least 2 hours. The laminin is then rinsed off with 2-3 changes of a few drops of L-15–air.

D.3 Loading a Neurochip with Neurons

A suspension of SCG neurons is prepared as described above, and three drops of this suspension are plated onto a neurochip prepared as described above. The neurochip is returned to the air incubator for approximately half an hour to allow many of the neurons to settle to the bottom of the basin. Approximately 2 mL of medium are then gently added to the dish holding the chip and the neurochip is carried to the stage of an upright microscope equipped with Nomarski optics for improved visibility of the transparent neurons.

The first procedure for moving of cells into the wells that was developed for this project by Dr. Pine used two differently shaped glass pipettes for manipulating the cell into the neuron well (See Fig.D-1). However, in the current method cells are manipulated into wells with the use of a glass microelectrode whose tip has been broken to about 20μm and melted into a smooth, round end. The terminal 2mm or so of the tip is bent at about 45° by holding the electrode over a red–hot platinum wire (the end result is approximately the shape of a hockey stick). The neurons, which at this stage have settled loosely on the bottom of the neurochip basin, are prodded and pulled with the manipulator until they are immediately over a well. Since most SCG cell bodies are larger than the main opening of the well, they must then be pushed in by lowering the stage of the microscope, putting the manipulator over the cell and well, and then raising the stage again.

Once each well has been filled with a neuron, the chip is left on the microscope stage for at least two hours. This appears to give enough time for the neurons to attach securely to the insides of the wells so that they are not dislodged when the neurochip is later moved. After this sitting time, other neurons in the vicinity of the wells are removed by suction with a glass microelectrode whose tip has been cut to 40μm and is attached through a patch–pipette electrode holder to plastic tubing and a syringe. This allows easier assessment of initial outgrowth from the wells by elimination of other possible sources of neurites.

The neurochip is then returned to the air incubator and left overnight. The next day, most of the medium is aspirated off and replaced with L-15–CO_2 with 10μmg/mL uridine and FUdR. The neurochip is subsequently kept in the CO_2 incubator.

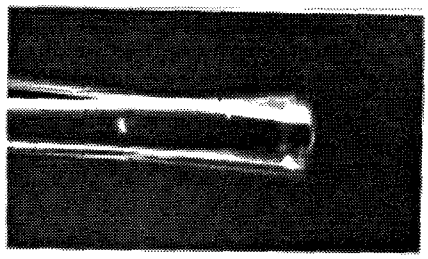

a)

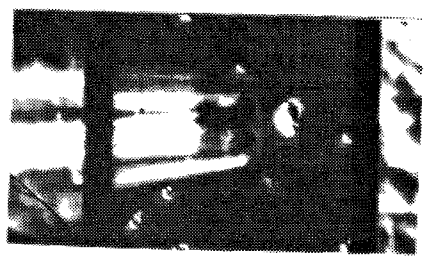

b)

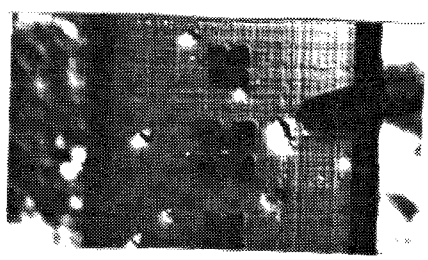

c)

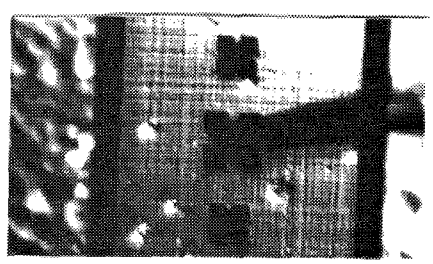

d)

Figure D-1: Major steps in the process of moving embryonic neurons in the wells: a) Neuron sucked and held in pipette while being moved to a well; b) Cell ejected from the pipette near a well; c) Pusher positioned to move cell over the well. The pipette used for carrying the cell has been moved out of view; d) Cell implanted in the well by a pusher.

References

[1] J.A. Appels et al. Local oxidation of silicon and its applications in semiconductor device technology. *Philips Res. Rep.*, 25(2):118–132, 1970.

[2] G. A. Banker and W. M. Cowan. Rat hippocampal neurons in dispersed cell culture. *Brain Research*, 126:397–425, 1977.

[3] E. Bassous, H.N. Yu, and V. Manisalco. Topology of silicon structures with recessed SiO_2. *J. Electrochem. Soc.*, pages 1729–1737, 1976.

[4] P. Benda et al. Dissociated cell cultures from fetal mouse hypothalamus. *Exp. Brain. Res.*, 23:29–47, 1975.

[5] C-B. Chien. *Voltage–sensitive dye recording from networks of cultured neurons.* Ph.D. thesis, California Institute of Technology, Pasadena, CA, 1990.

[6] C.-B. Chien and J. Pine. Voltage–sensitive dye recording of action potentials and synaptic potentials from sympathetic microcultures, 1991. Submitted to the Biophysical Journal.

[7] T.K. Garyantes and W.G. Regehr. Electrical activity increases growth cone calcium but fails to inhibit neurite outgrowth from rat sympathetic neurons. *J. Neurosci.*, 12:96–103, 1992.

[8] G. W. Gross et al. A new fixed array multimicroelectrode system designed for long term monitoring of extracellular single unit neuronal activity *in vitro*. *Neurosci. Lett.*, pages 101–105, 1977.

[9] G.W. Gross, A. Williams, and J.H. Lucas. Recording of spontaneous activity with photoetched microelectrode surfaces from mouse spinal neurons in culture. *Journal of Neuroscience Methods*, 5, 1982.

[10] P. Heinz. Economic analysis for a double side aligner at two sensor companies. Karl Suss America Inc., Publication No. 116.

[11] A. L. Hodgkin and A. F. Huxley. Resting and action potentials in single nerve fibres. *J. Physiol.*, 104:176–195, 1945.

[12] R. C. Jaeger. *Introduction to Microelectronic Fabrication.* Addison–Wesley Publishing Company, 1988.

[13] E.S. Kim, R.S. Muller, and R.S. Hijab. Front–to–back alignment using resist–patterned etch control and one etching step. *Journal of Microelectromechanical Systems*, 1(2):95–99, 1992.

[14] T. Kramer Garyantes. *The Effect on Electrical Stimulation on Neuronal Outgrowth and the Development of a New Method for Chronic Long–Term Stimulation and Recording from Groups of Neurons in Culture.* Ph.D. thesis, California Institute of Technology, Pasadena, CA, 1992.

[15] J. Krüger. Simultaneous individual recordings from many cerebral neurons: Techniques and results. *Rev. Physiol. Biochem. Pharmacol.*, 98:177–233, 1983.

[16] M. Kuperstein and H. Eichenbaum. Unit activity, evoked potentials and slow waves in the rat hippocampus and olfactory bulb recorded with a 24–channel microelectrode. *Neuroscience*, 15(3):703–712, 1985.

[17] H. Langeberg, 1988. Senior Thesis, California Institute of Technology.

[18] H. Lester, 1991. A Ten–Session Introduction for Biology 161: Neurobiology Laboratory Class.

[19] G. Ling and R. W. Gerard. The normal membrane potential of frog sartorius fibers. *J. Cell. Comp. Physiol.*, 34:383–396, 1949.

[20] R. E. Mains and P. H. Patterson. Primary cultures of dissociated sympathetic neurons. I. Establishment of long–term growth in culture and studies of differentiated properties. *J. Cell. Biol.*, 59:329–345, 1973.

[21] H. D. Mercer and R. L. White. Photolithographic fabrication and physiological performance of microelectrode arrays for neural stimulation. *IEEE Trans. Biomed. Eng.*, BME–25(6):494–500, 1978.

[22] K. Najafi and J. F. Hetke. Strength characterization of silicon microprobes in neurophysiological tissues. *IEEE Transactions on Biomedical Engineering*, 37(5):474–481, 1990.

[23] H. C. Nathanson and R. A. Wickstrom. Resonant gate silicon surface transistor with high–Q band–pass properties. *Applied Physics Letters*, 7(4):84–86, 1965.

[24] E. Neher and B Sakmann. The patch clamp technique. *Scientific American*, pages 46–51, 1992.

[25] P.G. Nelson and J.H. Peacock. Electrical activity in dissociated cell cultures from fetal mouse cerrebelum. *Brain Res.*, 61:163–174, 1973.

[26] J. O'Keefe and H. Bouma. Complex sensory properties of certain amygdala units in the freely moving cat. *Exp. Neurol.*, 23:384–398, 1969.

[27] J.H. Peacock, D. F. Rush, and L.H. Mathers. Morphology of dissociated hippocampal cutltures from fetal mice. *Brain Res.*, 169:231–246, 1979.

[28] G. L. Pearson, W. T. Read Jr., and W. L. Feldmann. Deformation and fracture of small silicon crystals. *Acta Metallurgica*, 5:181–191, 1957.

[29] M. Peckerar et al. Passive microelectrode arrays for recording of neural signals: A simplified fabrication process. *Rev. Sci Instrum.*, 62(9):2276–2280, 1991.

[30] J. R. Pfiester and J. R. Alvis. Novel germanium/boron channel–stop implantation for submicron CMOS, 1987. IEDM Technical Digest.

[31] J. R. Pfiester and J. R. Alvis. Improved CMOS field isolation using germanium/boron implantation. *IEEE Electron Device Lstters*, 9(8):391–393, 1988.

[32] R.S. Pickard. A review of printed circuit microelectrodes and their production. *J. Neurosci. Meth.*, 1:301–318, 1979.

[33] J. Pine. Recording action potentials from cultured neurons with extracellular micro-circuit electrodes. *Journal of Neuroscience Methods*, 2:19–31, 1980.

[34] J. Pine et al. Cultured neuron probe, 1994. Quarterly Progress Report No.4. Contract No. NO1-NS-3-2393.

[35] B. Puers and W. Sansen. Compensation structures for convex corner micromachining in silicon. *Sensors and Actuators*, A21–A23:1036–1041, 1990.

[36] W. G. Regehr et al. Progress in long–term electrical connections to cultured neurons using integrated circuits technology, 1988. 1988 IEEE Airlie House Conference on Synthetic Microstructures.

[37] W. G. Regehr et al. Sealing cultured neurons to embedded dish electrodes facilitates long–term stimulation and recording. *Journal of Neuroscience Methods*, 30:91–106, 1989.

[38] W.G. Regehr. *Neuron–Microdevice Connections.* Ph.D. thesis, California Institute of Technology, Pasadena, CA, 1992.

[39] LJ. Ristić, editor. *Sensor Technology and Devices.* Artech House, 1994.

[40] W. M. Runyan and K. E. Bean. *Semiconductor Integrated Circuit Processing Technology.* Addison–Wesley Publishing Company, 1990.

[41] H. Seidel et al. Anisotropic etching of crystalline silicon in alkaline solutions. *J. Electrochem. Soc*, pages 3626–3632, 1990.

[42] A. Stefanelli, E. Cataldi, and L.A. Ireadi. Specific synaptic systems in reaggregated spherules from dissociated chick cerrebelum cultivated *in vitro*. *Cell Tissue Res.*, 182:311–325, 1977.

[43] W. Stühmer, W. M. Roberts, and W. Almers. *The Loose Patch Clamp*, chapter 8, pages 123–132. Plenum Press, 1983.

[44] S. M. Sze. *VLSI Technology.* McGraw–Hill Book Company, 1988.

[45] O. Tabata et al. Anisotropic etching of silicon in TMAH solutions. *Sensors and Actuators*, 34:51–57, 1992.

[46] S. Tatić-Lučić et al. Silicon–micromachined neurochips for *in vitro* studies of cultured neural networks. In *Technical Digest, International Conference on Solid–State Sensors and Actuators: Transducers'93, Yokohama, Japan*, pages 943–946, 1993.

[47] S. Tatić-Lučić et al. Silicon–micromachined cultured neuron probes for *in vivo* studies of neural networks, 1994. To be presented at ASME Winter Annual Meeting, November 6-11, Chicago, IL.

[48] S. Tatić-Lučić and Y.-C. Tai. Novel extra accurate method for two–sided alignment on silicon wafers. *Sensors and Actuators A*, 41–42:573–577, 1994.

[49] C. A. Thomas Jr. et al. A miniature microelectrode array to monitor the bioelectric activity of cultured cells. *Experimental Cell Research*, 74:61–66, 1972.

[50] E. Trenkner and R.L. Sidman. Histogenesis of mouse cerrebelum in microwell structures. *J. Cell. Biol.*, 75:915–940, 1977.

[51] M. Verzeano. Activity of cerebral neurons in the transition from wakefulness to sleep. *Science*, 124:366–367, 1956.

[52] F. V. Warnock and P. P. Benham. *Mechanics of Solids and Strength of Materials.* Pitman, 1965.

[53] B. C. Wheeler and J. L. Novak. Current source density estimation using microelectrode array data from the hippocampal slice preparation. *IEEE Trans. Biomed. Eng*, BME–33(12):1204–1212, 1986.

[54] R.M. White and S.W. Wenzel. Inexpensive and accurate two–sided semiconductor wafer alignment. *Sensors and Actuators*, 13:391–395, 1988.

[55] K. D. Wise and K. Najafi. A micromachined integrated sensor with on–chip self–test capability, 1984. Digest 1984 IEEE Solid–State Sensor Conference.

[56] K. D. Wise, K. Najafi, and K. L. Drake. A multichannel microprobe for intracortical single–unit recording, 1984. Proc. IEEE/NSF Symp. on Biosensors.

[57] K.D. Wise, J.B. Angell, and A. Starr. An integrated circuit approach to extracellular microelectrodes. *IEEE Trans. Biomed. Eng.*, 17:238–246, 1970.

[58] S. Wolf and R.N. Tauber. *Silicon Processing for the VLSI Era*, volume 1. Lattice Press, 1986.

[59] T.-C. Wu, W. T. Stacy, and K. N. Ritz. The influence of the LOCOS processing parameters on the shape of the bird's beak structure. *J. Electrochem. Soc*, pages 1563–1566, 1983.

[60] X.-P. Wu and W.H. Ko. Compensating corner undercutting in anisotropic etching of silicon. *Sensors and Actuators*, 18:207–215, 1989.